Diploma thesis

Visualization of tumor-associated microbiota in lung cancer

16S rRNA FISH analysis in tumor tissue

submitted by

Jan Kleinherr

in partial fulfillment of the requirements for the degree of

Doktor der gesamten Heilkunde
(Dr. med. univ.)

at the

Medical University of Graz

Diagnostic and Research Institute (D&F) of Pathology

under the supervision of

Assoz. Prof. Priv.-Doz. Dr.med.univ. Gregor Gorkiewicz
+
Univ. FA Dr.med.univ. Martin Zacharias

Graz, 16.08.2024

Declaration of Academic Integrity:

I hereby confirm that the present diploma thesis is the result of my own independent scholarly work. I also confirm that in all cases, where material from the work of others (in books, articles, essays, dissertations, and on the internet) is acknowledged, quotations and paraphrases are clearly indicated. No material other than that cited in the reference list has been used. I have read and understood the Medical University's regulations and procedures concerning plagiarism.

Graz, 16.08.2024 Jan Kleinherr, eh

Acknowledgments:

First, I would like to thank Martin for his support! It was a great and friendly collaboration at eye level and was really fun! You were always available to support me with all my questions. Thank you very much for making this practical, research-based thesis possible for me!

A big thank you goes to Gregor, who supervised me with his expertise and suggested new ideas, new perspectives and new approaches in every lab meeting!

I would also like to thank my lab colleagues Barbara, Margit and the entire working group of Prof. Zatloukal for their daily practical help in the lab.

Finally, I would like to thank my fiancée and my family, who supported me during this time and gave me strength.

Zusammenfassung:

Hintergrund/Einleitung: Lungenkrebs ist und bleibt eine sehr schwere Diagnose, sodass sich auch das große, seit ca. 20 Jahren florierende Feld der Mikrobiomforschung mit dem Thema Lunge und Lungenkrebs beschäftigt hat. Nachdem vor einiger Zeit der Nachweis und die grobe Beschreibung eines spezifischen, respiratorischen Mikrobioms gelungen ist, beschreiben rezente Forschungsergebnisse eine lokale, mikrobielle Flora in soliden Tumoren, zu welchen auch die Lungentumoren gehören. Während für chronisch entzündliche Lungenerkrankungen eine Alteration des lokalen Mikrobioms festgestellt werden konnte, ist die Beschreibung des Lungenmikrobioms und des speziellen Tumormikrobioms in Lungentumoren noch nicht sehr ausführlich. Jedoch konnte eine Assoziation von Mikroben und Lungentumoren schon eindeutig gezeigt werden. Speziell Informationen über die räumliche Zuordnung der Mikroben im Tumorgewebe und die hier möglichen Rückschlüsse auf Karzinogenese und Pathophysiologie fehlen im Kontext der Lungentumoren aber noch weitestgehend.

Ziele: Unsere Versuchsreihe galt dem Ziel, die Lokalisation der Mikroben im Tumorgewebe zu identifizieren und zu beschreiben. So wollten wir eine wichtige Grundlage für das respiratorische Tumormikrobiom und weiterführende pathophysiologische Überlegungen, Forschungsprojekte und dessen Zusammenspiel mit der respiratorischen Karzinogenese und den Lungentumorzellen liefern.

Methoden: Als Grundlage wählten wir für die Visualisierung des respiratorischen Tumormikrobioms eine FISH-Analyse mit der panbakteriellen EUB338-Sonde gegen die 16S rRNA-Sequenz. Es wurde die H&E-Morphologie, genau wie die FISH-Morphologie in den DAPI- und den Sonden-spezifischen Wellenlängen detailliert mikroskopiert und ausgewertet. Mittels Bildverarbeitungstechniken wurden Einzelbilder übereinandergelegt, um die Aussagekraft zu verstärken.

Ergebnisse: Nach der Methodenetablierung, war es möglich verschiedene Gewebe mit verschiedenen Pathologien zu analysieren. Es konnten erfolgreich Bakterien in einer Appendizitis wie auch Colonkarzinom-assoziierte Bakterien dargestellt werden. In den eigentlichen Zielgeweben, den Lungenentzündungs- und

Lungentumor-Gewebeschnitten haben wir leider keine überzeugenden Signale generieren können.

Schlussfolgerung/Ausblick: Eine althergebrachte und etablierte Methode wie die FISH-Analyse bietet neben den neuen, technisch aufwändigen und teuren Methoden eine echte und aussagekräftige Ergänzung. Jedoch benötigt auch diese Methode eine intensive Etablierung. Wird diese Etablierung aufbauend auf unseren Ergebnissen fortgeführt, so sind auch schwer zu färbende Gewebe, wie die Lunge mit dieser Methode zu analysieren. Eine genaue Lokalisation des tumor-assoziierten Mikrobioms, genau wie Speziesbestimmungen mittels speziesspezifischer Sonden bietet eine weiterführende Grundlage für diagnostische Ansätze.

Structured abstract:

Background/Introduction: Lung cancer is and remains a very serious diagnosis and it is not surprising that the large field of microbiome research, which has been booming for around 20 years, has also focused on the topic of lungs and lung cancer. Following the successful detection and rough description of a specific respiratory microbiome not too long ago, recent research results describe a local microbial flora in solid tumors, including lung tumors. While an alteration of the local microbiome has been demonstrated for chronic inflammatory lung diseases, the description of the specific tumor microbiome in lung tumors is not yet very detailed. However, an association between microbes and lung tumors has already been clearly demonstrated. But particularly information on the spatial allocation of microbes in tumor tissue and the possible conclusions on carcinogenesis and pathophysiology in the context of lung tumors are still largely lacking.

Objectives/Aims: We tried to visualize the localization of tumor-associated microbiota in lung cancer with 16S rRNA FISH analysis. So, we tried to give some important information about the microbiome in tumors of the lungs to build a basis for further research about the pathophysiology between tumor cells, carcinogenesis and tumor-associated microbiota.

Methods: The performance of 16S rRNA FISH analysis with the EUB338 probe was the foundation of visualization of the microbiota in lung cancer tissue. Therefore, we compared H&E morphology with FISH morphology and merged images of probe signal with DAPI signal. We established pure bacteria cell blocks as positive controls, before testing inflammatory tissue (appendicitis and lung abscess cases) to then stain both colon carcinoma and lung carcinoma using the adapted protocol.

Results: After the establishment of the FISH method, we were able to analyze different pathologies. Successfully we stained microbes in appendicitis tissue and in colorectal cancer tissue. However, we were not able to generate a convincing staining result of lung abscess tissue and of lung cancer tissue.

Conclusion/Outlook: The FISH method is a well understood technique to visualize nucleic acids with a long history of use for different aims. It is a cheap

method in comparison to sophisticated analysis and it may be beneficial to invest work in establishment, to stain microbiota in tumor tissue. If the establishment process would be continued in further projects, there is a good chance of success. There remain a lot of further questions about the exact localization and distribution pattern of tumor-associated microbes and about potential diagnostic uses.

Table of content:

Abbreviations:

- °C - Degrees Celsius
- 16S rRNA – 16S ribosomal ribonucleic acid
- ALK - anaplastic lymphoma kinase
- approx. - approximately
- BC - Before Christ
- BCG - Bacillus Calmette-Guerin
- BSA - Bovine serum albumine
- CD – Cluster of differentiation
- CF – cystic fibrosis
- COPD - Chronic obstructive pulmonary disease
- CT - computed tomography
    - PET-CT - Positron emission tomography–computed tomography
- Cy-3 labled - Tetramethylrhodamine (TRITC) = fluorescent dye oligonucleotide labled
- DAPI - 4′,6-diamidino-2-phenylindole
- DNA - Desoxyribonucleic acid
- EBV - Epstein-Barr virus
- EGFR - Epidermal Growth Factor Receptor
- et al. = et alii - and others
- ESMO - European Society for Medical Oncology
- EUB338 Probe/(S-D-Bact-0338-a-A-18) Probe - Bacteria specific sequence
- EX – Extinction
- FDA - Food and Drug Administration
- FFPE - formalin-fixed paraffin-embedded
- FISH – Fluorescence in situ hybridization
- g – Gramm
- GFP - green fluorescent protein
- GIMP - GNU Image Manipulation Program
- HBV - hepatitis B virus
- HCl – Hydrochloride
- HCV - hepatitis C virus
- H&E-Stain - Hematoxylin-Eosin stain
- HHV-8 - Kaposi's sarcoma herpesvirus
- HPV - human papillomavirus

- HTLV - human T-cell lymphotropic virus
- MCC - mucociliar clearance
- MCPyV - Merkel cell polyomavirus
- MET - Mesenchymal-epithelial transition
- mg - Milligramm
- ml - Milliliter
- mM – Millimolar
- min – Minutes
- MRI - magnetic resonance imaging
- NaCl – Natriumchloride
- NaOH - Sodium hydroxide
- ng - Nanogramm
- nm – Nanometers
- NSCLC – Non small cell lung cancer
- NTRK - neurotrophic tyrosinereceptor kinase
- PCR – Polymerase chain reaction
- PD-L1 - programmed death-ligand 1
- QM - Quality management system
- RNA - Ribonucleic acid
    - tRNA – transfer RNA
    - smRNA - small modulatory RNA
    - mRNA – messenger RNA
- SCLC – Small cell lung cancer
- SDS - Sodium dodecyl sulfate
- TNM - Tumor (T), Nodes (N), Metastases (M)
- TRIS - Tris(hydroxymethyl)aminomethan
- TVEC - Talimogene laherparepvec
- UICC – Union for international Cancer Control
- µl – Microliter

List of figures:

List of tables:

1. Introduction:

1.1. Lung cancer:

The diagnosis of lung cancer continues to be a life-limiting diagnosis associated with high morbidity and mortality. According to Statistic Austria, 2302 new diagnoses among women and 2901 new diagnoses among men were registered in Austria in 2022. In terms of cancer-related deaths, lung cancer now ranks first among men (approx. 21%) and women (approx. 18%) (1). This statistic emphasizes the clinical and social relevance of this topic right from the start.

1.1.1. Epidemiology and entities:

The most common types of lung tumors are the small cell lung cancers (SCLCs) (~15-20%) and the group of non-small cell lung cancers (NSCLCs) (~80-85%), which includes adenocarcinoma (~35-45%), squamous cell carcinoma (~15-30%), large cell carcinoma (~5-10%), other neuroendocrine tumors than SCLCs (~1-5%) and sarcomatoid carcinoma (<1%) (Percentage values = Diseases per 100,000 persons/year, age European standard). The incidence in Europe is given as approx. 52/100,000/year and is around 3 times higher in men. The exception here is adenocarcinoma, which occurs 6 times more frequent in women than in men. Adenocarcinoma is also the most common diagnosis among non-smokers. The peak incidence is at 55-60 years of age (2–8).

1.1.2. Localization:

The most common entities of lung tumors can generally be distinguished by the location of the primary tumor. Adenocarcinomas are typically diagnosed in the peripheral parts of the bronchial tree and are then classified under the descriptive term of peripheral lung tumors (approx. 25-30%). On the other hand, there is the descriptive term of central lung tumors (approx. 60-70%). These generally include squamous cell carcinomas and SCLCs. The smallest group is formed by so-called diffuse-infiltrating ("pneumonic") lung tumors with approx. 3% (5,9).

1.1.3. Risk factors:

The overriding risk factor for the development of lung cancer is tobacco consumption (5–7,9). Approximately 85% of lung cancers develop as a direct result of cigarette smoking (5). Of around 7000 chemical substances in tobacco smoke, around 60 substances have been classified as highly carcinogenic according to animal

experiments. If the incidence rate is shown as a function of cigarette consumption, the significance can also be demonstrated in numbers. There is an increase in the incidence of lung tumors with a cigarette consumption of 10 cigarettes per day compared to non-smokers by the factor 15 and a further increase with a cigarette consumption of 40 cigarettes per day by the factor 4 (15x4=60) (9). If cigarette consumption begins in adolescence, the risk of lung cancer increases by the factor x30 (5). In addition to polycyclic aromatic hydrocarbons and harmful metal bonds, cigarette smoke also contains substances which, due to their low boiling point, occur in a primarily gaseous state in cigarette smoke (e.g. N-nitroso compounds and nitrosamines) and first condense in the bronchioloalveolar periphery (9). These substances are associated with an increase in the incidence of adenocarcinomas in connection with changes in smoking behavior (depth of inhalation) and changes in the form of consumption (e.g. e-cigarettes, light cigarettes), because these substances can cause damage deep in the periphery due to these properties. The significance of fine dust pollution in the carcinogenesis of adenocarcinoma in the lung is also being discussed (4). Other risk factors for lung cancer development often include workplace exposure to asbestos, arsenic, wood dust, scars in the lungs (so-called scar carcinomas) and often iatrogenic exposure to radioactive radiation (5,9).

1.1.4. Symptoms:

Early diagnosis of lung tumors is a major challenge even in today's central European healthcare system. Unfortunately, initial symptoms are either non-existent or very unspecific. Cough, dyspnea and chest pain can be typical, just like the known B-symptoms (fever, chills, night sweats, unintentional weight loss). However, the list of differential diagnoses is very long. It is important that a more detailed investigation is recommended, especially for coughs that are new or have changed in character and last longer than 3-4 weeks under optimal therapy. A very short history of bronchial asthma, bronchitis and recurrent pneumonia in patients >40 years of age are also always suspicious for cancer. Symptoms such as hemoptysis, recurrent paresis, phrenic nerve paralysis and superior inflow congestion are often clinically easier to classify as suspected of lung cancer but are generally late symptoms (5). The Horner symptom complex of miosis + ptosis + (apparent) enophthalmos with possible intercostal neuralgia, plexus neuralgia and destruction of the 1st rib would

be a classic picture of a so-called Pancoast tumor. This is localized at the top of the lung and can thus damage nearby nerve cords. Furthermore, paraneoplastic syndromes are a not-so-rare manifestation of lung tumors. They are often caused by SCLC. Endocrinopathies such as Cushing's syndrome, Bartter-Schwartz syndrome (SIADH), PTHrP-induced tumor hypercalcemia, insulin-like-growth-factor-II (IGF-II) induced hypoglycemia can become clinically manifest, just as paraneoplastic neuropathies and myopathies such as Lambert-Eaton syndrome, polymyositis and dermatomyositis can (5–7).

1.1.5. Diagnosis:

If a lung carcinoma is clinically suspected, the diagnostic tool of first choice is imaging. A chest X-ray is often performed in two planes. The following computed tomography (CT) is usually more detailed. Histological diagnosis can be made by endobronchial or transcutaneous biopsy methods or surgical methods. Positron emission tomography + computed tomography (PET-CT), sonography of the abdomen and cranial magnetic resonance imaging (MRI) should also be performed in a subsequent step to exclude distant metastases (5–7,10). In addition to the traditional assessment of histomorphology in combination with immunohistochemical behavior (first and foremost the PD-L1 *(programmed death-ligand 1)* tests) for diagnosis confirmation, various molecular pathological methods are becoming increasingly important predicting the response to therapy (8). Depending on the stage of the tumor, various mutations are considered relevant for therapy and should be investigated before starting treatment. Examples include ALK *(anaplastic lymphoma kinase)* translocation, EGFR *(Epidermal Growth Factor Receptor)* exon 18-21 mutations, BRAF V600E mutations, ROS1 rearrangements, NTRK *(neurotrophic tyrosinereceptor kinase)* 1-3 rearrangements, MET-*(Mesenchymal-epithelial transition)* exon 14 skipping mutations/amplifications, RET rearrangements, KRAS G12C mutations, to name the most relevant ones according to the current ESMO (European Society for Medical Oncology) guidelines (11).

1.1.6. Metastasis:

The regional lymph nodes are affected relatively early by lung carcinoma and spread along the physiological pathways. It should be mentioned here that so-called skip lesions can occur and individual lymph node stations can be skipped (9). Classical localizations of distant metastases of lung carcinomas are the lung itself, the liver,

the brain, the adrenal gland and the skeleton (5–7,9). A CUP (cancer of unknown primary) syndrome, in which the primary tumor cannot be diagnosed with certainty when a distant metastasis is diagnosed, is based on a lung carcinoma in 27% of cases (5). An important differential diagnosis to primary lung carcinoma are secondary tumors of the lung = metastases to the lung (9).

1.1.7. Therapy:

The treatment options have increased significantly with the possibility of individually targeted immunotherapy, which is why the complexity of treatment regimens has increased significantly. If operability is given, a lung carcinoma should be resected in toto. Conventional radiotherapy and chemotherapy still have their place in treatment regimens. However, these often move into second or third line or are being combined with new immunotherapy options at an early stage. The exact pathways are far beyond the content of this thesis and can be found in the current guidelines at any time (5–7,10).

1.1.8. Prognosis:

The most important prognosis-relevant factors are i) the histological tumor subtype, ii) the tumor stage, iii) patient-specific characteristics such as age, gender, comorbidities and general condition. While the 5-year survival rate for stage IA NSCLC (T1, N0, M0) is around 70%, it is only 20-25% for stage IIIA. The rates for women are always slightly more favorable than those for men. The prognosis for SCLC is still very poor. After a typically good response to chemotherapy, relapse occurs quickly and the chance for cure is only around 5%. Even the 5-year survival rate for SCLC is <10%, regardless of gender (2–5).

1.2. Human microbiome:

Over the past 20 years, we have gained an immense amount of knowledge about the human microbiome and its interactions and reactions, therefore our understanding of these complex relationships is becoming increasingly detailed. Figure 1. shows this immense increase in knowledge graphically. While in 1956 only one single publication on the search term "microbiome" was published, in 2010, for the first time, there were more than 1,000 publications with 1,178. In 2023, 27,963 publications were published on this topic and has therefore risen rapidly by a multiple in around a decade. These data are limited to the search term for "microbiome" in the National Library of Medicine ("PubMed").

Figure 1. PubMed search: "Microbiome" -> Results by year

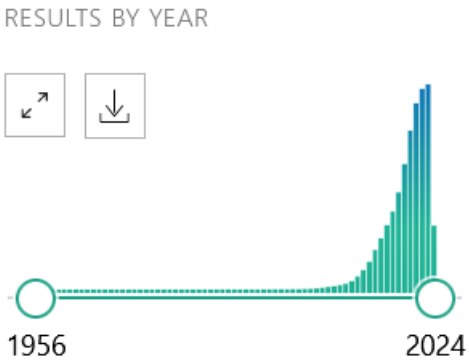

Results by year: 1956 – 1, 2010 – 1,178, 2023 – 27,963
Link: https://pubmed.ncbi.nlm.nih.gov/?term=microbiome

In the natural sciences, and therefore also in medicine, definitions of terms are always very relevant to ensure that everyone is talking about the same thing. Defining a field as dynamic as the human microbiome is not easy. As Figure 1. shows, new findings in this field are added almost daily. A table of definitions (Table 1.) from the work of T. Requena and M. Velascob has been taken over here to provide an overview of some terms, that are frequently used in the research field of the human microbiome and are perhaps not always differentiated with the necessary clarity.

Table 1. General concepts and definitions

Concept	Definition
Microbiota	Collection of microorganisms that populate a habitat, with populations of stable species (autochthonous) and other variables (allochthonous)
Microbiome	Includes the microorganisms, its genomes and the environmental conditions present in a habitat
Metagenome	Collection of genomes of the members of a microbiota
Metabolome	Metabolite flows and contents
Metatranscriptome	Expression and regulation of microbiota's genes
Metaproteome	Collection of proteins that reflect the microbiota's activity
Hologenome	Host's genome and metagenome, which together constitute an ecosystem. Reflects the microorganisms' importance for the host' biology
Dysbiosis	Imbalance in microbiota populations and/or functions. Also related to changes in diversity

This table was taken with kind permission directly from the work of T. Requena and M. Velascob (12).

To further clarify the central concept of the microbiome, Figure 2. was taken from Berg et al.´s work. This work provides a good overview of the huge field of the microbiome, which includes far more than just human health (e.g. agriculture, horticulture, aquaculture, food processing…) and discusses the difficult task of a standardized definition in detail (13).

Figure 2. Definition Microbiome

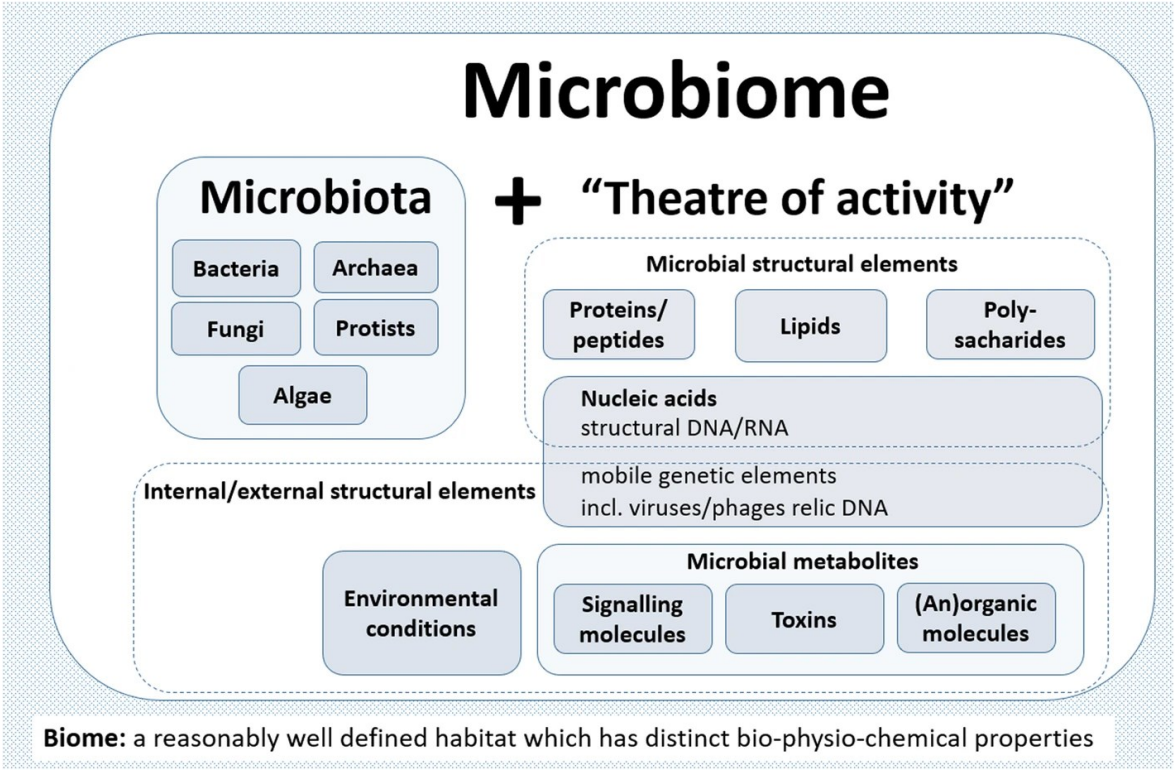

"A schematic highlighting the composition of the term microbiome containing both the microbiota (community of microorganisms) and their "theatre of activity" (structural elements, metabolites/signal molecules, and the surrounding environmental conditions)" - cited and transferred from the work of Berg et al. (13). Link: https://microbiomejournal.biomedcentral.com/articles/10.1186/s40168-020-00875-0#rightslink

1.2.1. The human bacteria:

In this study, we focused exclusively on the bacterial component of the human microbiome.

The number and distribution of bacteria found in the human body has been described by Sender R., Fuchs S. and Milo R. and states that there are approx. $3x10^3$ different species in a total number of around $3.8x10^{13}$ bacteria. Of these, ~97% are found in the colon and ~3% are found outside the colon (14). „Knowledge

of physiological conditions is always a prerequisite for the interpretation of findings of pathological conditions“, as my supervisors always like to say.

Research has already made great progress in the field of descriptive microbiome research, in which the present microorganisms are identified, quantified and described in terms of their physiological relative abundance (see following chapters). In the area of functionality and in a detailed understanding of the relationship between host, microbiome (changes) and health/disease, we are still at the beginning. To give a rough overview of functionalities, Figure 3., taken directly from Kostic's commentary, shows a visual summary of atypical phenotypes of a germ-free mouse model, that have regressed after recolonization with a physiological mouse microbiome. By improving pathologies, this image allows conclusions about the physiological function of the microbiome (15).

Figure 3. Selection of functions of the microbiome

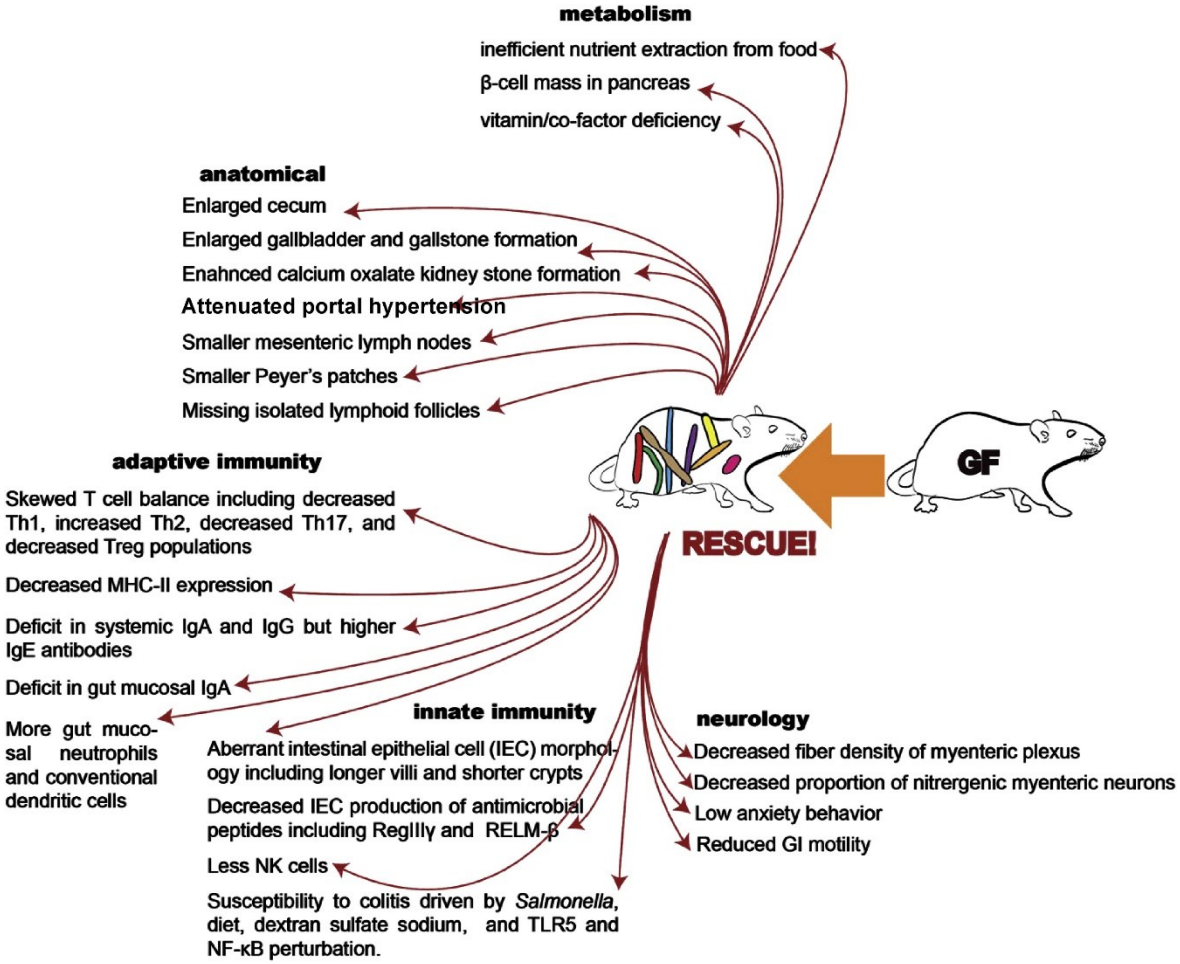

“Select germ-free phenotypes that can be at least partially rescued upon colonization with a mouse microbiome” cited and transferred with kind permission directly from the commentary of A. Kostic (15).

Describing the composition of the bacterial microbiome of the entire human body would exceed the volume of this thesis, so we decided to describe here the two organ systems from which we collected our samples (see M&M - chapter 2.1.1.). Therefore, the composition of the physiological bacterial microbiome of the colon and the lung is described below.

1.2.1.1. Bacterial microbiome of the colon - physiological composition:

The gut microbiome is the best-researched area of microbiome research. It contains the largest number and diversity of microorganisms in the human body. In numbers, about 3000 different species from 11 phyla are reported. The majority (approx. 90%) consists of *Firmicutes* and *Bacteroidetes.* Other phyla are the *Actinobacteria* (especially *Bifidobacterium spp.*), *Proteobacteria*, *Fusobacteria* and *Verrucomicrobia*. Among the *Firmicutes*, Gram-positive *Clostridiodes spp.*, *Lactobacillus spp.*, *Bacillus spp.*, *Clostridium spp.*, *Enterococcus spp.* and *Ruminicoccus spp*. are mainly found, whereby approx. 95% of these are formed by *Clostridium spp.*. Among the *Bacteroidetes*, Gram-negative *Bacteroides spp.* and *Prevotella spp.* are mainly found (12,16). Just to touch briefly on the complexity of the topic, one important aspect is that these bacteria should by no means be considered individually but must rather be understood as a communicating collective. Both, intraspecies communication via autoinducers and interspecies communication via so-called quorum sensing must be considered (16). In a healthy gut microbiome, the main representatives of the *Firmicutes* and the *Bacteroidetes* are represented in approx. equal proportions. If there is an imbalance in this distribution, associations have been made for example with increased inflammation (16,17). As already outlined in Figure 3., the functions of the intestinal microbiome are also very diverse and not yet understood in detail. However, many associations have already been established between changes in the intestinal microbiome and diseases such as chronic inflammatory bowel disease, coeliac disease or small intestinal overgrowth syndrome (16,18,19). In some cases, it has been possible to assign a certain role to a species, so that in the case of *Akkermansia muciniphilia*, a healthy metabolic state and an anti-inflammatory effect can be assumed (20,21). The same applies to *Faecalibacterium prausnitzii* (22). In contrast, the biofilm

forming *Bacteroides fragilis* has been associated with inflamed mucosal areas in IBD patients (23).

1.2.1.2. Bacterial microbiome of the lung - physiological composition:

The phyla of *Bacteroidetes*, *Proteobacteria* and *Firmicutes* dominate the composition of the lung microbiome. They are followed by *Actinobacteria*. *Prevotella*, *Veillonella*, *Fusobacteria*, *Cyanobacteria* and *Streptococcus* are also detectable. *Tropheryma whipplei* can sometimes be detected in very small quantities (12,16,24–26).

The direct connection to the outside environment, the nasopharynx and the oral cavity makes it possible to understand the transfer of bacteria to the lungs through microaspirations from these areas (26). In physiological conditions, the bacterial load decreases from central to peripheral parts of the lung and a sensitive balance is created between the transfer of new bacteria and the elimination of those germs, primarily by the mucociliary clearance (MCC) (12,16,27). The relevance of this clearance becomes clear in the example of cystic fibrosis (CF) (28). In this clinical picture the MCC is severely impaired, what has a direct impact on the composition of the lung microbiome. Other chronic lung diseases such as bronchial asthma or chronic obstructive lung disease (COPD) also change the microbiome of the lungs (16,29,30). Regarding CF, Frayman et al. were able to determine a significant reduction in microbiome diversity in children with CF using 16S rRNA sequencing of BAL samples (21 CF children and 10 non-CF children) (28). However, the mass of bacteria in the lungs is relatively low and is estimated in older studies to be in the range of 4.5 - 8.5 log copies/ml (31,32). In their work, Sze et al. calculated the number of bacteria in lung tissue at 10-100 bacteria per 1,000 human cells (33).

To illustrate the concept of communicating biomass briefly mentioned in 1.2.1.1. using the shown examples of the microbiomes from the colon and lung, the work of Wang Q., Li F., Liang B. et al. should be briefly mentioned. They used a metagenome analysis of 36 adult asthma patients and identified a change in the gut microbiome. The changes consisted of a reduction of butyrate-producing bacteria such as *Cryptococcus eutactus* and *F. prausnitzii* and an increased detection of *Clostridium bolteae, Clostridium ramosum, Clostridium spiroforme* and *Eggerthella lenta* (34). Some of the latter bacteria are also increasingly found in IBD patients (16,18,19).

1.3. Tumor microbiome:

Recently, a sub-area of microbiome research has emerged as a very interesting and promising topic. The tumor microbiome describes those microorganisms that are found locally in tumor tissue. In recent years, there has been increasing evidence that these resident microorganisms in tumors may play an important role in carcinogenesis and tumor progression, (35). In this work, we have focused exclusively on the bacterial component of the tumor microbiome.

1.3.1. History of tumor-associated microbiota:

The idea of a connection between microbial organisms and carcinogenesis is by no means a new one. The often-quoted Ebers Papyrus of 1550 BC (36) already spoke of a tumor (here: swelling) therapy that included, among other things, the generation of an infection through an incision. In the 19th century, both Wilhelm Busch and Fridrich Fehleisen described a tumor regression that they were able to attribute to an infection with *Streptocoocus pyogenes* (37–39), before William Coley, a pioneer of vaccination therapy, used a bacterial cocktail of *Streptococcus spp.* and *Serratia spp.* to treat terminal cancer patients. He achieved a disease-free interval of >10 years in 60/210 patients (40). Livingstone-Wheeler V. then put forward the theory that the origin of cancer development lies in the bacterium *Progenitor cryptocides*. However, this theory was not confirmed and the described "germ of origin for carcinogenesis" turned out to be a germ of the physiological skin flora (*Staphylococcus epidermidis*) (41).

In addition to bacteria, viruses are of course also involved in carcinogenesis. As White M. K., Pagano J. S. and Khalili K. describe in their review, about 20% of all human cancer diagnoses are directly linked to an infectious cause. However, the number of proven causal links between viruses and the development of cancer is still limited. Epstein-Barr virus (EBV), hepatitis B virus (HBV), human papillomavirus (HPV), human T-cell lymphotropic virus (HTLV), hepatitis C virus (HCV), Kaposi's sarcoma herpesvirus (HHV-8) and Merkel cell polyomavirus (MCPyV) are clearly oncogenic (42). Zapatka M., Borozan I., Brewer D. S. et al. were able to detect viruses in 382 tumor genomes and 68 tumor transcriptomes in sequence analyses of 2658 tumors across 38 tumor types. The largest number of tumor types were samples from liver, esophagus, stomach, pancreas, colon/rectum, head/neck and

cervix. A high prevalence of well-known onco-viruses EBV, HBV, HPV was detected (43).

1.3.2. Influence of human microbiome and tumor microbiome on carcinogenesis, tumor progression and therapeutic options:

Since the association of microorganisms and carcinogenesis described above has a long history, in-depth research into the connections is still relatively recent. However, it is already evident that most organs have an individual microbiome and are not sterile, as was believed for a long time (15,24,44–46). The tumors of solid organs are colonized by extra- and intracellular microbial organisms (24,45–47). The significance of the microbes for carcinogenesis in detail is still unclear. However, some studies have already shown a clear interaction in various areas:

A recent study by Galeano Niño J. L. et al. made an important contribution to a better understanding of the relationship between carcinogenesis/tumor progression and the intratumoral microbiome. Here it is shown that the intratumoral microbiome is highly organized in niches and that these colonized niches show clear differences to the surrounding tumor tissue (tumor heterogeneity). Thus, colonized tumor areas show reduced vascularization and a lower presence of Ki-67 positive malignant cells than other tumor areas. A direct influence on the genetic alteration of tumor cells as well as on metastasis by intratumoral bacteria could also be shown (48). Fu et al. also investigated the connection between intratumoral bacteria and tumor metastasis. (47). They were able to prove with the help of a green fluorescent protein (GFP)-labeled *Staphylococcus xylosus* in a breast cancer mouse model, which was injected directly into the primary tumor, that intratumoral pathogens can participate in and influence the path of metastasis. The recombinant *S. xylosus* was detected in 80% of lung metastases. Furthermore, it was shown that antibiotic therapy of the primary tumor was able to reduce the occurrence of lung metastases by a factor of 3 (47).

Therapeutic influence of the microbiome has been shown in the areas of *i)* chemotherapy (49), *ii)* hormone therapy (50), *iii)* radiotherapy (51,52) and *iv)* immunotherapy (53–60): *i)* Geller et al. hypothesized that intratumoral bacteria in pancreatic ductal adenocarcinoma are capable of leading to resistance to the chemotherapeutic agent gemcitabine (49). *ii)* Pernigoni et al. were able to demonstrate the influence of the intestinal microbiome on the development of

endocrine resistance to castration-resistant prostate cancer via bacterial-induced production of androgens (50). *iii)* Shiao et al. investigated the effects of the gastrointestinal bacterial and fungal microbiome on the effectiveness of radiotherapy in more detail and were able to demonstrate that there are also modulations of therapy effectiveness in this context. While depletion of commensal bacteria led to a reduced effectiveness of radiotherapy in melanoma and breast cancer mouse models, the opposite effect was observed when commensal fungi were depleted (51). *iv)* There is evidence that the gut microbiome plays a decisive role in influencing immunotherapy. For example, Tanoue et al. identified 11 bacterial strains that are associated with a healthy gut microbiome composition and can interact to induce Interferon-γ+ CD8 T cells, mediate resistance to the intracellular pathogen *Listeria* and increase the efficacy of immune checkpoint inhibitors on tumor growth (58).

There are also innovative approaches in the field of diagnostics (61–65) and prognostics (48,66–70). For example, Poore et al. have provided some initial evidence for a blood test based on microbial patterns, in which these bacterial patterns allow the diagnosis of different types of cancer (62). Kwong et al. were able to establish a connection between bacteremia of various bacteria (*Streptococcus gallolyticus, Bacteroides fragilis, Fusobacterium nucleatum, Peptostreptococcus species* and some other bacteria) and colorectal carcinoma and postulate a further diagnostic tool here (61). Prognostically, for example, a specific intratumoral microbiome signature was identified in the work of Riequelme et al. that is associated with longer survival in pancreatic adenocarcinoma. This signature consisted of *Pseudoxanthomonas, Streptomyces, Saccharopolyspora* and *Bacillus clausii* (68).

New approaches to antitumor therapy have also been developed based on findings on the tumor microbiome (71–77). For example, several recent studies have highlighted the topic of "programmable bacteria" and the associated potential cancer therapy (72,74–77). To take just one example, Chowdhury et al. used a non-pathogenic E. coli strain. This lyses specifically in the tumor microenvironment and releases an anti-CD47 nanobody - an anti-phagocytic receptor that is typically overexpressed in many types of cancer. Among other things, an increased migration rate of tumor-infiltrating T cells, tumor regression, a reduced incidence of

metastases and an increased survival rate were demonstrated in mouse models (75).

Two FDA-certified antitumor therapies on a microbial basis are already on the market. Current microbial therapies against tumors include BCG therapy (Bacillus Calmette-Guerin) for superficial, non-muscle invasive bladder cancer (NMIBC) (78) and oncolytic viral therapy with Talimogene laherparepvec (TVEC) in advanced melanoma (71).

The mass of evidence relating to this topic has finally led to the adaption that the standard work „The hallmarks of cancer" of Hanahan and Weinberg (79) now also contains the sub-item „Polymorphic Microbiomes" in a revised version „Hallmarks of Cancer: New Dimensions" (80).

1.3.3. Tumor-associated microbiota in lungs:

As far as the topic of tumor-associated microbes in lung tumors is concerned, we are still at the beginning of research compared to the evidence for the intestinal microbiome. Nevertheless, there is clear evidence of a microbial influence of resident lung bacteria on lung pathologies (29,30,81–83), including lung tumors (69,84–87). In an important step, it was found that chronic inflammation, which is associated with most common lung diseases, is also associated with the development of lung cancer (88). Furthermore, it was shown that exacerbations of chronic inflammatory lung diseases such as COPD, bronchial asthma and CF are associated with a change in the local microbial composition (26,89). The next major milestone in tumor microbiome research in lung tumors was achieved by Jin et al., who were able to show that the local microbial lung flora has a direct influence on the interaction between inflammation and adenocarcinomas of the lung via the activation of lung-resident γδ T cells. Bacteria-free mice or mice pre-treated with antibiotics were significantly better protected against the development of a KRAS-mutated lung tumor with TP-53 loss of function (84).

The study by Nejman et al. (46), examined samples from the ovary, pancreas, breast, bone and glioblastoma multiforme as well as samples from the lung. Here, the measured bacterial load in lung tumors was approx. 1-10 bacteria per 40ng DNA of the lung tumor. Based on these data, Sepich-Poore et al. calculated an average extrapolation that describes an expected number of bacteria in tumor tissue of approx. 1 bacterium per 147 tumor cells (approx. 0.68%) (90). Compared with data

on bacterial abundance in the colon, this number is extremely low. Therefore, the exact localization of the microbes is a particular challenge in the lung context, if the low density of the expected bacteria in lung tumor tissue is considered and has not yet been clarified in detail.

1.4. Fluorescence in situ hybridization:

One way of determining the localization of microbes within tissue is via fluorescence in situ hybridization (FISH). FISH is a traditional method for the detection of specific gene sequences using specially configured probes that bind complementarily to this gene sequence. Under optimal environmental conditions and with an optimized protocol, this binding is very specific (91–93).

1.4.1. History of FISH development:

The development of in situ hybridization (ISH) began with the work of Gall et al. (94) in 1969, in which radioactive probes were used. In 1977, Rudkin and Stollar (95) were able to carry out FISH for the first time. This was an indirect method that required, among other things, antibodies for visualization. Direct FISH without the need for antibodies was finally introduced in 1980 by Baumann et al. (96). With the publication of the first RNA-FISH by Singer and Ward (97) in 1982, actin messenger RNA (mRNA) from chicken skeletal muscle could be visualized. Since then, there have been countless adaptations and further developments of FISH. A few in our opinion relevant adaptations are shown in the results section and many more possible adaptations that we believe could lead to an even better FISH of bacteria in the tissue context are discussed in the discussion section.

Nowadays, there are numerous highly technologized niche applications of FISH in combination with other methods. For example, small modulatory RNA (smFISH) is used simultaneously with immunofluorescence and flow cytometry, as shown by Arrigucci et al. (98). Today, it is also possible to use padlock probes to visualize mutations, as El-Heliebi et al. demonstrated in colorectal cancer (99).

1.4.2. FISH principal:

The principle of FISH is based on the detection of nucleic acids as a molecular cytogenetic method. Direct-fluorescent probes or indirect-fluorescent probes are used, whereby the latter must be made detectable by an additional enzymatic or immunological step (Figure 4.). The probes are selected/configured complementary to the nucleic acid sequence to be detected, to achieve specific binding and thus be

able to detect the local assignment of the signal in a spatial context. Since the probes can be configured to pretty much any base sequence imaginable, there are many different target sequences in several different materials that could potentially be considered for FISH analysis. From classical detection of chromosome aberrations to subcellular detection of mRNA expression patterns of various genes at the single cell level, a wide range of applications in clinical diagnostics and research is available today. The material for FISH can be cells, tissue sections or even whole-mounts. The basic procedure of FISH is always similar and can also be found in this work in the M&M section. The material must be prepared for the so-called hybridization = annealing of the probes to the target sequence. This takes place during tissue preparation = pre-hybridization. After hybridization, various washing steps = post-hybridization follow (91–93). In addition to our methodology, the M&M section also describes the individual steps and their importance for the method. The Discussion section then presents some suggestions that could improve this method in the FISH context. In general, the selection of the probe is an essential first challenge. The next step is to optimize the basic conditions to make the binding of probe and target sequence as specific as possible and to eliminate interfering signals as far as possible. Here, the non-specific and specific penetration of the targets, buffer compositions and buffer concentrations, pH settings, hybridization times and washing steps are certainly key points of the methodology (92).

A well-known example of the clinical-diagnostic application of the FISH method is the detection of chromosome aberrations, particularly in the context of the discovery of the Philadelphia chromosome t(9;22)(q34;q11), which leads to the ABL1/BCR fusion gene (91). Rowley J. D. was the first to describe this in 1973 as a translocation that causes a specific malignancy, chronic myeloid leukemia (CML) (100). This causality of translocations/gene fusions and malignancy was summarized in the review by Mitelman F., Johansson B. and Mertens F. (101). In their review, Cui et al. have summarized a good overview of typical changes in the context of hematopoietic and lymphoid neoplasms and the associated probes (91).

Figure 4. The principle of fluorescence in situ hybridization

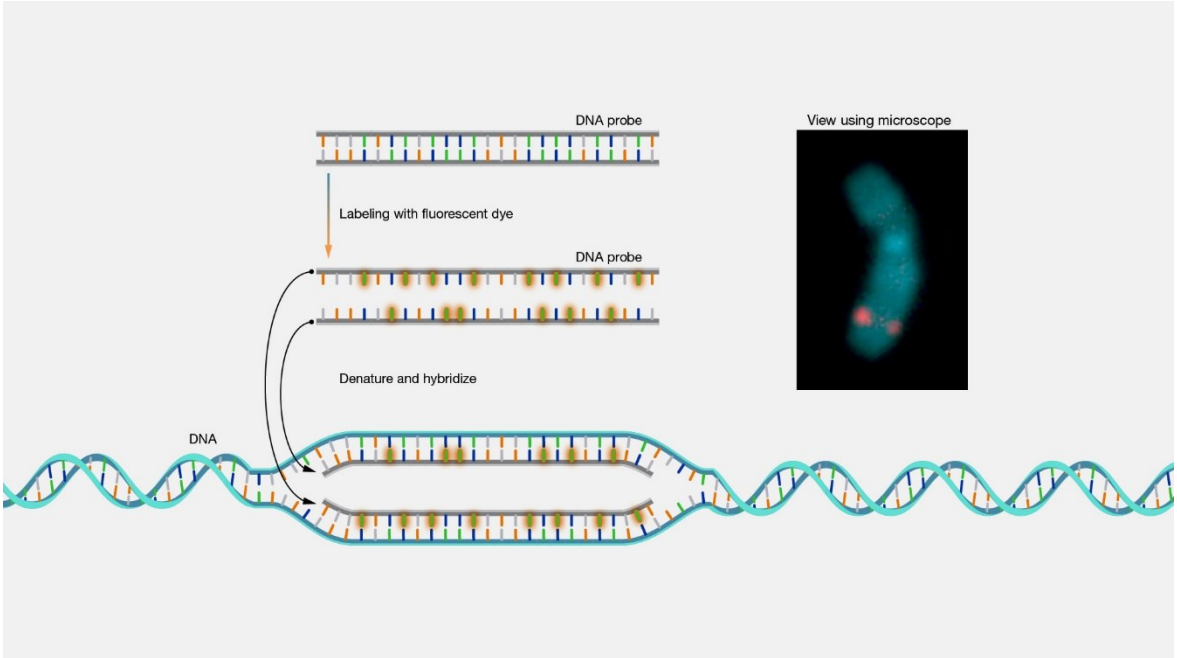

General schematic illustration of DNA-FISH principle, directly taken from the website of the National Human Genome Research Institute, Link: https://www.genome.gov/genetics-glossary/Fluorescence-In-Situ-Hybridization

1.4.2.1. 16S rRNA FISH:

The 16S region of ribosomal RNA (rRNA) is a region of the 30S subunit of prokaryotic ribosomes. It represents a highly conserved gene in bacteria and is thus detectable in most bacteria. However, hypervariable regions (V1 - V9) also allow species identification based on the 16S region. Using differently configured probes, panbacterial regions can be specifically marked or even species determinations can be realized (102,103). For example, Shah et al. describe the possibility of malaria species diagnostics via FISH (104). In this work, we used an EUB-338 probe to label and detect the entirety of the bacteria. Our "target" is therefore the EUB-338 18-digit base sequence (5'- GCT GCC TCC CGT AGG AGT -3') of the bacterial 16S rRNA. The probe was therefore configured complementary to this base sequence. This probe is connected to the Cy-3 (Tetramethylrhodamine (TRITC) = fluorescent dye) fluorophore (105,106). This is a direct FISH analysis (92,93).

1.5. Study aim:

The main goal of this study was the development of a structured 16S rRNA FISH protocol for formalin-fixed paraffin-embedded (FFPE) treated and trimmed tumor tissue slides to visualize and localize tumor-associated microbiota.

2. Material and Methods:

2.1. Material:

For the first steps of establishment, we used pure bacterial cell blocks. We then carried out the first analyses in the tissue context with highly inflammatory tissue from the intestine and lungs before testing our FISH method in the tumor context with tumor samples from the colon and lungs.

2.1.1. Pure bacteria cell block:

A high dose of bacteria (*Eschericha coli*, *Staphylococcus aureus* and *Mycobacterium spp.)* was dissolved sterilely from blood agar plates, brought into solution, mixed with fibrin as a natural binding agent and concentrated by mild centrifugation. The bacterial mixture was then poured out and embedded, to form a cuttable cell block, which we were able to use for our first experiments and generally as a positive control.

2.1.2. Tissue:

Furthermore, we used human routine tissue from the Institute of Pathology at the Medical University of Graz. According to the certification of this institute, the following material was treated as required by the QM-established standard-operating-procedure (SOP). After the macroscopic assessment, the tissue was incubated in 4% formalin and poured in a FFPE block. We did our test series with tissue from cases with appendicitis [exact diagnosis: „acute ulcerophlegmonous appendicitis + mesenteriolum phlegmon + fibrinous purulent periappendicitis"], lungabscess [exact diagnosis: „abscess forming infarct pneumonia"], adenocarcinoma of the colon [exact diagnosis: „6 cm large, ulcerated, low-grade (formerly G2) adenocarcinoma with spread into the fatty tissue. Peritumoral abscess, covered perforation and accompanying acute peritonitis. High grade tumor cell dissociation at the invasion front (high grade tumor budding)", TNM: (UICC 8., 2017): pT3 N0 (0/42) R0 L0 V0 Pn1 G2] and adenocarcinoma of the lung [exact

diagnosis: „Several foci of adenocarcinoma of the lung with a partially dense inflammatory reaction“, TNM: (UICC 8., 2017): rpT3 pN0 (0/17) R0 (local)].

2.2. Methods:

As methods of visualization of tissue sections, we have used the conventional H&E and Gram stains for overview and assessment of the individual tissue components. We have tried to interpret these in connection with our FISH test series.

2.2.1. H&E staining and Gram staining:

Gram stain and hematoxilin & eosin (H&E) stain was performed according to the QM-established SOP in the Institute of Pathology - Medical University of Graz.

2.2.2. Detailed FISH protocol:

In the following, we would like to present a detailed step-by-step guide to the protocol we ultimately used. For reasons of comprehensibility, we have also included the functions of individual steps and of individual reagents.

2.2.2.1. Tissue preparation/unspecific permeabilization:

In this series of tests, we treated pure bacteria cell blocks (2.1.1.) as a positive control. Furthermore, we tested specimens from acute appendicitis, acute lung abscess, colorectal cancer and lung cancer (exact diagnosis see above). We prepared 5µm sections of FFPE blocks to perform FISH analysis. Formalin fixation effects covalent links in DNA, lipids and peptides or other macromolecules and thus causes a correct/in vivo localization of tissue components on the slide as well as less enzymatic digestion. Formalin treatment is the first step of unspecific permeabilization of tissue and bacteria (92). 4% formalin was used in these samples.

2.2.2.2. Heating:

The slides were incubated at 60°C for 1h to melt the paraffin on the tissue and facilitate the next step.

2.2.2.3. Xylol/descending alcohol series:

Next was treatment with xylol (two times 10min), before the slides were incubated 5min in 100% alcohol - 1,5min at room air to dry - 3min each in 90%-/70%-/50%-alcohol. The solutions were in approx. 80 ml cuvettes. After descending alcohol series, the slides can stay in distilled water for a while. In this xylol and descending alcohol series, milieu in the tissue changes from hydrophobic paraffin milieu (milieu

to store the slides) into the hydrophilic milieu, which is the correct one to perform FISH analysis (all ingredients based on aqueous solutions) (107).

2.2.2.4. Specific, enzymatic permeabilization:

These steps were done in a Dako Cytomation Hybridizier (108), which was transformed into a humid chamber by placing some wet wipes in the corners. The whole Dako Cytomation Hybridizier was placed, if necessary, on a shaker for cuvettes to create continuous agitation. The tissue was circled by a hydrophobic barrier pen to minimize the necessary amount of enzyme and to concentrate the enzymes at the target region. For each step of the enzymatic permeabilization, 200µl of enzyme was gently pipetted on the tissue and incubated 30min at 37°C. We treated the tissue with a combination of 1. lysozyme, 2. lysostaphin from *Staphylococcus staphylolyticus* and 3. proteinase K. Between every enzymatic step, the slides were washed in d. distilled water cuvettes.

1. The correct lysozyme (Sigma, 62970-1G-F) concentration of 20mg/ml was achieved by a 10mM TRIS-HCl (10812846001, Merck) buffer, pH8. 0,079g TRIS-HCl were solved in 50ml d. distilled water and 1000mg lysozyme stock solution was mixed with 50ml TRIS-HCl buffer.
2. The correct lysostaphin (L7386, Sigma) concentration of 0,2mg/ml was achieved by 0,05M TRIS-HCl/0,145M NaCl (S7653, Sigma) buffer, pH7,4. 0,788g TRIS-HCl /100ml d. distilled water and 0,847g NaCl/100ml d. distilled water were weighed and lysostaphin 1MG stock solution was combined with 5000µl buffer.
3. The correct proteinase K (2609517, Thermo Fisher, 1,25ml, 20mg/ml) concentration of 0,2mg/ml was achieved by dilution with 10mM TRIS-HCl buffer, pH7,5. 0,16g TRIS-HCl/100ml d. distilled water were generated and 990µl of this buffer were combined with 10µl of proteinase K stock solution.

Firstly, we gently pipetted 200µl of 20 mg/ml lysozyme (Sigma, 62970-1G-F) on the slide, to permeabilize mainly Gram-negative bacteria (Figure 22.) by hydrolyzing the β(1–4) glucoside linkages of glycosaminoglycans - mucopolysaccharides in the cell walls of these bacteria (109). Secondly, we gently pipetted 200µl of 0,2mg/ml lysostaphin from *Staphylococcus staphylolyticus* (L7386, Sigma, 1MG) on the slide. This lysostaphin can cleave staphylococcal peptidoglycan-specific pentaglycine cross bridges (110,111). Thirdly, we gently pipetted 200µl of 0,2mg/ml of proteinase

K (2609517, Thermo Fisher 1,25ml, 20mg/ml) on the slide. Proteinase K is able to hydrolyze peptidoglycans in bacterial cell walls (112).

2.2.2.5. Stop enzymatic reaction:

To stop enzymatic reaction, the slides were incubated 1min in a cuvette (~80ml) filled with pure methanol (Merck: Methanol for analysis, 1874509 713) (92).

2.2.2.6. Hybridization:

After 15min incubation in hybridization buffer (see below) in a cuvette (~80ml) at 46°C under continuous agitation, we mixed the hybridization buffer with the EUB338 probe (EUB, MBD0033, Sigma, Cy3-labled) or the nonsense probe (non-EUB, MBD0035, Sigma, Cy3-labled) in a concentration of 1ng/ml and incubated this mixture at 46°C again in the Dako Cytomation Hybridizier transformed into a humid chamber under continuous agitation for 2h. We created a 1:20 solution from stock solution of probes (5µl probe + 95µl d. distilled water). Then, after 15min of incubation in the cuvette (~80ml) full of hybridization buffer, we took 27µl hybridization buffer from this cuvette and pipetted it carefully on the slide. In this buffer bubble we gently pipetted 3µl of the 1:20 probe solution (1:20 + 1:10 = 1:200), to create a working concentration of 1ng/ml. We made sure to mix this buffer-probe solution without losing the fluid outside the hydrophobic barrier pen area. We tried to create a cover glass with a small piece of a parafilm-placeholder in each corner to create some space between the slide and the cover glass, but also to make sure that the distribution and the humid environment is optimal for the whole hybridization time.

The hybridization buffer (100ml) consists of 20% formamide (Sigma, F7503, 1L) - 20ml/100ml, 20 mmol/l TRIS-HCl – 0,32g/100ml, 2% Sodium dodecyl sulfate - SDS (L3771, Sigma) – 2g/100ml and 0,9% NaCl – 5,26g/100ml. The solvent is d. distilled water and the container was filled up to 100ml. The pH adjustment was done with HCl and NaOH to create pH7. The formamide content effects a lower temperature for annealing of probes at the target 16S rRNA sequence, while the SDS-content support as a detergence the unspecific permeabilization of bacteria (92).

2.2.2.7. Post-hybridization wash step I:

The slides were washed in 48°C pre-heated wash buffer (see below) for 15min at 46°C under continuous agitation in a cuvette (~80ml) under light protection, to remove unspecific bindings. [Make sure to wash positive panbacterial probe and

negative nonsense probe in two different cuvettes to avoid crosslinking on your separate slides!] Wash buffer (100ml) consisted of 10mM TRIS-HCl – 0,16g/100ml, 2% SDS – 2g/100ml and 0,0225M NaCl – 1,32g/100ml. The solvent was d. distilled water and the container was filled up to 100ml. PH adjustment was done with HCl and NaOH to create pH7.

2.2.2.8. Post-hybridization wash step II:

The slides were washed short but active with tap water, to remove unspecific bindings. After that, the slides dried light protected at room temperature.

2.2.2.9. DAPI counterstaining:

A counterstaining with 4',6-Diamidino-2-phenylindol (DAPI) was performed and the slides were stored at 4°C. DAPI is a molecule which stains core elements (113).

2.2.2.10. Microscopy:

The fluorescence microscope we used was a Nikon Eclipse Ci. Three pictures were taken from each region of interest: DAPI image (DAPI: EX387nm), background image (green: EX494nm) and probe-signal image (orange: EX543nm; Cy-3 absorption maximum is 555nm (114)). As Eichinger et al. and Spindler et al. (115,116) had described, we defined the green filter (green: EX494nm) as background.

2.2.2.11. Digital image processing:

With GIMP-Software (GNU Image Manipulation Program), we were able to overlay DAPI images with probe-signal images and thus study the spatial relationships of DAPI positive nuclei and probe-signal positive bacteria. After creating the difference between target signal (orange: EX543nm) and background (green: EX494nm), we performed an overlay of the created „difference“ image with DAPI image (DAPI: EX387nm).

3. Results:

Since the main goal of this study revolved around establishing a FISH protocol for staining tumor-associated microbiota in FFPE treated and 5µm trimmed slides of tumor tissue, we described the results as a timeline of adaptions starting with the original protocol of Madhusudhan et al. (117) followed by some inspirations of Fu et al. (47), Nejman et al. (46) and Young et al. (92).

3.1. Original FISH protocols:

We tested the exact protocol of Madhusudhan et al. (117) and of Fu et al. (47) with pure bacteria cell blocks and with described inflammatory tissue from an appendicitis case and a lung abscess case.

3.1.1. Pure bacteria cell block:

In the beginning we started with some staining series of our described, self-made pure bacteria cell blocks. We took three different types of bacteria (*Eschericha coli* + *Staphylococcus aureus* + *Mycobacterium spp.*), to try to represent the high diversity of the structure and the cell wall components in the kingdom of bacteria. Cell block material served as a positive control for our first FISH test runs. First, we checked the success of the cell block production described in 2.1.1. in H&E staining (Figure 5.) and in Gram staining (Figure 6.). The morphological characteristics of the different bacteria can be better identified in the Gram stain than in the H&E stain. *Staphylococcus aureus* is found in typical Gram-positive cluster cocci, while Gram-negative, rounded *Eschericha coli* rods are found individually and in groups. The acid-resistant *Mycobacteria spp.* are difficult to identify. Above all, the appearance in Gram stain is easily transferable to FISH morphology. We compared the results of exact reproduction of the protocols of Madhusudhan et al. (117) (Figure 7. + 8.) and of Fu et al. (47) (Figure 9. + 10.). We performed both protocols in the original procedure with the positive EUB338 probe and with the negative non-EUB/nonsense probe as a negative control. Figure 7. shows a strong positive signal for *E. colis* and for mycobacteria. The *Staph. aureus* signal intensity is rather weak. In the negative control (non-EUB probe), we received a correct negative signal in both runs (Figure 8. + 10.), which is easily recognizable compared with DAPI counterstain. In these non-EUB negative control figures (Figure 8. + 10.), we were also able to verify the correctness of our background definition. If the probe extinction (orange spectrum: 543nm) is compared with the background extinction (green spectrum: 494nm), these images in Figures 8. + 10. are very similar.

Figure 5. Cell block of Staph. aureus + E. coli + Mycobact., H&E staining

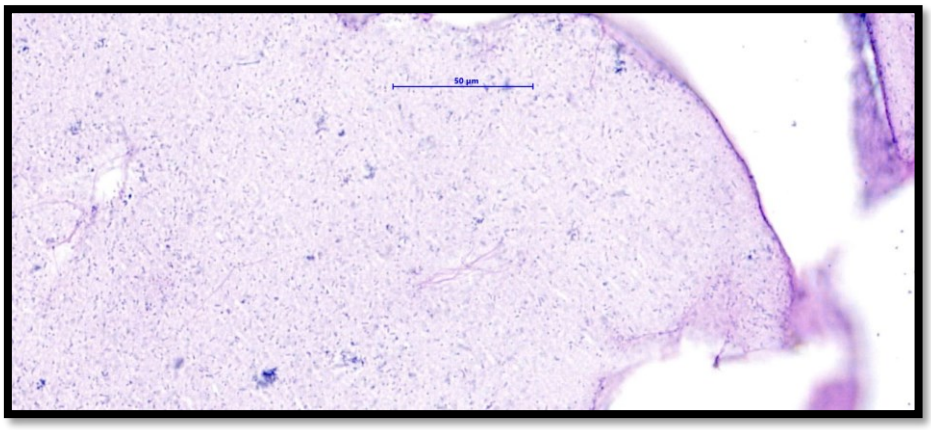

Pure bacteria (*Staph. aureus* - Gram positive, *E. coli* - Gram negative, acid-resistant *Mycobacteria spp*.) are in a fibrin environment on the section

Figure 6. Cell block of Staph. aureus + E. coli + Mycobact., Gram staining

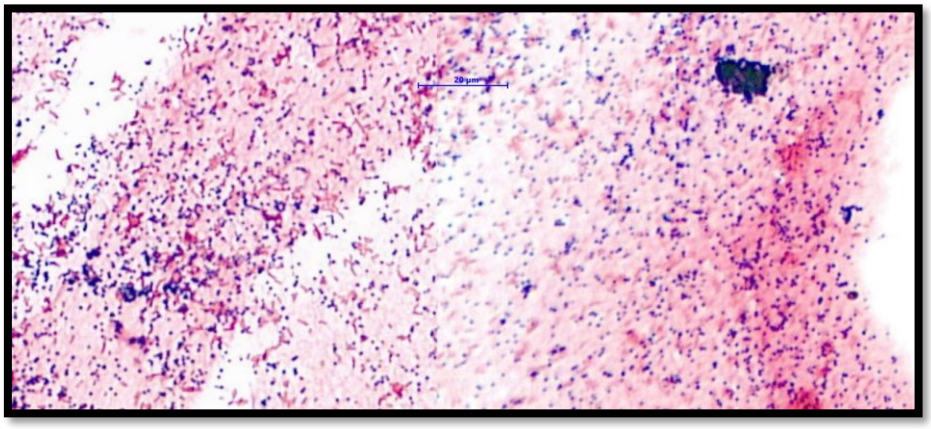

Pure bacteria (*Staph. aureus* - Gram positive, *E. coli* - Gram negative, acid-resistant *Mycobacteria spp*.) are in a fibrin environment on the section, whereby the *Mycobacterium spp*. are very difficult to identify in these stains.

In Figure 9., all 3 bacterial species tested can be detected well, although the background signal is significantly stronger here. Thus, in a comparison of the two original protocols, the advantage of bacterial detection lies on the side of the Fu et al. (47) protocol, while the advantage of the low background signal and rapid performance lies on the side of the Madhusudhan et al. (117) protocol.

Figure 7. Cell block of Staph. aureus + E. coli + Mycobact., FISH staining: EUB338, original protocol: Madhusudhan et al.

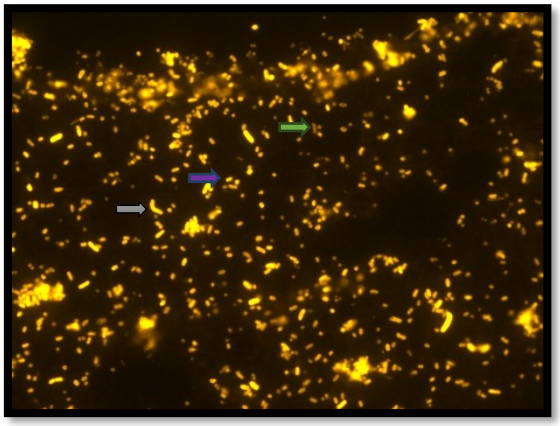

7.1. Probe - EX543nm

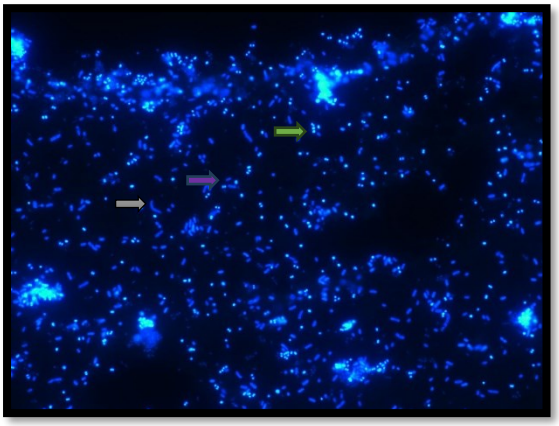

7.2. DAPI - EX387nm

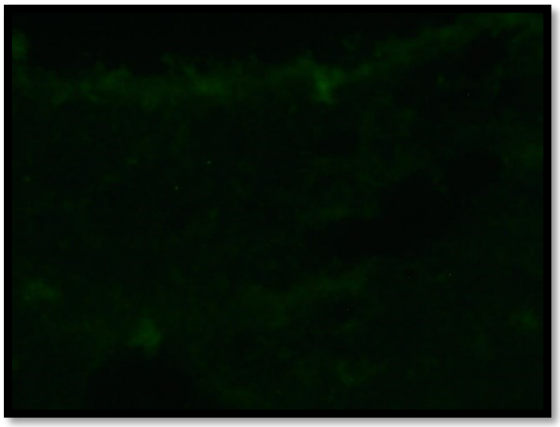

7.3. Background EX494nm

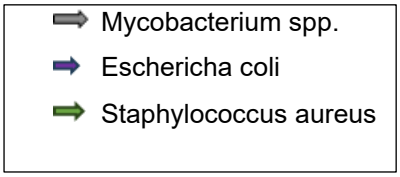

Strong positive signal of E. coli + Mycobact. spp., weakly positive signal of Staph. aureus. The background shows nearly no signal.

Figure 8. Cell block of Staph. aureus + E. coli + Mycobact., FISH staining: Non-EUB338, original protocol: Madhusudhan et al.

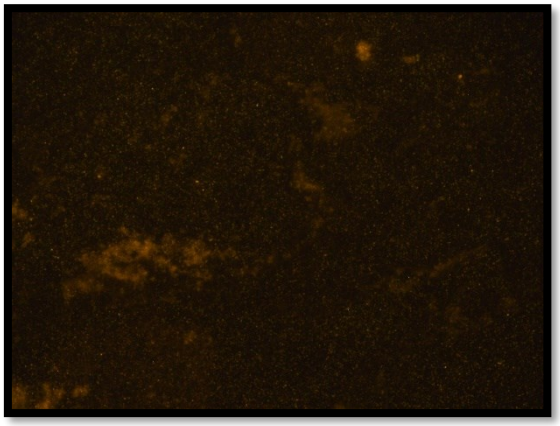

8.1. Probe - EX543nm

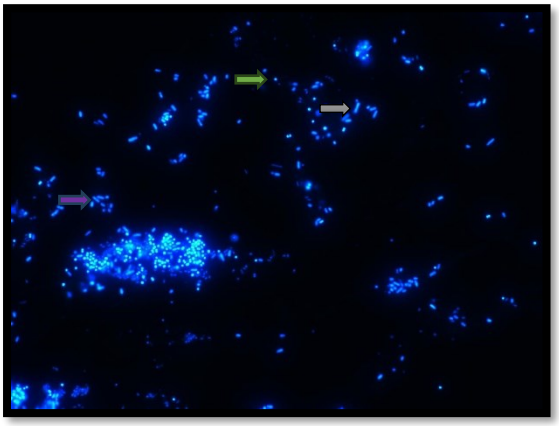

8.2. DAPI - EX387nm

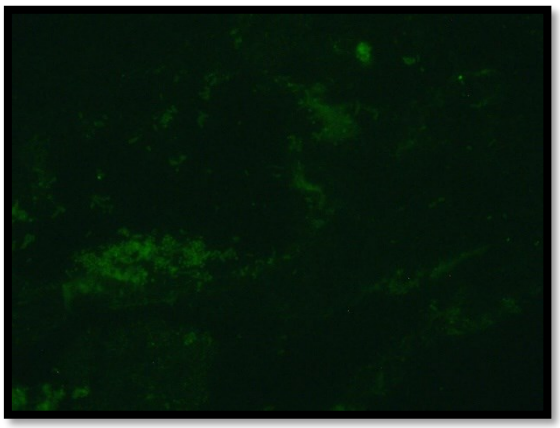

8.3. Background EX494nm

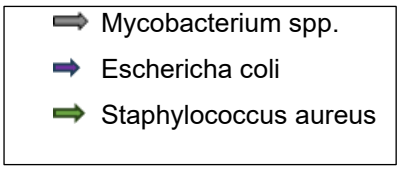

Correct negative results with non-EUB probe. Probe signal and background signal nearly similar.

Figure 9. Cell block of Staph. aureus + E. coli + Mycobact., FISH staining: EUB338, original protocol: Fu et al.

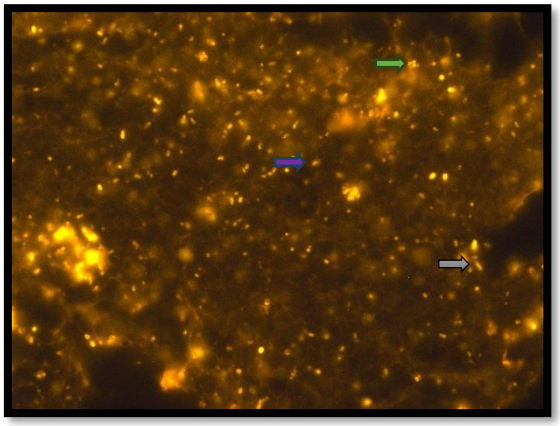

9.1. Probe - EX543nm

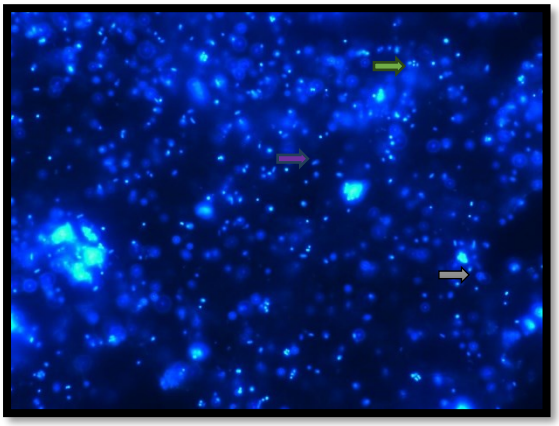

9.2. DAPI - EX387nm

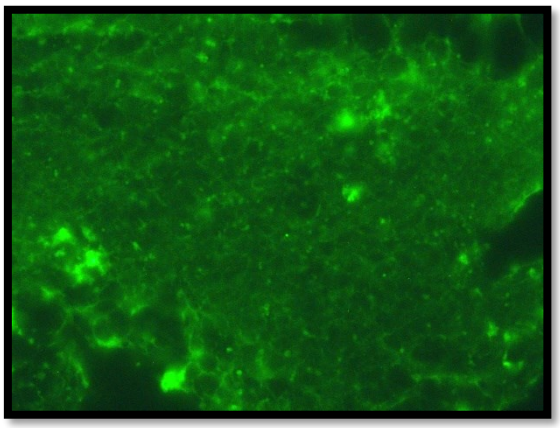

9.3. Background EX494nm

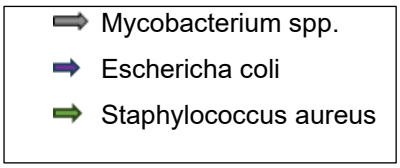

Correct positive signals from all 3 bacterial species. More background signal recognizable in the green range.

Figure 10. Cell block of Staph. aureus + E. coli + Mycobact., FISH staining: Non-EUB338, original protocol: Fu et al.

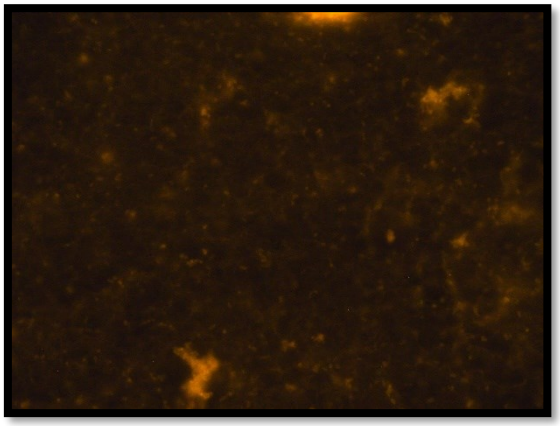

10.1. Probe - EX543nm

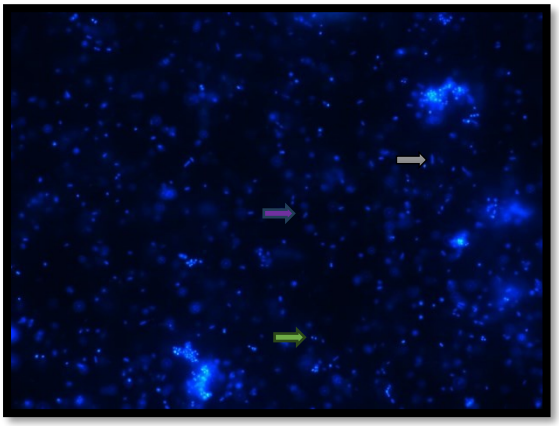

10.2. DAPI - EX387nm

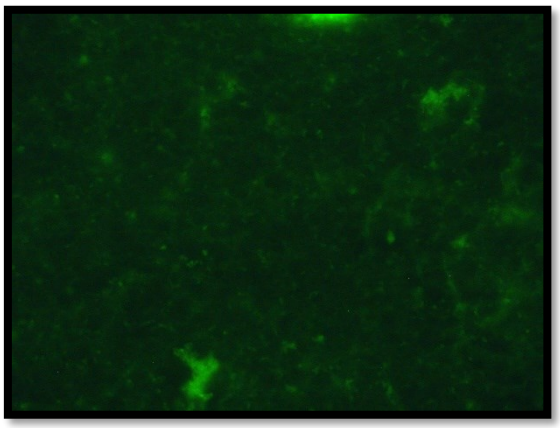

10.3. Background EX494nm

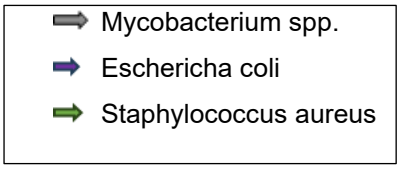

Correct negative results with non-EUB probe. Probe signal and background signal nearly similar.

3.1.2. Inflammatory tissue:

We suspected that the staining performance of pure bacteria cell blocks might be different as staining bacteria in a tissue context. Therefore, we tested the original protocols of Madhusudhan et al. (117) and of Fu et al. (47) also in FFPE tissue. To do so, we selected an acute appendicitis and a lung abscess as pathologies with a likely high abundance of bacteria. We detected the high concentration of bacteria even in H&E staining (Figure 14.), in addition to all usual signs of acute inflammation such as dense infiltration of neutrophils, edema and hemorrhage.

3.1.2.1. Acute appendicitis:

Figure 11. shows an overview of the acute appendicitis case in H&E staining from two cross sections and the appendix tip. Already in this overview the high number

of inflammatory cells, hemorrhage spots and a mixture of inflammatory cells, cellular detritus and blood organized in a fibrin network that fills the lumen almost completely is recognizable.

Figure 11. Acute appendicitis, H&E staining, overview

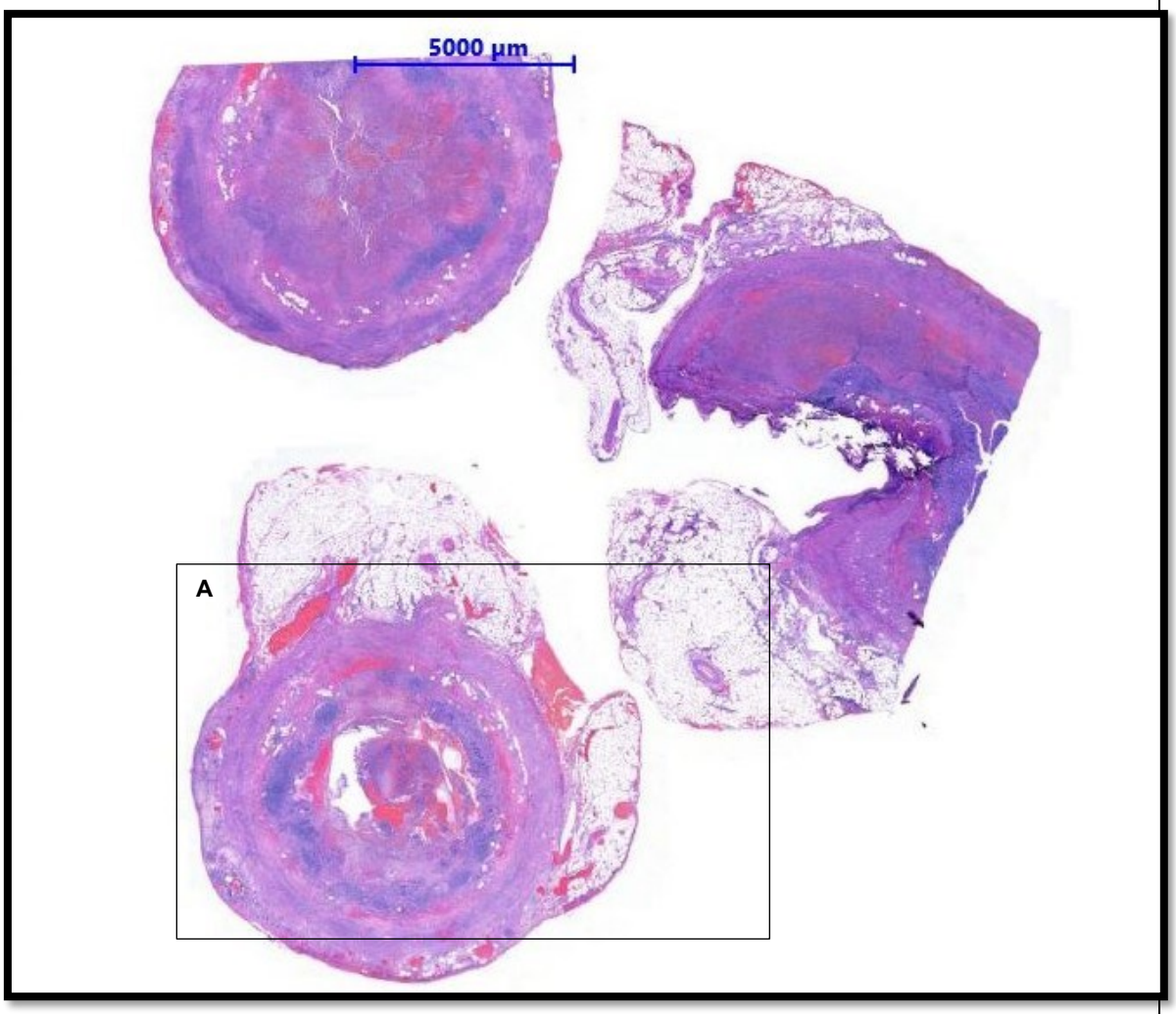

Inflammatory cells, hemorrhage, mixture of inflammatory cells + cellular detritus + blood organized in a fibrin network fills lumen almost completely.

Figure 12. (=Figure 11. - A) shows all typical signs of inflammation mentioned more clearly, just like Figure 13. (=Figure 12. – B) and 14. (=Figure 12. – C) do. Figure 13. includes the termination of the appendix mucosa during the inflammatory reaction. On closer inspection at Figure 14., there are some bacteria noticeable in the edematous substance.

Figure 12. Magnification of Figure 11.-A

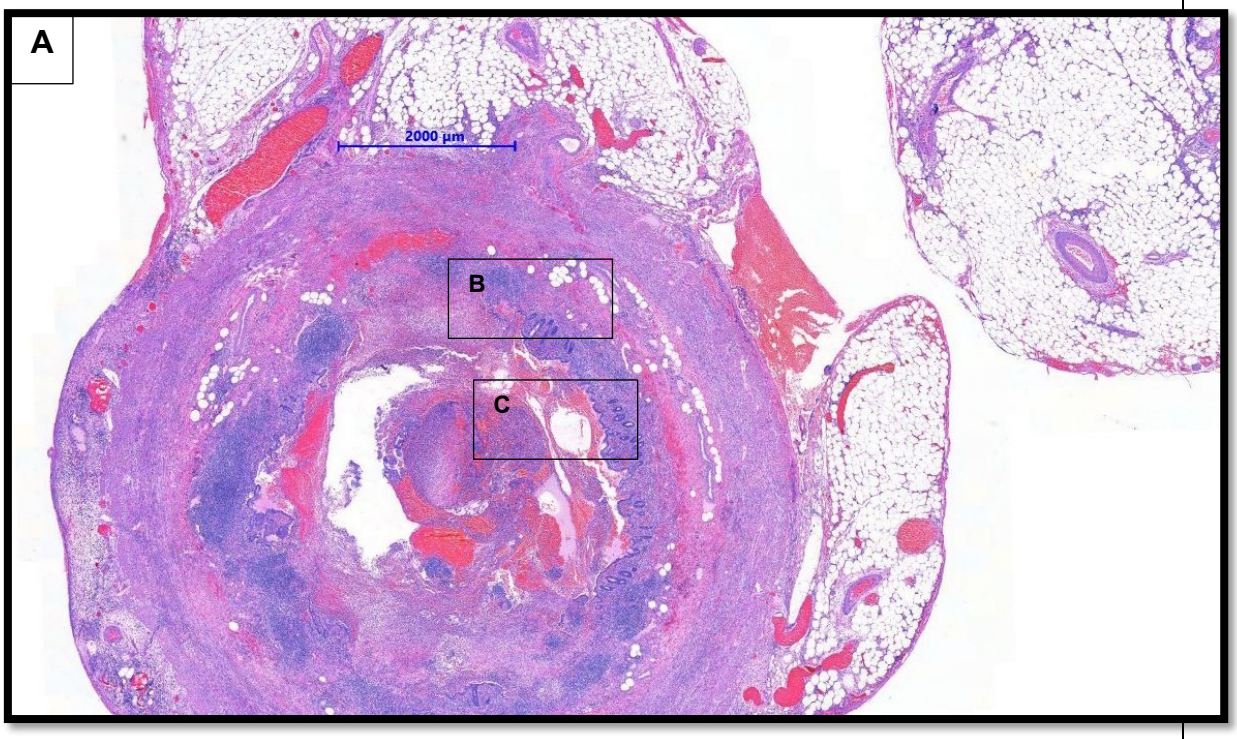

Inflammatory cells, hemorrhage, mixture of inflammatory cells + cellular detritus + blood organized in a fibrin network fills lumen almost completely.

Figure 13. Magnification of Figure 12.-B

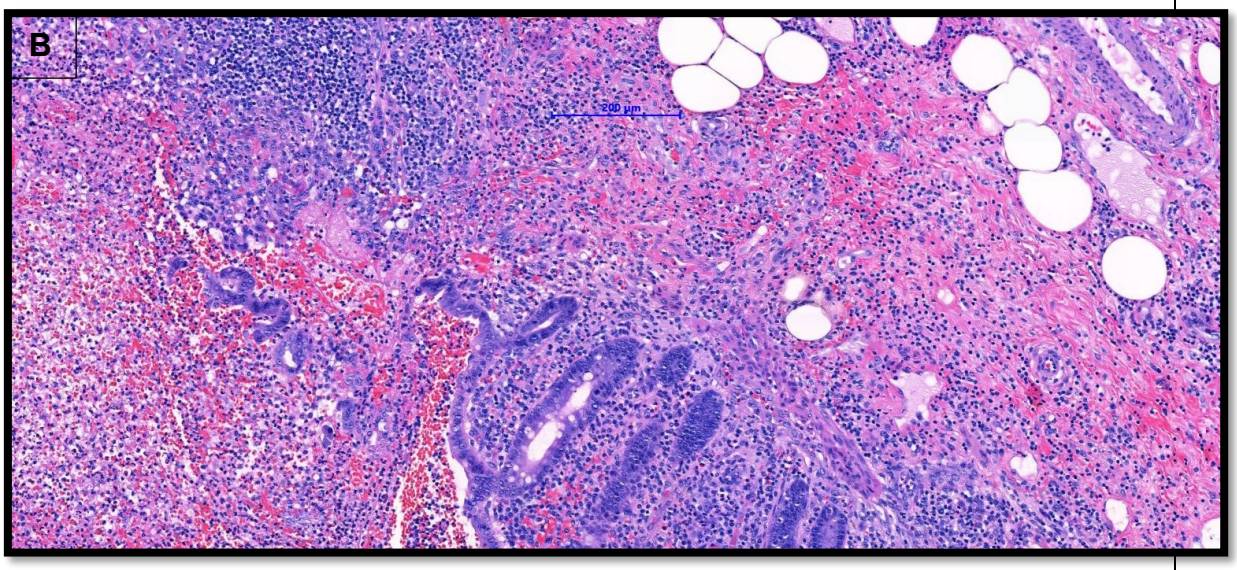

Termination of appendix mucosa, high abundance inflammatory cells and hemorrhage in the mucosa and in the lumen.

Figure 14. Magnification of Figure 12.-C

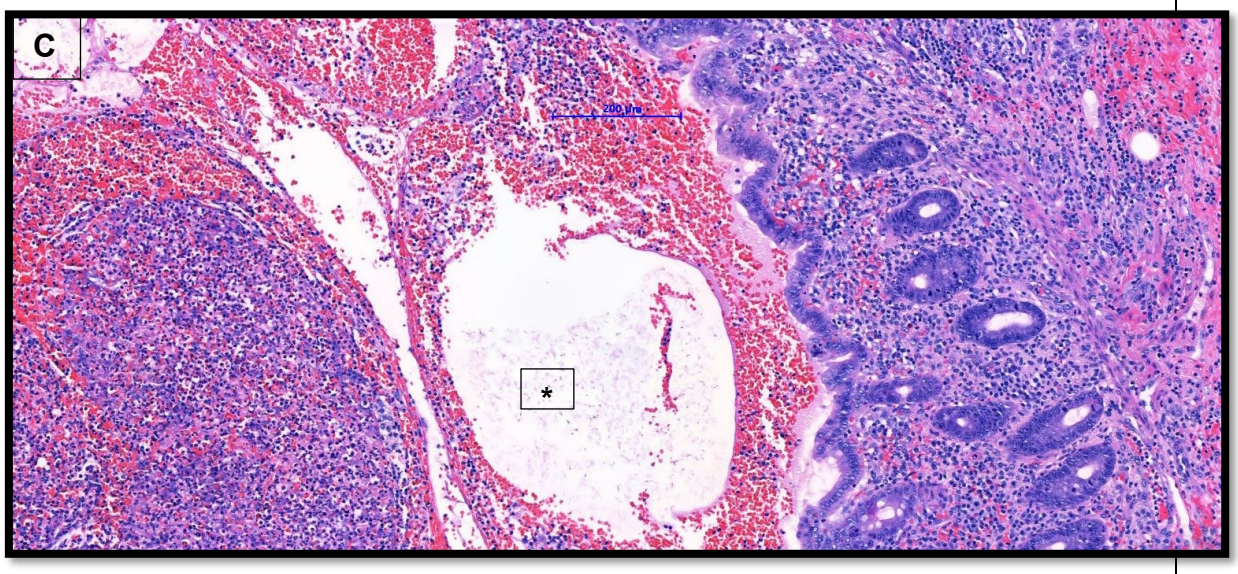

Inflammatory lumen - right sided: appendix wall, left sided: filled lumen, bacteria in the edematous substance (*).

We have tried to roughly align H&E images (Figure 15. – A) and DAPI x4 overview images (Figure 16.1.). However, it must be mentioned that the 100%-correct regional allocation was difficult because of different sectional planes (each section causes an offset of the sectional plane by at least 5µm). For future testing it may be useful to perform the different staining methods with well-established protocols in one section series. Then the offset of sectional planes is minimized by 5µm and the morphology is probably still so similar that an exact regional classification is possible.

Figure 15. Magnification of Figure 11. - upper cross section

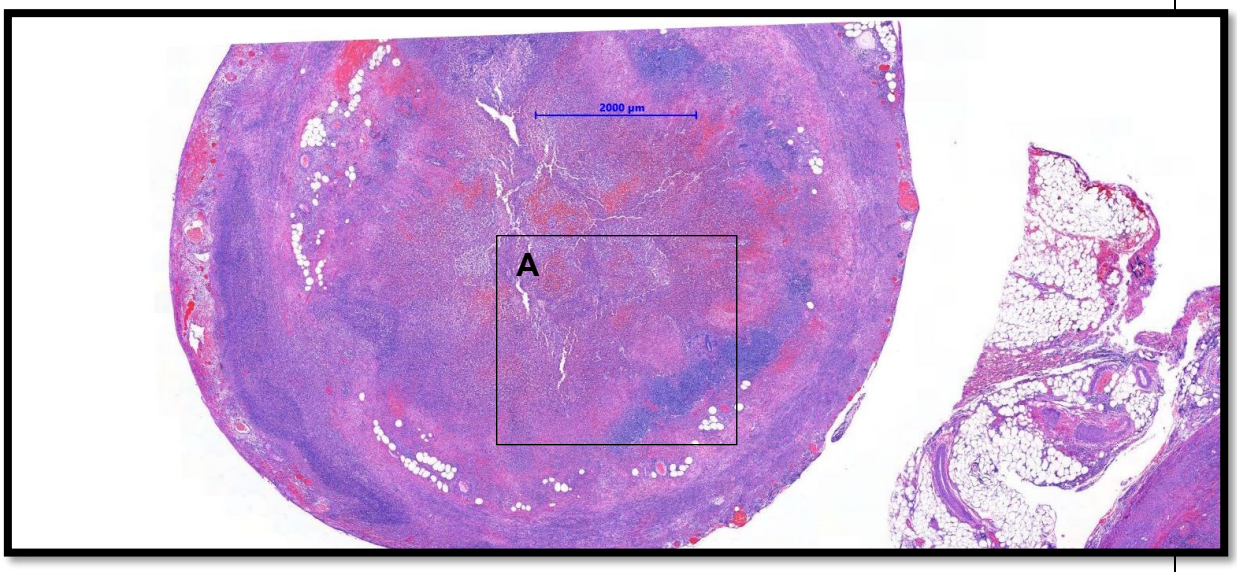

Rough H&E <-> DAPI (Figure 16.1.) allocation

To reproduce the magnification steps from DAPI x4 (Figure 16.1.) to DAPI x100 (Figure 16.2.), further images are provided in supplements. With the original protocol of Madhusudhan et al. (117) we detected some rod-shaped bacteria in the inflammatory wall and in the inflammatory filled lumen, but signal intensity was quite low (Figure 16.3.). Also, unspecific signal was quite strong (Figure 16.4.). On closer inspection, it is possible to interpret the arrangement of the rod-shaped bacteria in relation to the cell nuclei (Figure 16.6.). These are located very close to each other. With the protocol of Fu et al. (47) we were not able to detect any bacteria at all.

Figure 16. Acute appendicitis, FISH staining, original protocol: Madhusudhan et al.

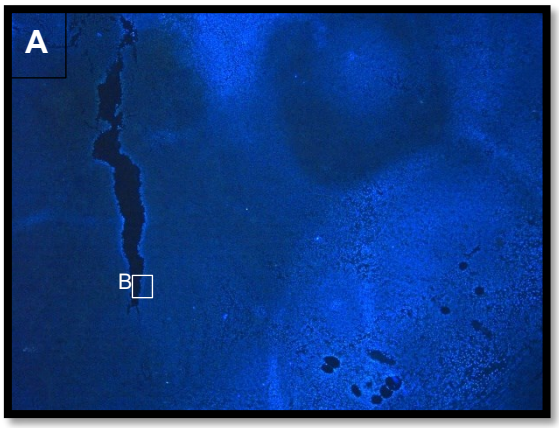

16.1. DAPI - EX387nm, x4
rough H&E (Figure 15.–A) <-> DAPI allocation

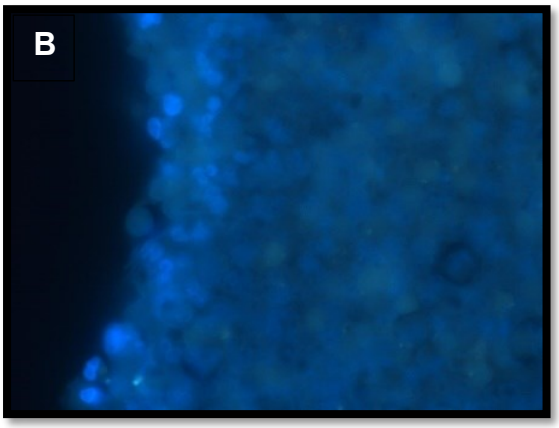

16.2. DAPI - EX387nm x100
magnification of 16.1.-B

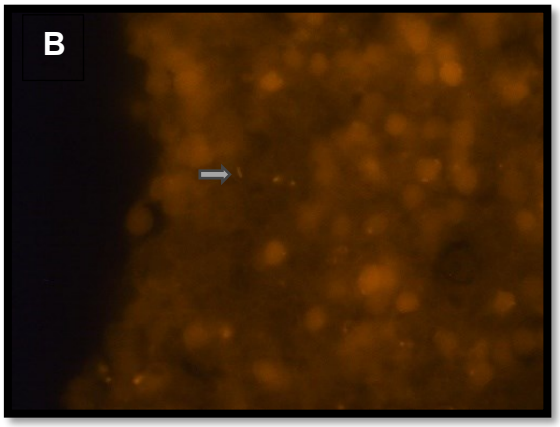

16.3. Probe - EX543nm, x100

Rod-shaped bacteria (⇨) recognizable
in probe-filter

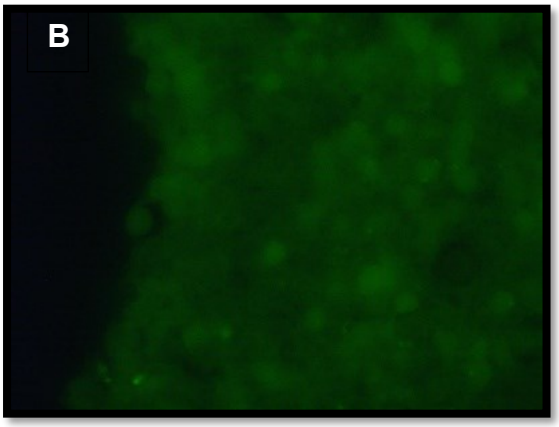

16.4. Background EX494nm

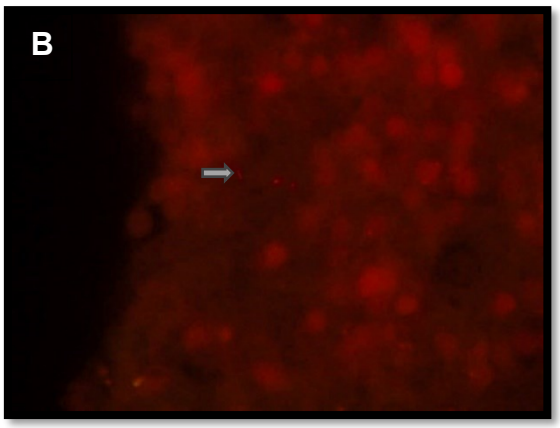

16.5. difference probe - background

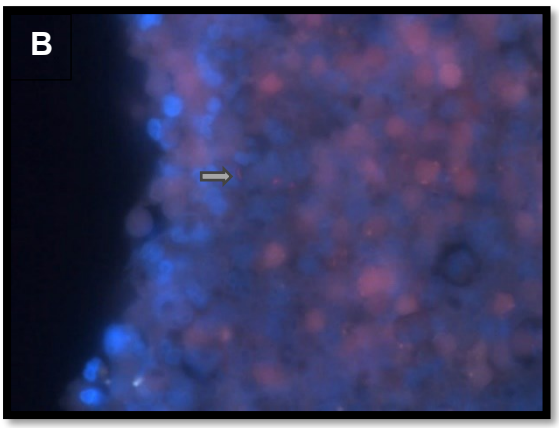

16.6. overlay „difference“ with DAPI

Arrangement of rod-shaped bacteria (⇨) in relation to the cell nuclei, unspecific signals quite strong, for a detailed image sequence of DAPI magnifications see supplements..

3.1.2.2. Acute lung abscess:

The H&E staining shows the histomorphology of an abscessing infarct pneumonia (Figure 17.). Usual signs of acute inflammation in the lung with alveolar structures filled with a mixture of inflammatory cells, fibrin, edema and cellular detritus, massive hemorrhages and a complete loss of architecture in the area of the abscessing process (Figure 17. -19.) are recognizable. At higher magnifications (Figure 18. + 19.), the normal architecture of lung parenchyma is completely lost. Figure 19. shows a massive hemorrhage and a formed abscess in direct positional relationship.

Figure 17. Lung abscess, H&E staining, overview

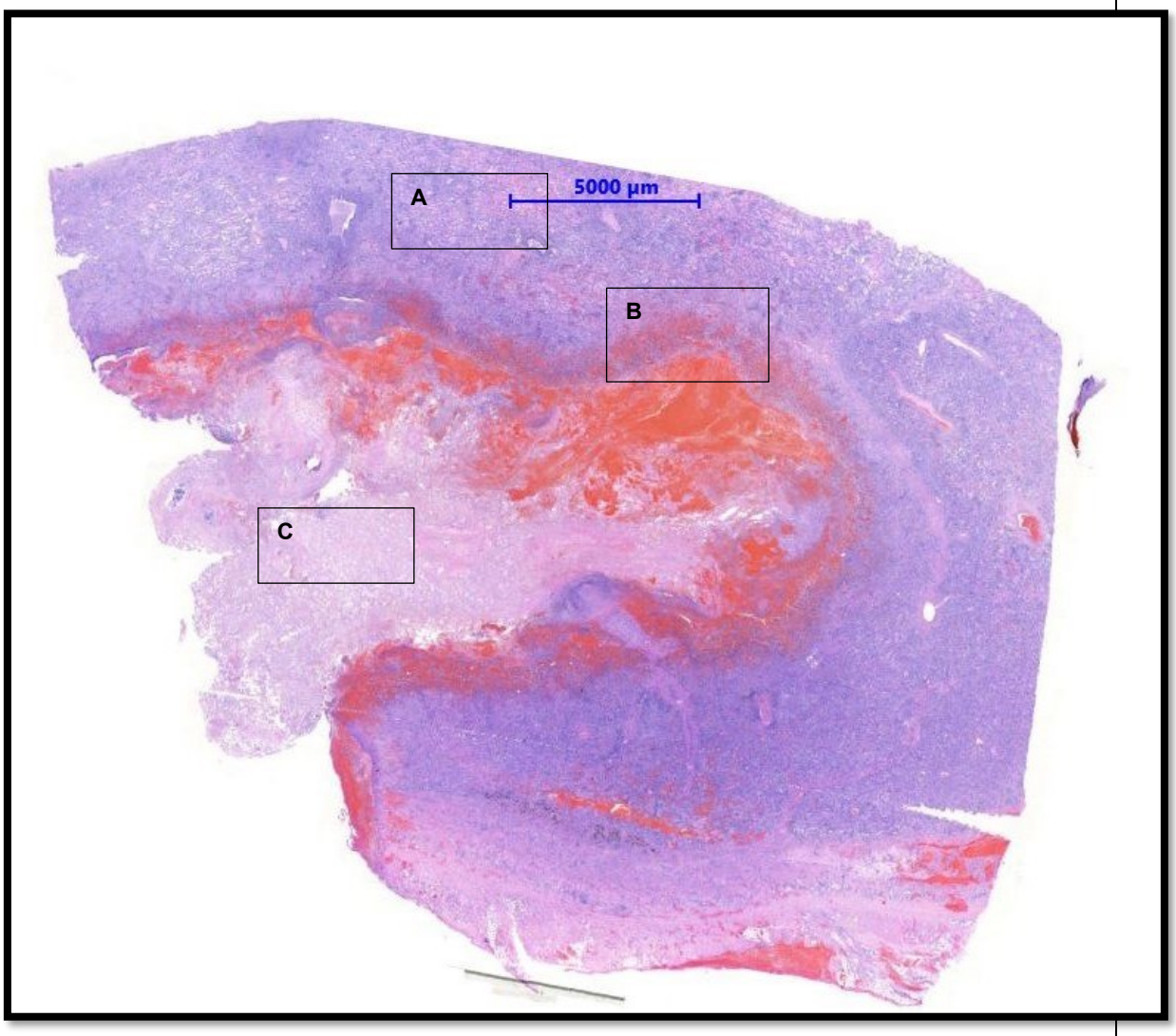

Lung abscess, loss of alveolar architecture, massive infiltration of inflammatory cells, massive hemorrhages.

We have tried to roughly align H&E images (Figure 17. – C) and DAPI images (Figure 20.1. + Figure 21.1.). If the DAPI x60 (Figure 20.3). image in Figure 20. and the DAPI x100 (Figure 21.1.) image in Figure 21. are inspected, clear coccoid-like structures are recognizable that stand out from the surrounding DAPI background. If you look at the corresponding probe images (Figure 20.4. + 21.2.) with this knowledge, no specific signals are recognizable here. Rather, it should be noted that the signals in the probe spectrum are very similar to the signals in the background spectrum. Accordingly, we were not able to specifically stain the DAPI positive cocci with the probe using either the protocol of Madhusudhan et al. (117) or the protocol of Fu et al. (47). Many of the cocci were located in the middle of the abscess where we tried a rough allocation between H&E images and DAPI images.

Figure 18. Magnification of Figure 17.-A

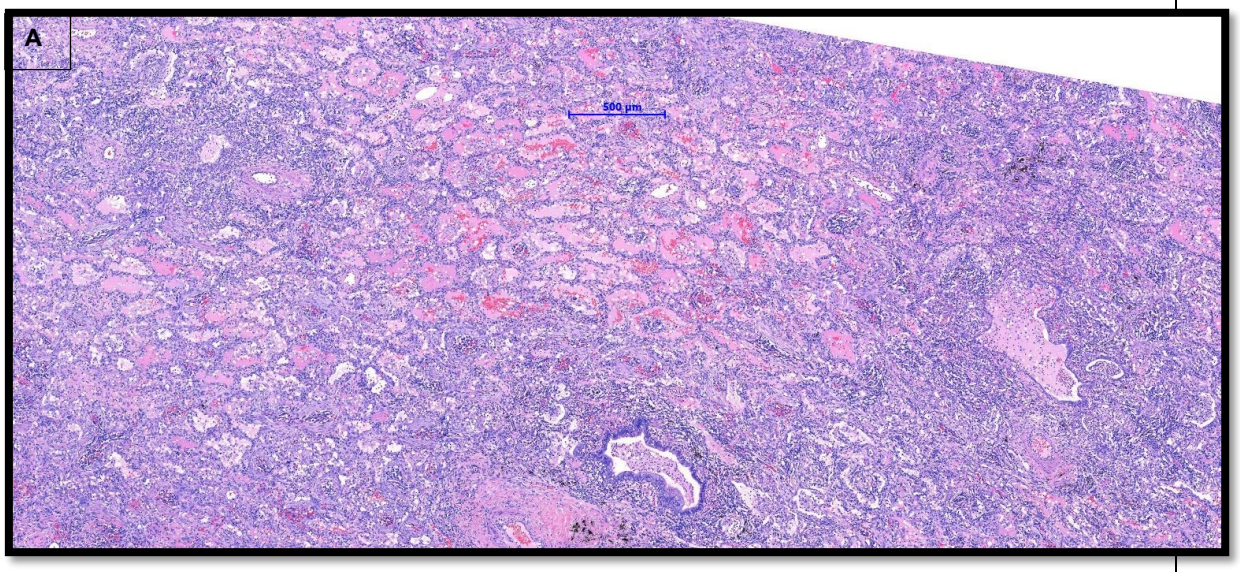

Alveolar architecture lost, edema + erythrocytes + inflammatory cells + cell-detritus in nearly all alveoli.

Figure 19. Magnification of Figure 17.-B

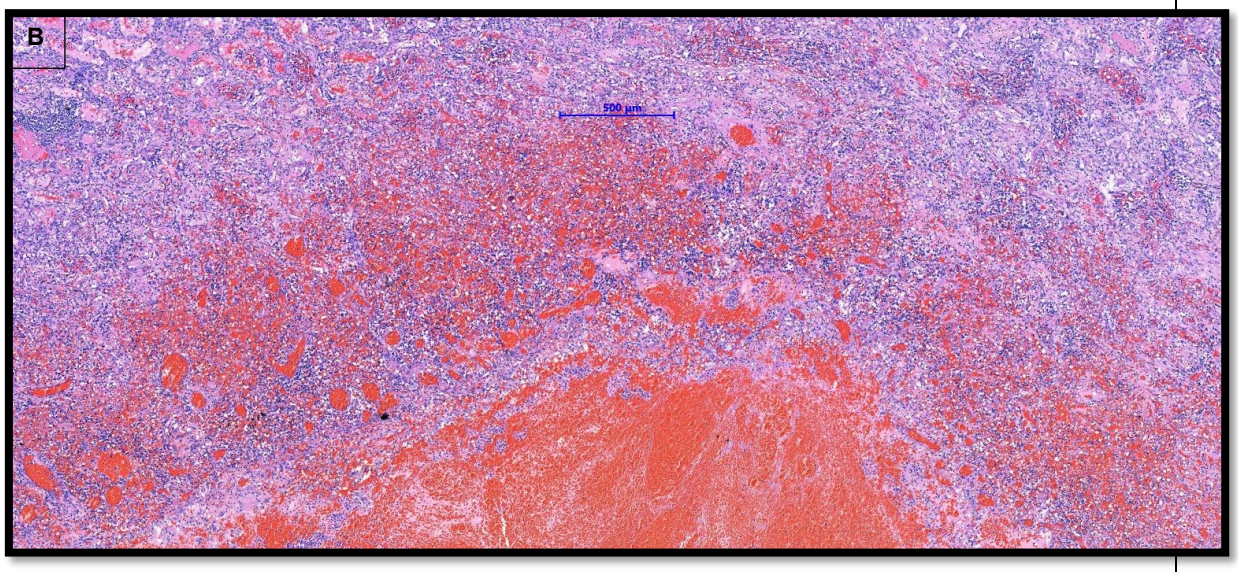

Massive hemorrhage + loss of alveolar architecture near the abscess.

Figure 20. Lung abscess, FISH staining, protocol: Madhusudhan et al.

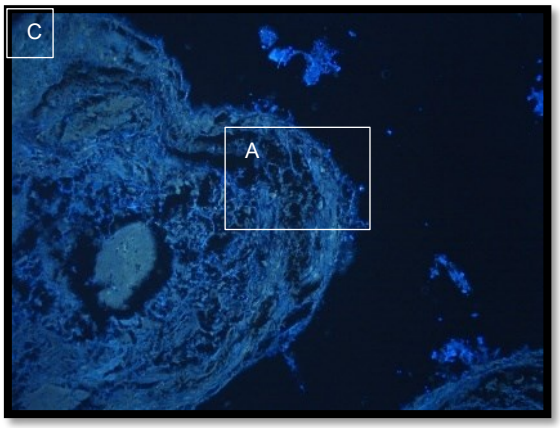

20.1. DAPI - EX387nm, x4

Rough H&E (Figure 17.-C) <-> DAPI allocation

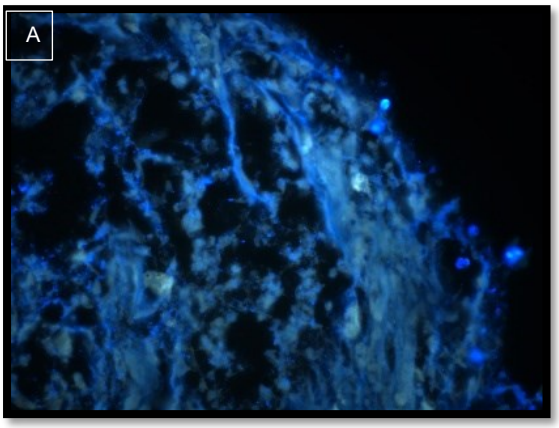

20.2. DAPI - EX387nm, x40

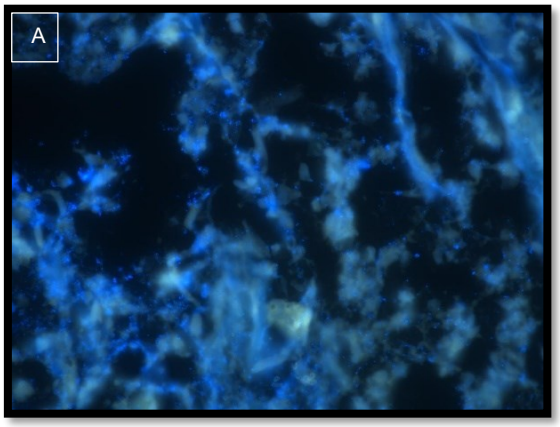

20.3. DAPI - EX387nm, x60,

Cocci recognizable

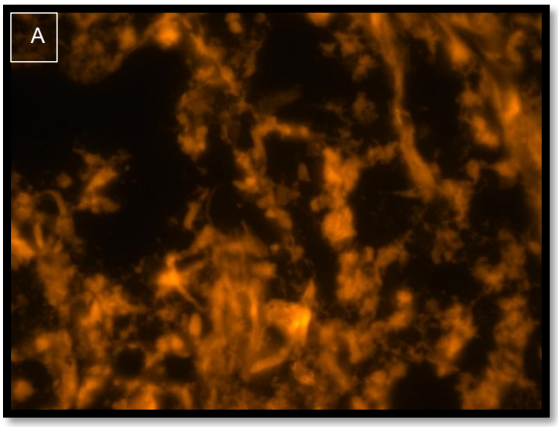

20.4. Probe - EX543nm, x60 – No Signal

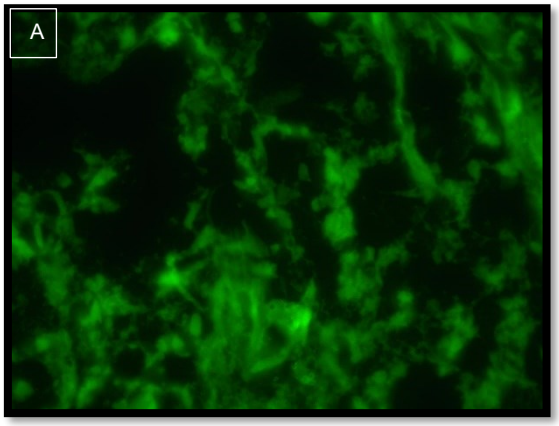

20.5. Background EX494nm, x60

Cocci in DAPI x60 staining, no specific signal in probe staining. Probe filter and background filter are nearly similar.

Figure 21. Lung abscess, FISH staining, original protocol: Fu et al.

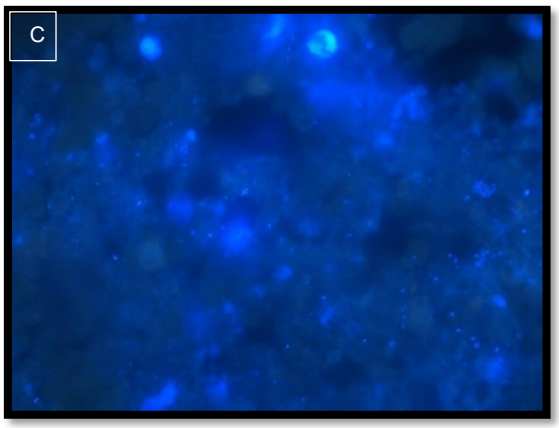

21.1. DAPI - EX387nm, x100,
Cocci recognizable
Rough H&E (Figure 17. - C) <-> DAPI allocation

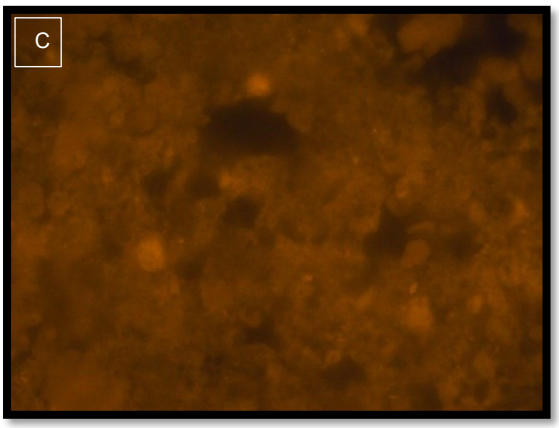

21.2. Probe - EX543nm, x100 – No Signal

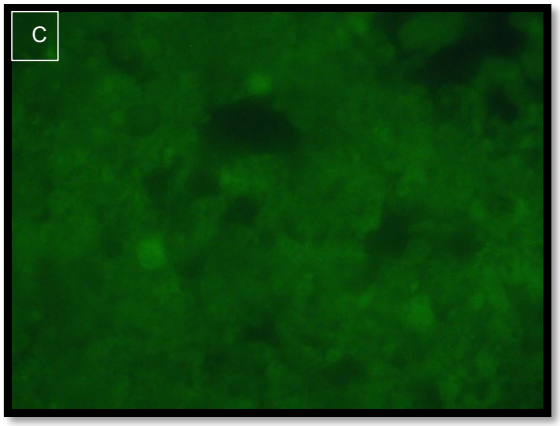

21.3. Background EX494nm x100

Cocci in DAPI staining, no specific signal in probe staining. Probe filter and background filter are nearly similar.

3.1.3. Summary of initial results:

After the review of demonstrated results in 3.1.1. and 3.1.2., we decided to take the protocol of Madhusudhan et al. (117) as our basis – see also Table 2.

In 3.1.1., probe signal was in a good intensity, background signal was quite weak and the hands-on time was lower. Nevertheless, in the protocol of Madhusudhan et al. (117) the staining results of Gram-positive cocci were not as intense as we wanted it to be (Figure 7.) - the sensitivity of the FISH was therefore not yet optimal. However, the background signal was very weak and nonsense (non-EUB) test series was correct negative - the specificity here was therefore very good.

In 3.1.2. we saw with the protocol of Madhusudhan et al. (117) a positive signal just in the appendicitis. Here, however, the intensity of the specific bacterial signal was still relatively weak compared to the relatively strong background signal - the sensitivity in the tissue context was therefore significantly worse than in the cell block context. In the lung abscess we were neither with the protocol of Madhusudhan et al. (117) nor with the protocol of Fu et al. (47) able to produce a specific positive probe signal.

Furthermore, we wanted to adjust the required quantity of enzymes to an optimum, so as not to consume unnecessarily large quantities. So, we tested the specific permeabilization only with proteinase K as Nejman et al. (46) did it as well as the combination of enzymes - as it was done in the protocol of Fu et al. (47). But we wanted to make sure that the concentrations are high enough to have an effect, so we performed dilution series with lysostaphin and proteinase K and demonstrated the effect of lysozyme.

3.2. Enzyme dilution series:

Since Nejman et al. (46) were able to perform the specific permeabilization just with proteinase K and Fu et al. (47) used a significantly lower concentration of the enzymes than Madhusudhan et al. (117) did, we wanted to make sure that the specific permeabilization with every single enzyme are non-redundant steps and tested every enzyme by its own.

3.2.1. Lysozyme:

First, we tested the effect of lysozyme on staining quality. Therefore, we performed the original FISH-protocol of Madhusudhan et al. (117) with the cell block, but the specific permeabilization was done only with 20mg/ml lysozyme. We clearly saw a specific signal just in Gram-negative *E. coli* and in acid-resistant *Mycobacterium spp.* (Figure 22.), as it was to be expected from the known function of the lysozyme described above.

Figure 22. Cell block of Staph. aureus + E. coli + Mycobact., FISH staining, protocol: Madhusudhan et al., just lysozyme, 20mg/ml

22.1. Probe - EX543nm

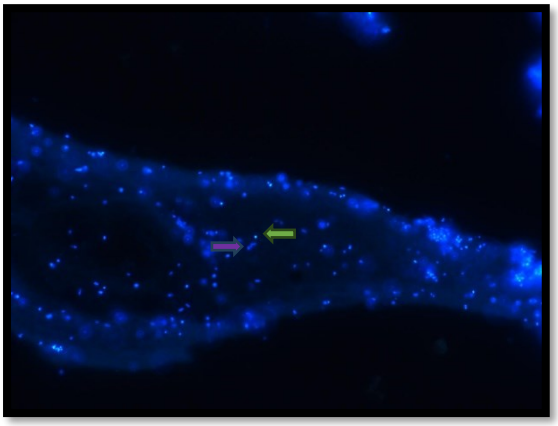

22.2. DAPI - EX387nm

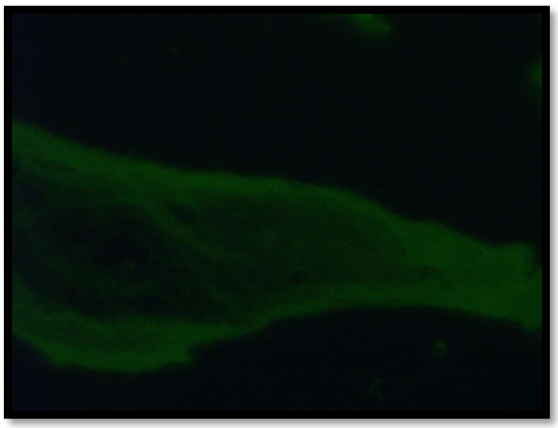

22.3. Background EX494nm

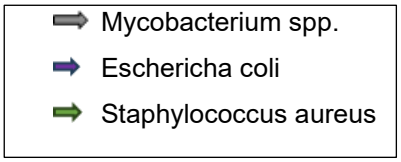

E. coli in 22.1. + 22.2. positive, Staph. aureus in 22.1. negative (lighter green arrow) and in 22.2. positive (more intense green arrow), Mycobacterium spp. missing here. Background shows nearly no signal, just the fibrin.

3.2.2. Lysostaphin:

While Fu et al. (47) only used 0.05mg/ml, Madhusudhan et al. (117) used 20x as much - 1mg/ml. To evaluate the best and lowest possible concentration of lysostaphin, we tested concentrations from 0,05mg/ml (Figure 23.), 0,1mg/ml (not shown), 0,2mg/ml (Figure 25.), 0,5mg/ml (not shown) up to 1mg/ml (Figure 24.). With 0,05mg/ml (Figure 23.) we saw nearly no staining at all, with just a slightly better staining at 0,1mg/ml (not shown). The difference between 0,2mg/ml (Figure 25.), 0,5mg/ml (not shown) and 1mg/ml (Figure 24.) were not significant, so we decided to use 0,2mg/ml (Figure 25.) lysostaphin in our adapted protocol.

Figure 23. Cell block of Staph. aureus + E. coli + Mycobact., FISH staining, protocol: Madhusudhan et al. just lysostaphin, 0,05mg/ml

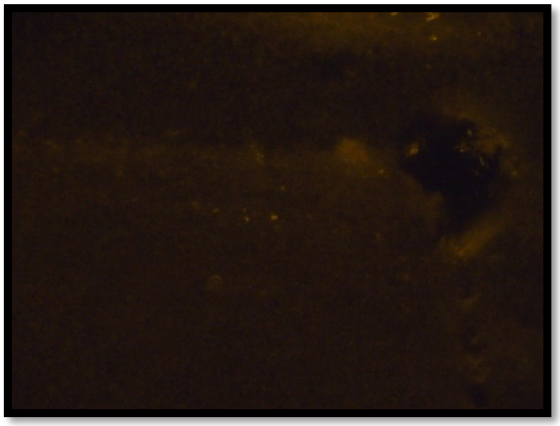

23.1. Probe - EX543nm

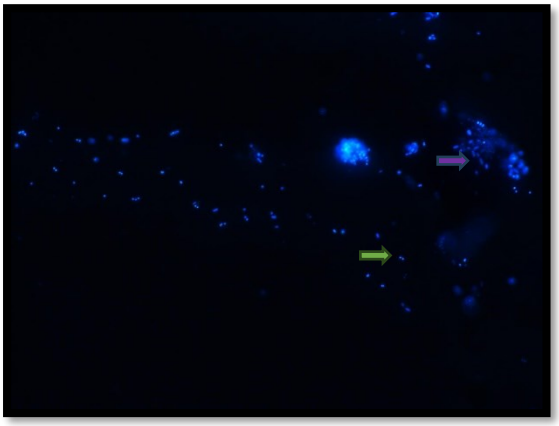

23.2. DAPI - EX387nm

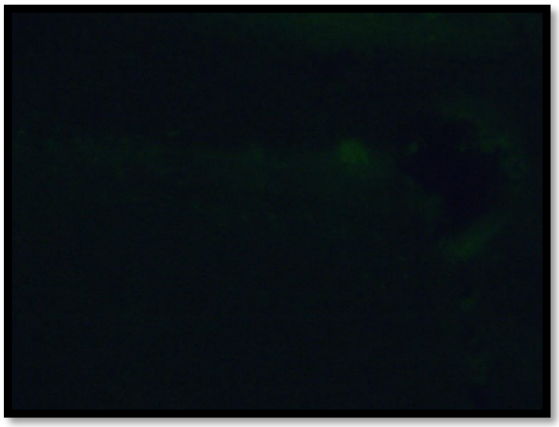

23.3. Background EX494nm

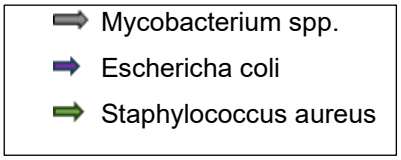

Weak signal, Mycobacterium spp. missing here.

Figure 24. Cell block of Staph. aureus + E. coli + Mycobact., FISH staining, protocol: Madhusudhan et al., just lysostaphin, 1mg/ml

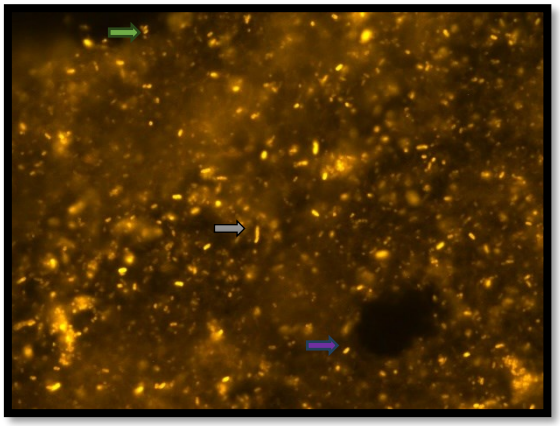

24.1. Probe - EX543nm

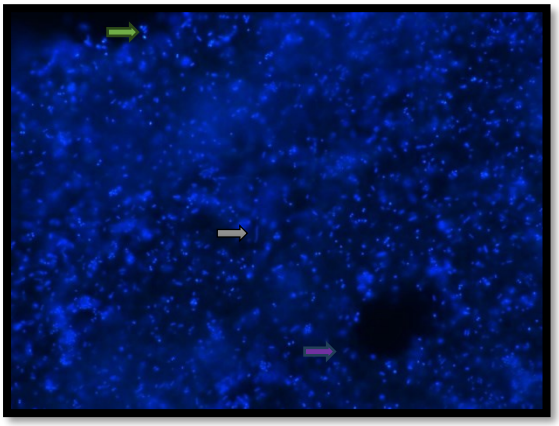

24.2. DAPI - EX387nm

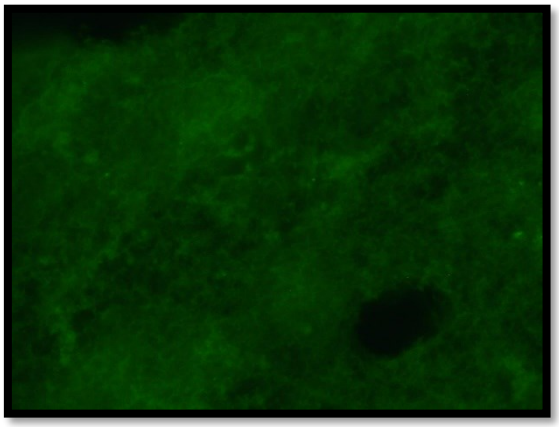

24.3. Background EX494nm

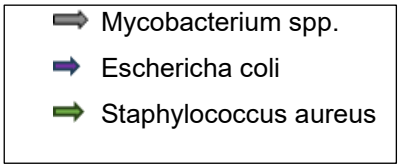

All three bacteria positive.

Figure 25. Cell block of Staph. aureus + E. coli + Mycobact., FISH staining, protocol: Madhusudhan et al., just lysostaphin, 0,2mg/ml

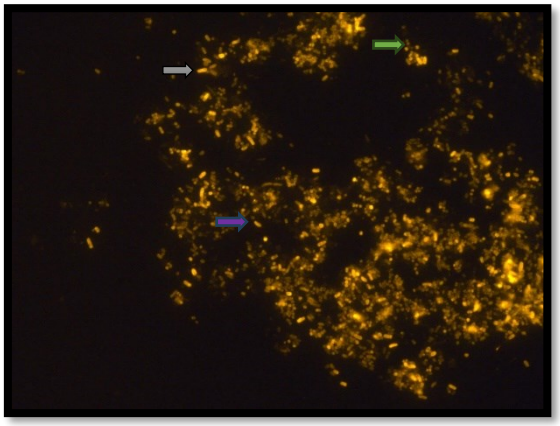

25.1. Probe - EX543nm

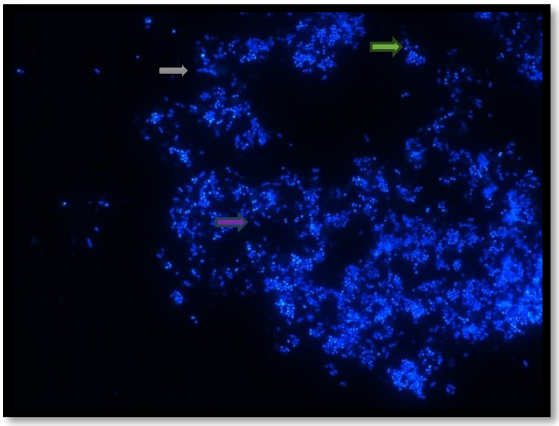

25.2. DAPI - EX387nm

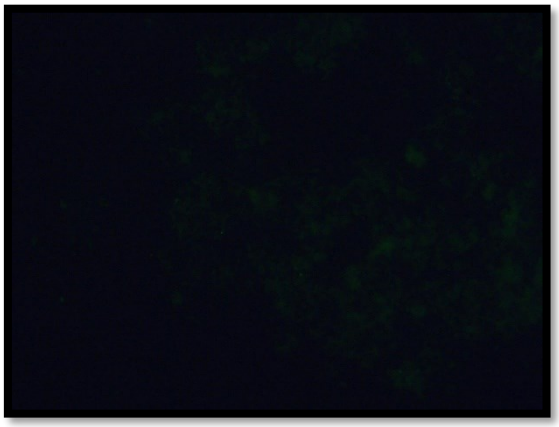

25.3. Background EX494nm

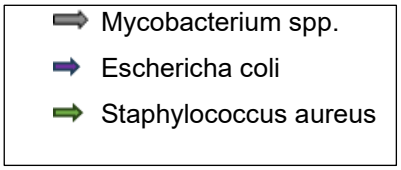

All three bacteria positive, cocci less intense

3.2.3. Proteinase K:

Nejman et al. (46) performed the specific permeabilization only with 10µg/ml proteinase K. In the protocol of Fu et al. (47), they used all three enzymes with also 10µg/ml proteinase K. Therefore, we wanted to visualize the effect of proteinase K as an unspecific proteinase with cell block material. We started with 0,1mg/ml (Figure 26.) and went up from 0,2.mg/ml (Figure 27.), 0,5mg/ml (not shown) up to 1mg/ml (not shown). With 0,1mg/ml (Figure 26.) and 0,2mg/ml (Figure 27.) we were able to demonstrate the effect of proteinase K just in the Gram-negative bacteria and in the acid-resistant *Mycobacterium spp.* In the Gram-positive cocci we saw no signal at all. With the concentration of 0,5mg/ml (not shown) we saw a loss of signal-intensity and a loss of morphological features of the bacteria, which was even

stronger with 1mg/ml (not shown). So, we decided to adapt our protocol with a proteinase K concentration of 0,2mg/ml (Figure 27.), even though the cell block results were slightly better with 0,1mg/ml. Since we wanted to specifically stain bacteria in the tumor tissue context, we decided on the higher concentration of 0.2 mg/ml (Figure 27.).

Figure 26. Cell block of Staph. aureus + E. coli + Mycobact., FISH staining, protocol: Madhusudhan et al., just proteinase K, 0,1mg/ml

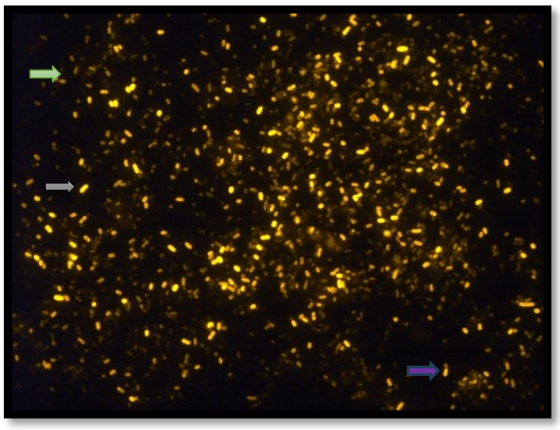

26.1. Probe - EX543nm

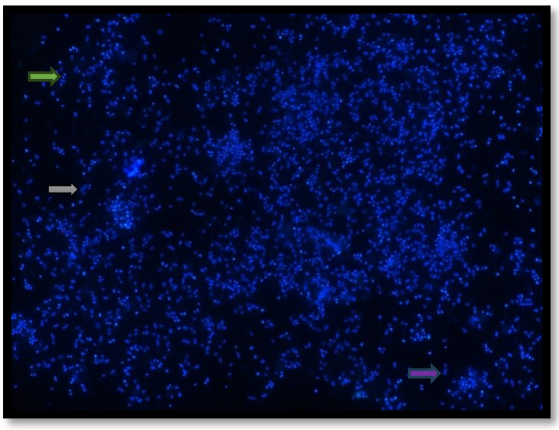

26.2. DAPI - EX387nm

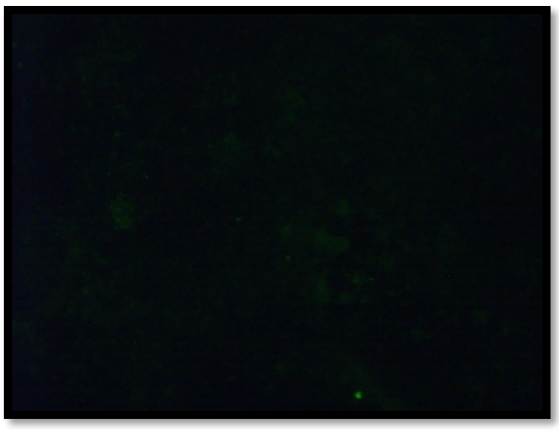

26.3. Background EX494nm

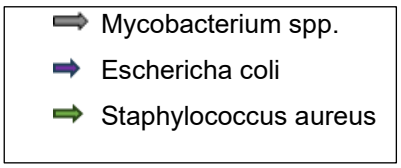

Positive E. coli and Mycobacterium spp. signals in 26.1. + 26.2., no positive signal from Staph. aureus in 26.1. (lighter green arrow) with a signal in 26.2 (more intense green arrow).

Figure 27. Cell block of Staph. aureus + E. coli + Mycobact., FISH staining, protocol: Madhusudhan et al., just proteinase K, 0,2mg/ml

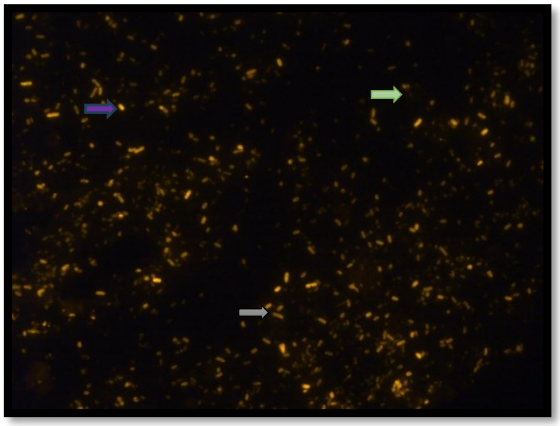

27.1. Probe - EX543nm

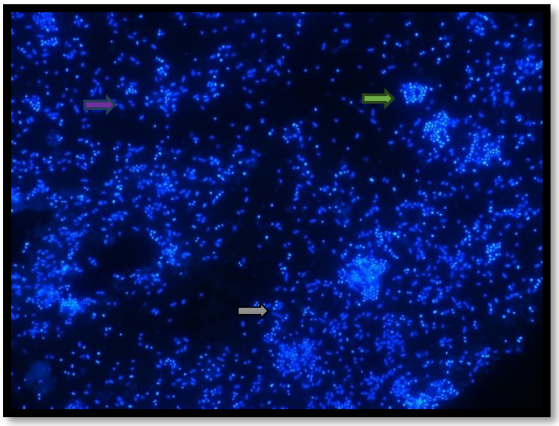

27.2. DAPI - EX387nm

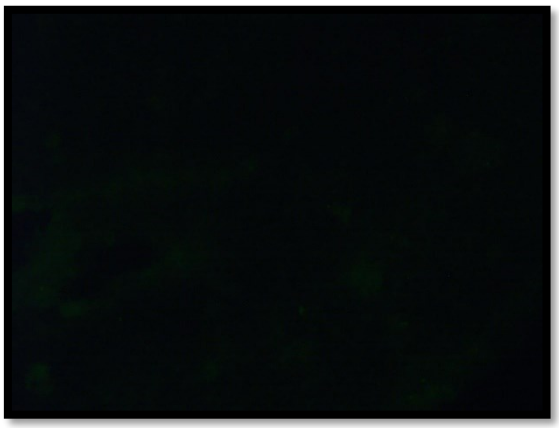

27.3. Background EX494nm

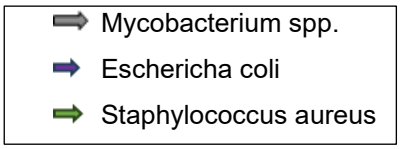

Weakly positive signal in E. coli and in Mycobacterium spp., no positive signal from Staph. aureus in 27.1. (lighter green arrow) with a signal in 27.2. (more intense green arrow).

3.3. Adapted FISH protocol:

With the described adaptations in the specific enzymatic permeabilization, we performed the FISH-protocol as it is shown in the Material and Methods section.

3.3.1. Pure bacteria cell block:

In this cell block staining we recognized that the permeabilization for pure bacteria must not be as strong as it needs to be in the tissue context. We saw some bacteria which were clearly over-digested with a loss of their signal intensity and a loss of their morphology (Figure 28.).

Figure 28. Cell block of Staph. aureus + E. coli + Mycobact., FISH staining, adapted protocol

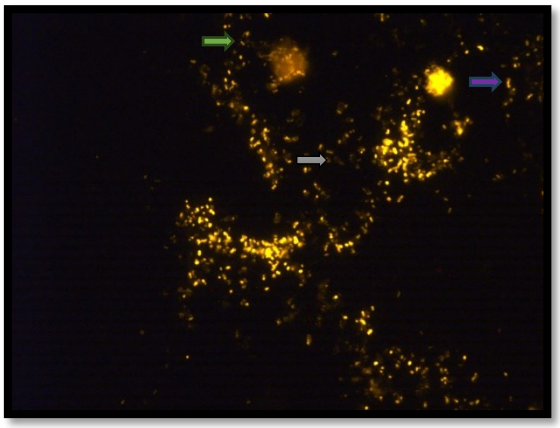

28.1. Probe - EX543nm

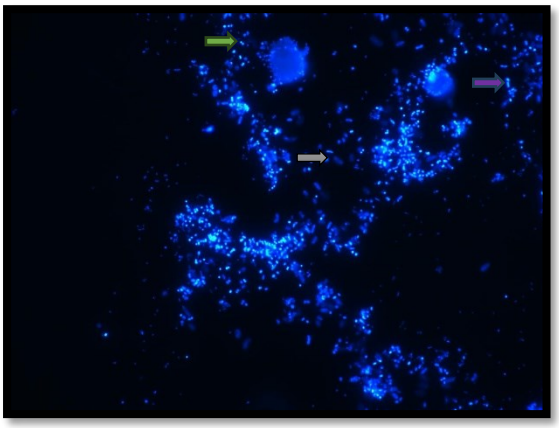

28.2. DAPI - EX387nm

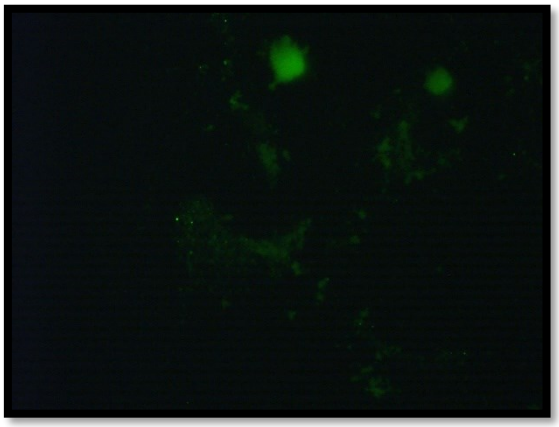

28.3. Background EX494nm

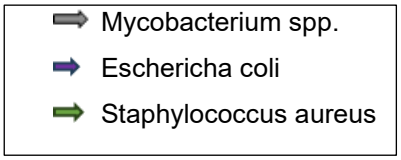

Some E. colis appear distended, some DAPI positive Mycobacterium spp. with loss of probe signal.

3.3.2. Inflammatory tissue:

At the same time as the cell bock staining series, we tested inflammatory tissues with the adapted protocol to be able to directly compare the results of the cell block and the results of the inflammatory tissue. At this point, however, the results in the tissue context were more important to us, as we obviously precisely need this tissue context for our study aim.

3.3.2.1. Acute appendicitis:

We have tried to roughly align H&E images (Figure 29. – A) and DAPI images (Figure 30.1.). For a detailed description of the H&E overview shown in Figure 29. see Figures 11.-14.

Figure 29. Acute appendicitis, H&E staining, overview

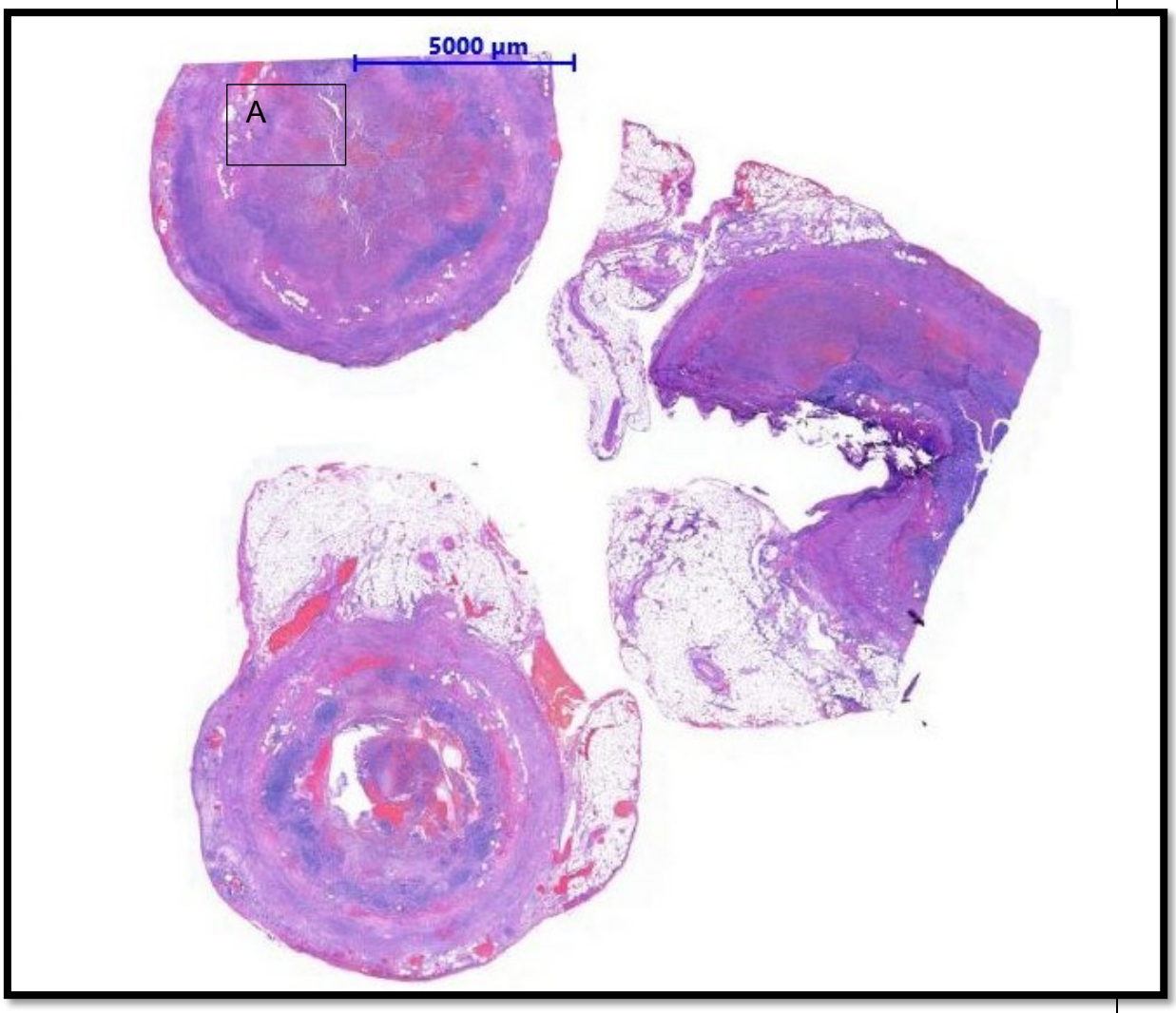

Rough H&E <-> DAPI x4 (Figure 30.1.) allocation, detailed description see Figures 11.-14.

In FISH analysis with our adapted protocol, we detected rod-shape bacteria in this acute appendicitis case (Figure 30.3. + 31.2.). The bacteria showed a very specific, intense signal and were - with some microscopy experience - good to detect (Figure 30.3. + 31.2.) beside the unspecific signal and the autofluorescence/background signal (Figure 30.4. + 31.3.). Even in a 40x magnification, bacteria were well and clearly visible (Figure 32.1.). We were therefore able to achieve a significant improvement in our method with the adaptations we made - at least for appendicitis. We were also able to show that (at least in some of the bacteria found in tissues) morphology remains intact and is clearly detectable. With digital image processing we were able to demonstrate the pattern of the bacteria in relation to the cell nuclei (Figure 30.6. + 31.5.).

Figure 30. Aute appendicitis, FISH staining, adapted protocol

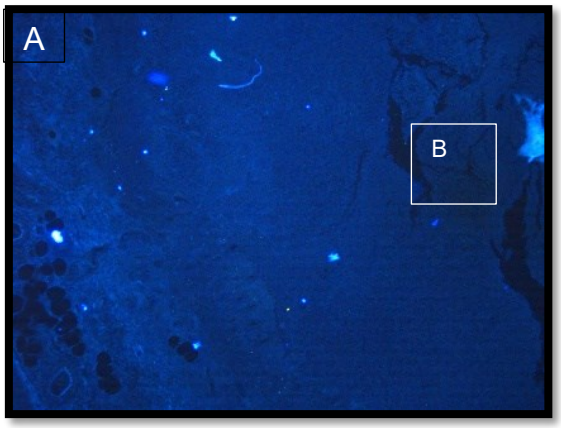

30.1. DAPI - EX387nm, x4

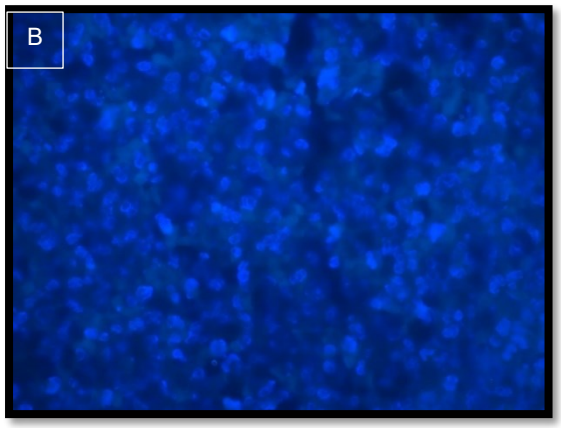

30.2. DAPI - EX387nm, x60

Rough H&E (Figure 29.-A) <-> DAPI allocation

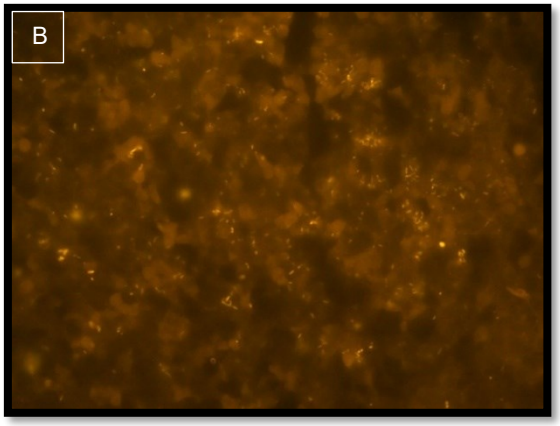

30.3. Probe - EX543nm, x60

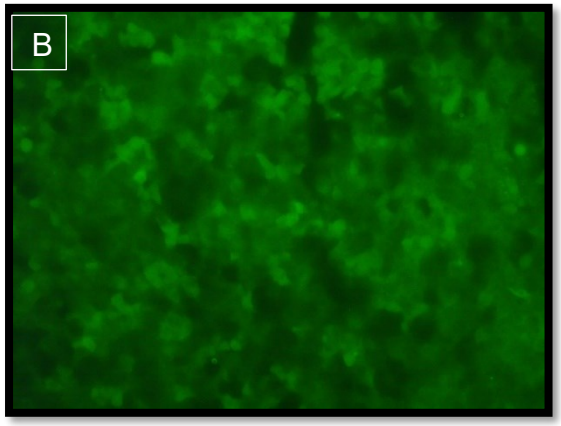

30.4. Background EX494nm, x60

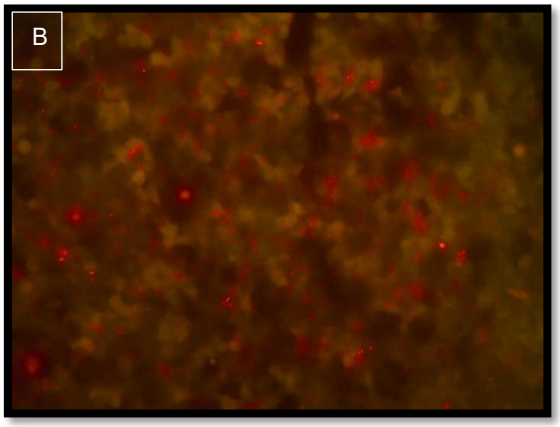

30.5. difference probe - background

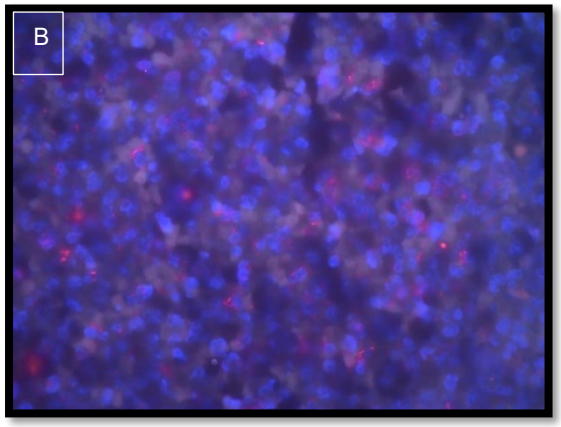

30.6. overlay „difference“ + DAPI

Image series - different extinctions and processed images, specific rod shaped-bacterial signals in Probe, for detailed magnification and localization see supplements.

Figure 31. Acute appendicitis, FISH staining, adapted protocol

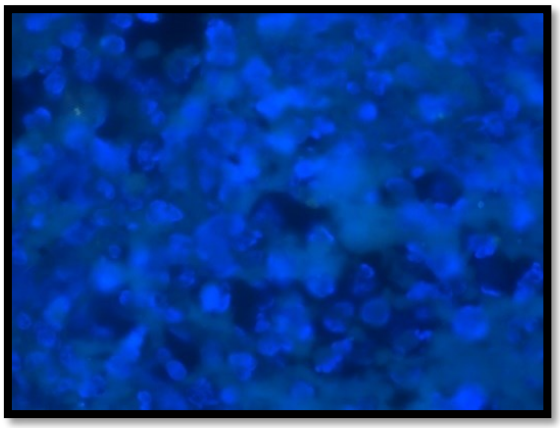

31.1. DAPI - EX387nm, x100

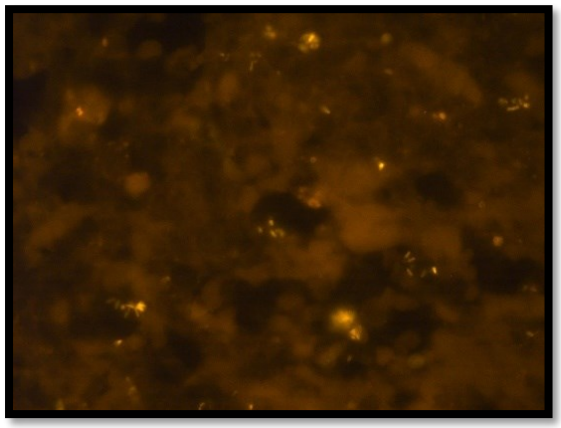

31.2. Probe - EX543nm, x100

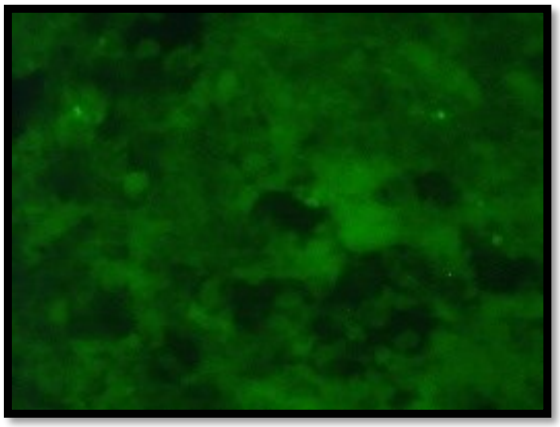

31.3 Background EX494nm, x100

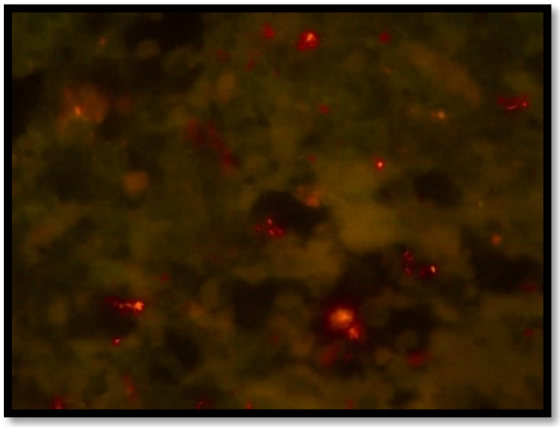

31.4. difference Probe - Background

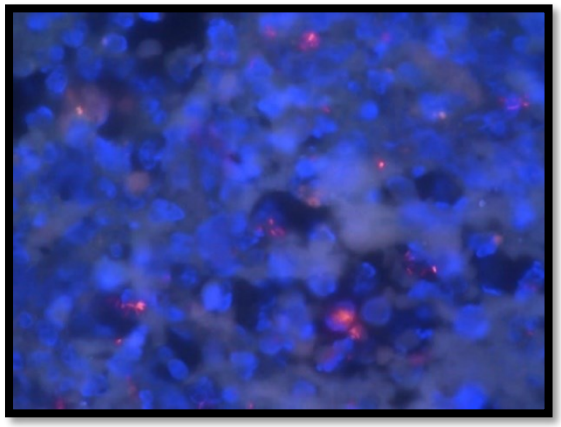

31.5. overlay „difference“ + DAPI

Image series - different extinctions and processed images, specific rod-shaped bacterial signals in Probe 31.2.

The bacteria are mainly grouped directly around the cell nuclei, although some are probably also located intracellularly. This is difficult to confirm in individual cases. Of course, it remains questionable whether we were able to stain all bacteria in this image section. It remains also unclear why these bacteria are not found in the DAPI counterstain (Figure 30.2. vs. 30.3. / Figure 31.1. vs. 31.2.). It is possible that they are being overlaid by nuclei material.

Figure 32. 40x and 60x magnification with a larger image section as shown in Figure 31. - Probe

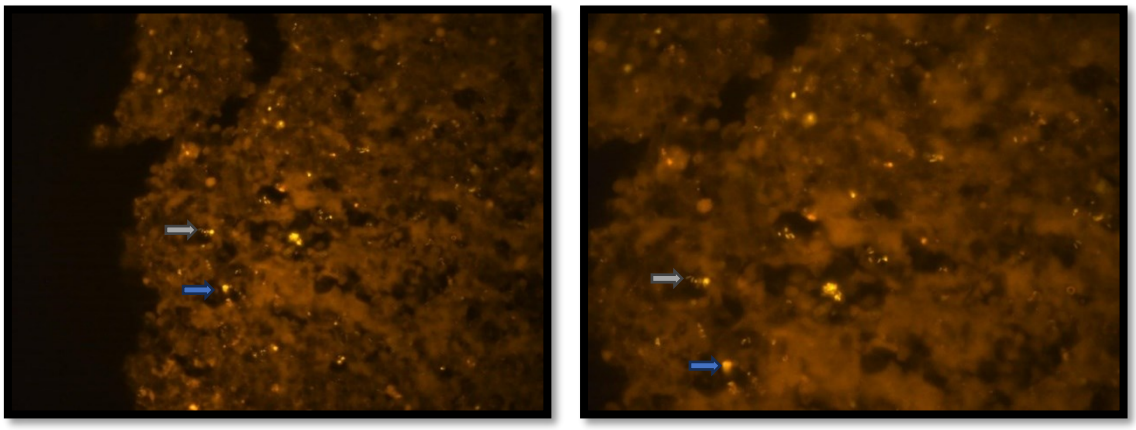

32.1. Probe - EX543nm, x40 32.2. Probe - EX543nm, x60

Specific rod-shaped bacterial signals (⇨)in probe-filter beside unspecific signals (➡).

3.3.2.2. Acute lung abscess:

We have tried to roughly align H&E images (Figure 33. – A) and DAPI images (Figure 34.1.). For a detailed description of the H&E overview shown in Figure 33. see Figures 17-19. In the lung abscess we detected cocci clearly in the DAPI filter (Figure 34.1.), as we did with the original protocol of Madhusudhan et al. (117). Unfortunately, we were still unable to detect these bacterial signals in the probe filter (Figure 34.2.) due to the massive autofluorescence and unspecific signals (Figure 34.3.). These massive autofluorescence and unspecific signals are easy to understand if you compare the background signal (Figure 34.3.) with the probe signal (Figure 34.2.) and realize that it is almost identical.

Figure 33. Lung abscess, H&E staining, overview

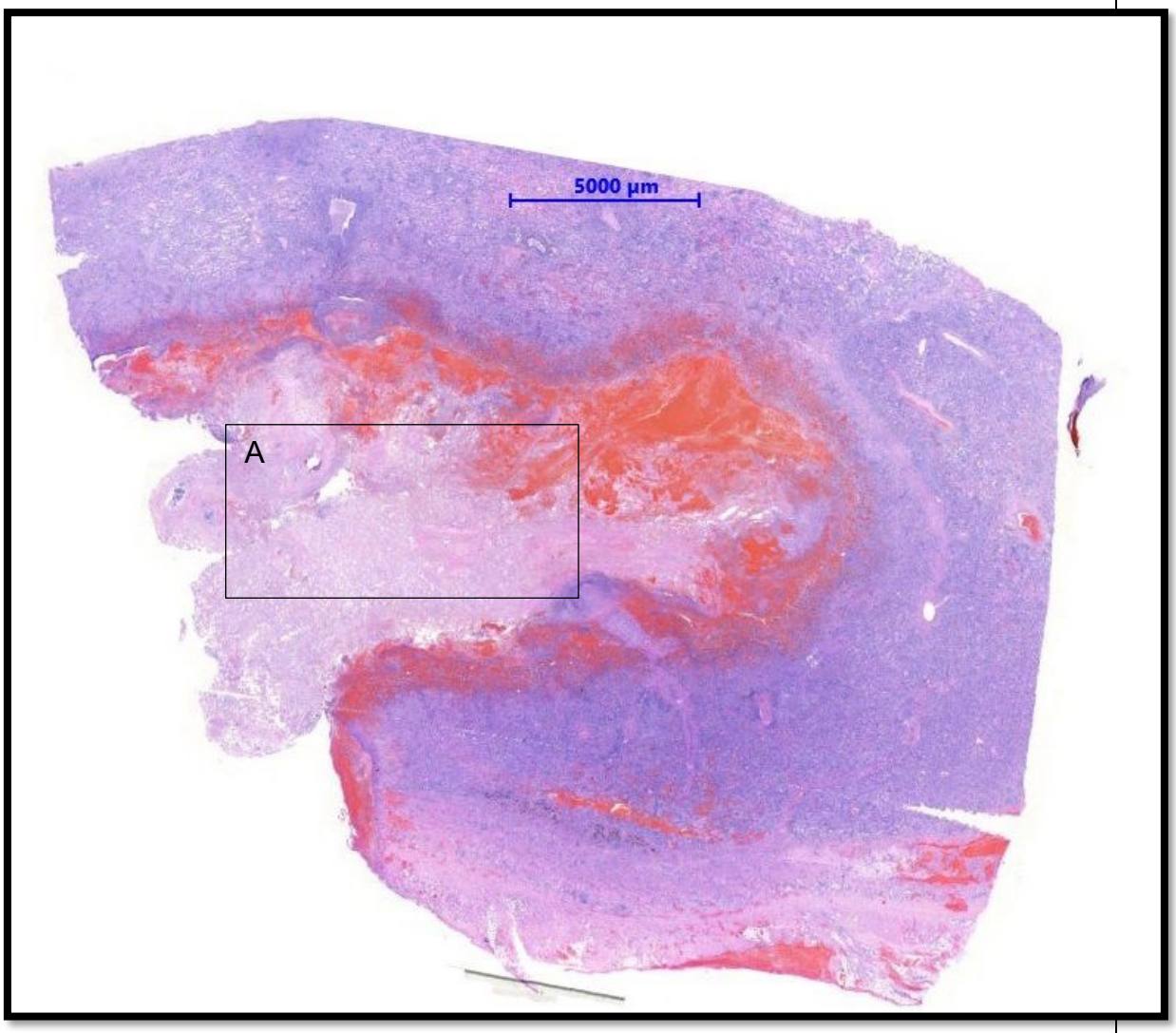

Rough H&E <-> DAPI (Figure 34.1.) allocation – detailed description see Figure 17.-19.

Figure 34. Lung abscess, FISH staining, adapted protocol

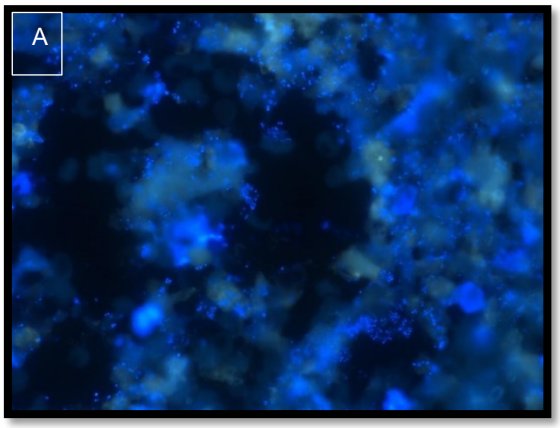

34.1. DAPI - EX387nm, x100

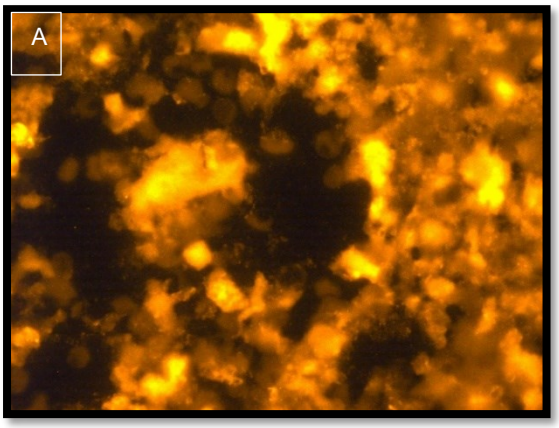

34.2. Probe - EX543nm, x100

Rough H&E (Figure 33.-A) <-> DAPI allocation

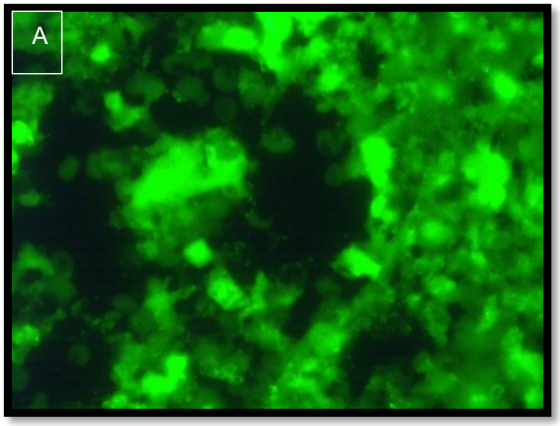

34.3. Background - EX494nm, x100

Cocci in DAPI filter, which are not detectable in probe filter. Probe filter and background filter are nearly similar.

3.3.3. Tumor tissue:

After we had at least in appendicitis material convincing results, we tested two types of cancer. The consideration of testing colon cancer, although lung cancer was our primary target tissue, was identical to previous consideration of testing inflammatory tissue. The expected bacterial load is significantly higher in the colon and therefore also in colon carcinoma than in the lungs and in lung carcinoma (46). Secondly, we were not able to produce a positive bacterial signal in the lung abscess material, but we were able to produce a positive bacterial signal in the appendicitis material.

3.3.3.1. Adenocarcinoma of the colon:

The overview image of H&E staining shows a typically high cell density in the area of the colon mucosa. Isolated areas of high cell density extend to the neighboring peritoneal fatty tissue (Figure 35.). In addition to the classic glandular tumor formations of an adenocarcinoma (Figure 36.), clear inflammatory infiltrated necrotic/abscessing areas (Figure 37.) can be identified in H&E staining. At the cellular level, all typical malignancy criteria of tumor cells can be found (Figure 36.).

Figure 35. Adenocarcinoma of the colon H&E staining, overview

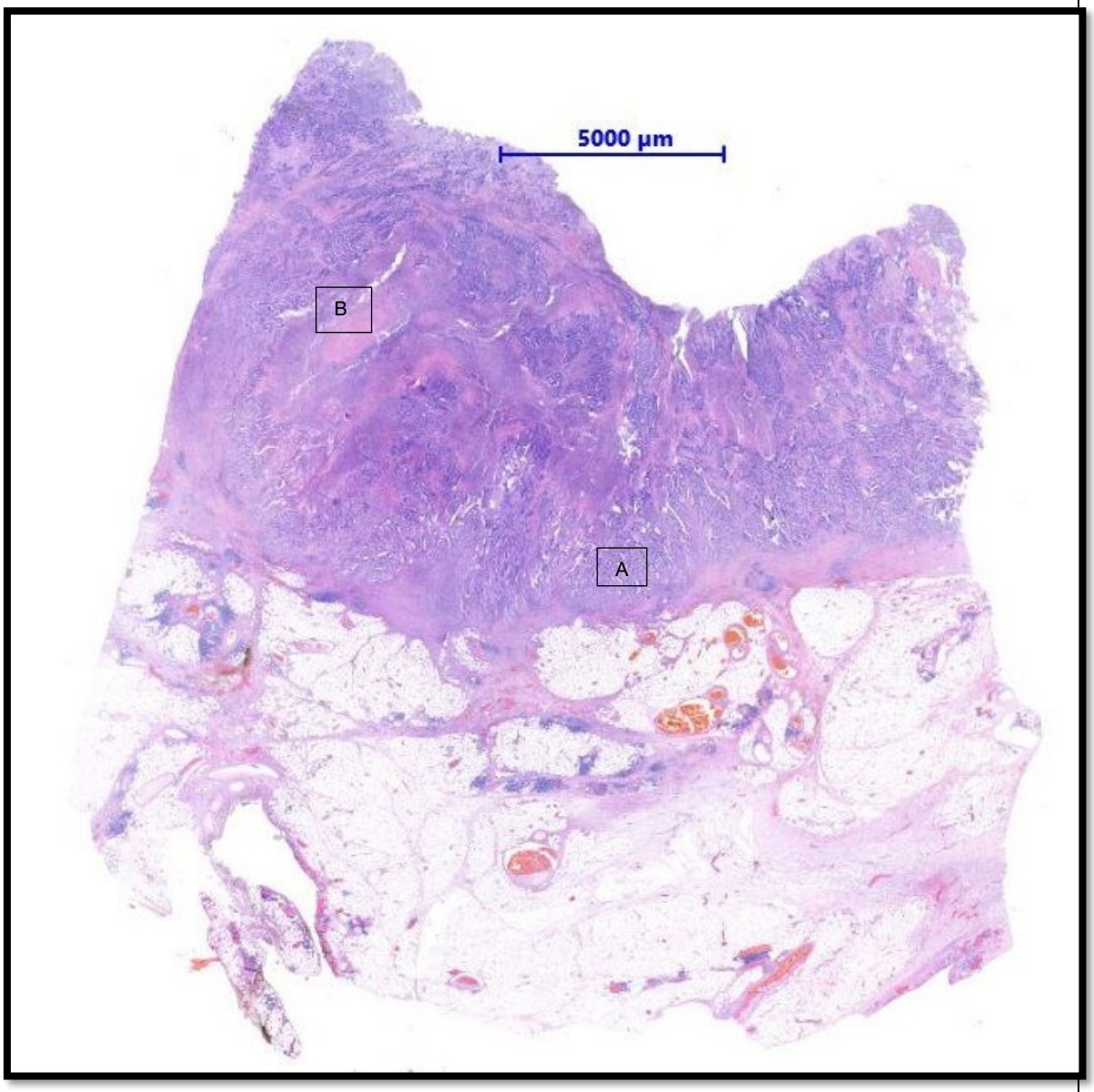

High mucosal cell density, areas of necrosis, fatty tissue infiltration

Figure 36. Magnification of Figure 35. - A

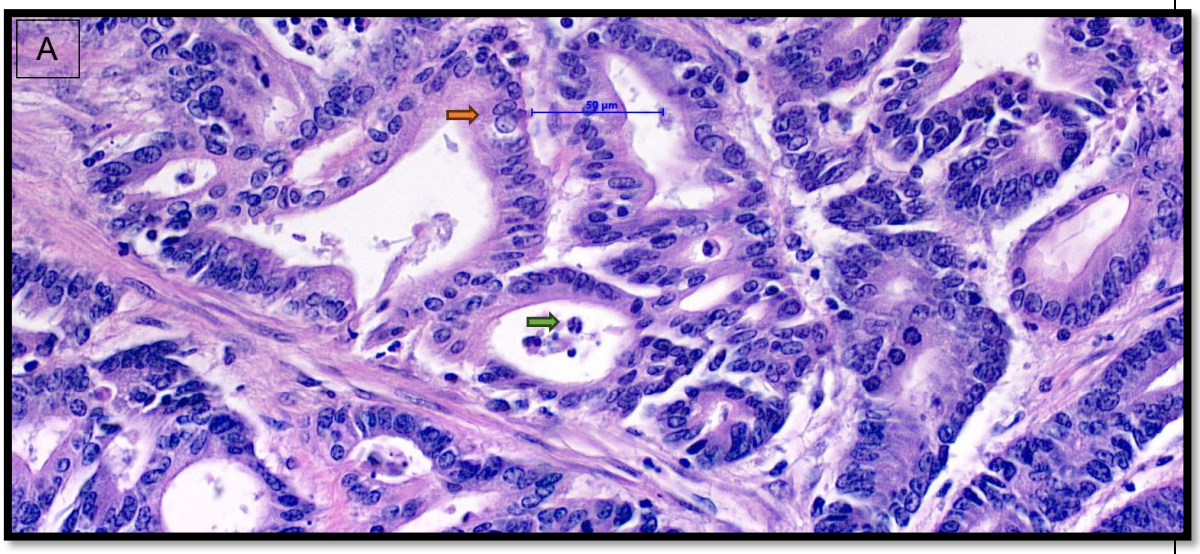

Classic nuclear malignancy criteria (⇨) of general pathology, typical adenocarcinoma formations, individual inflammatory cells (⇨)

Figure 37. Magnification of Figure 35.-B

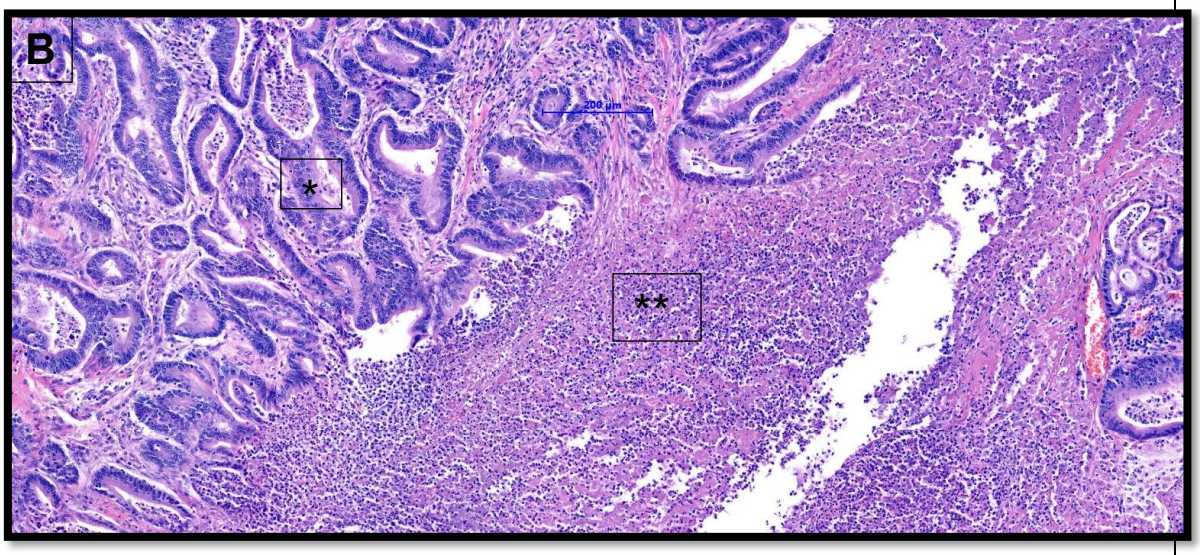

Tumor formations (*), massive necrosis/abscess formations (**)

In this adenocarcinoma of the right sided colon, we were able to detect bacteria. In the FISH analysis these bacteria are clearly identified in the probe filter (Figure 38.6. + 38.9.) and negative in the background filter (Figure 38.7. + 38.10.). In some cases, they showed a positive staining in the DAPI-filter in others they did not. In all 3 filters used (Figure 38. - DAPI, probe, background), the unspecific interference signals are clearly visible, which can lead to an imitation of bacterial signals.

Figure 38. Adenocarcinoma of the colon, FISH staining, adapted protocol

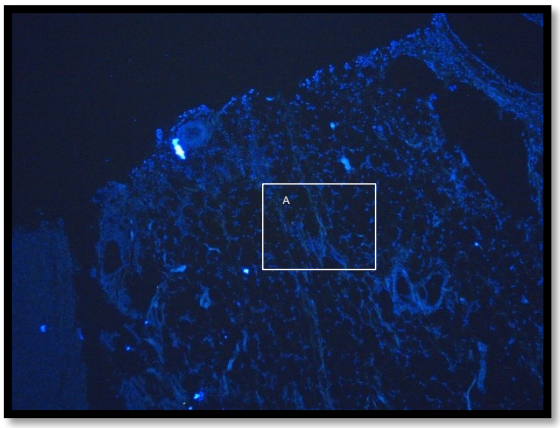

38.1. DAPI - EX387nm, x4

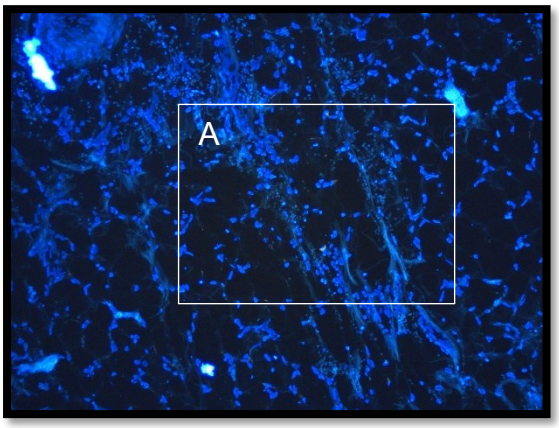

38.2. DAPI - EX387nm, x10

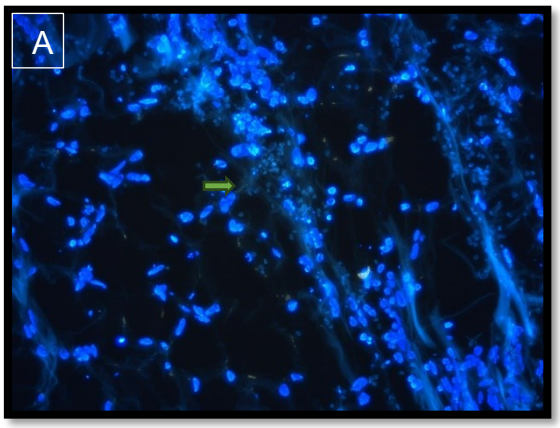

38.3. DAPI - EX387nm, x20

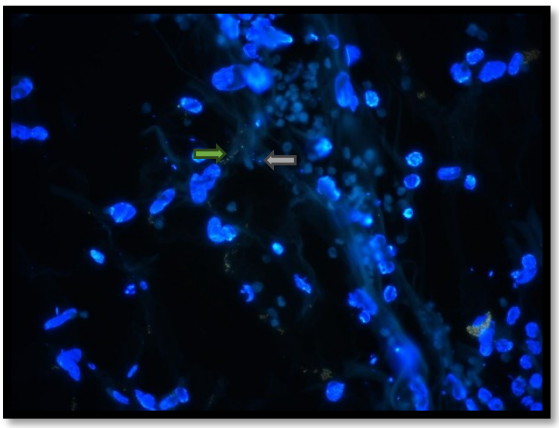

38.4. DAPI - EX387nm, x40

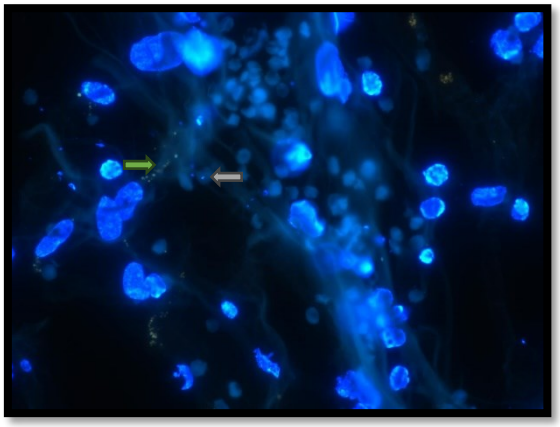

38.5. DAPI - EX387nm, x60

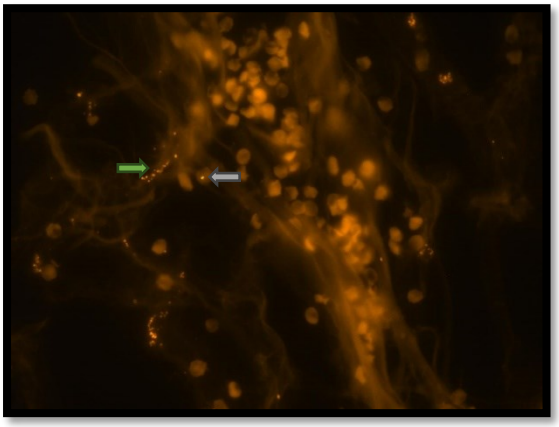

38.6. Probe - EX543nm, x60

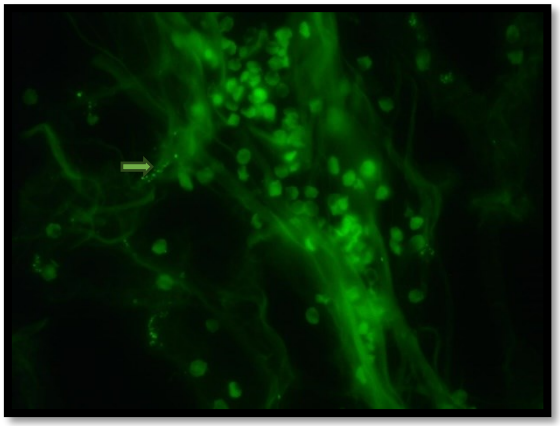

38.7. Background - EX494nm, x60

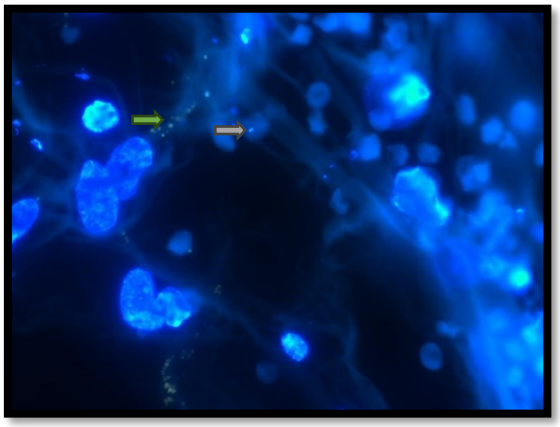

38.8. DAPI - EX387nm, x100

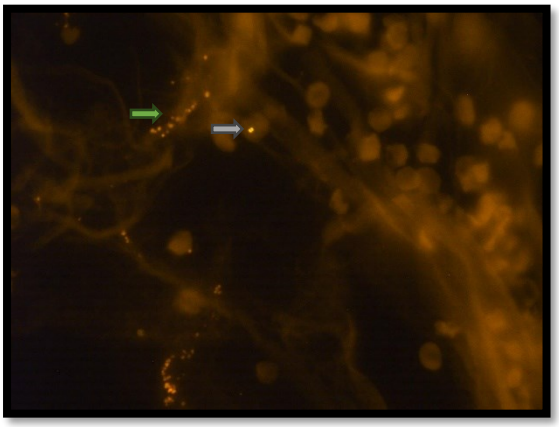

38.9. Probe - EX543nm, x100

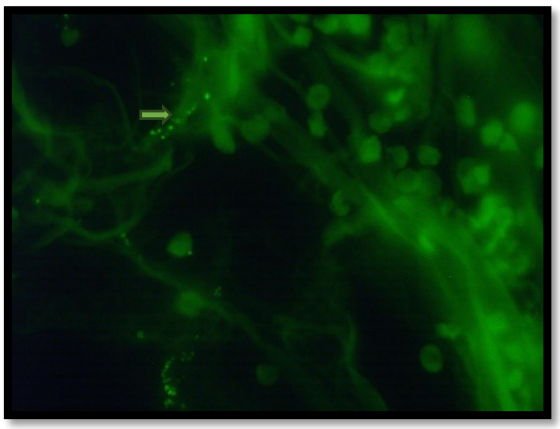

38.10. Background - EX494nm, x100

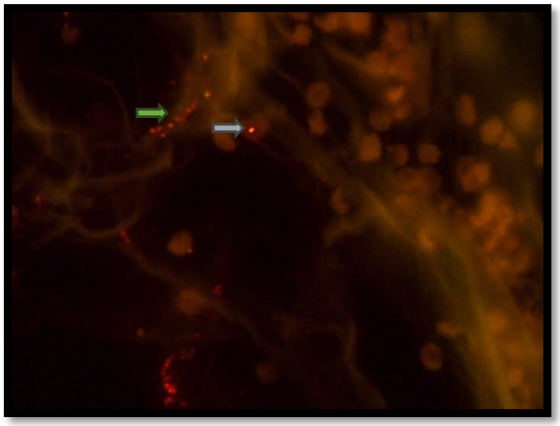

38.11. difference background – probe

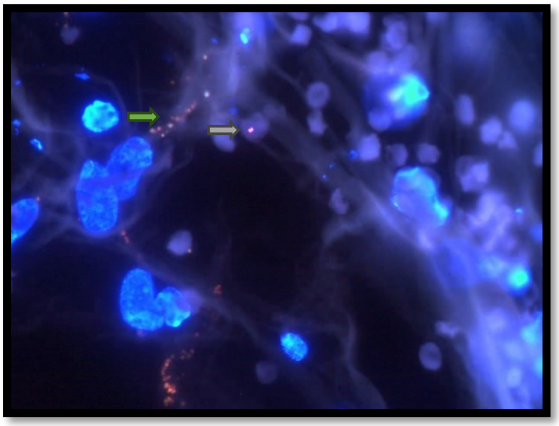

38.12. overlay „difference“ + DAPI

Specific bacterial signals (⇨) next to unspecific interfering signals (⇨), more results/images in supplements.

In this case, a synoptic view and combined interpretation of the microscopy images of all three extinctions used, is helpful. With digital processed images we were able to describe the localization of these bacteria in the direct surrounding to malignant, de-rounded, polymorphic tumor nuclei (Figure 38.12.). Whether the localization of this detected bacteria is directly intracellular or just in direct surrounding, is difficult to determine. A rough local assignment between H&E and FISH was unfortunately no longer feasible due to the time intervals and the spatial intervals between the cuts. The supplement contains several other positive bacterial findings, in which coccoid and rod-shaped bacterial signals can be recognized in direct surroundings to clearly malignant nuclei.

3.3.3.2. Adenocarcinoma of the lung:

We stained an adenocarcinoma of the lung with inflammatory components. In H&E staining all typical adenocarcinoma features like invasive glandular formations that grow destructively into healthy lung tissue (Figure 39.) on a clearly definable invasion front (Figure 40.) and all typical cellular atypia such as a shifted nuclear-to-cytoplasm-ratio in favor of the nucleus, hyperchromasia, a clear polymorphism of the nuclei, etc. (Figure 41.) can be recognized. The inflammatory component can also be clearly identified (inflammatory cells in Figure 41.), which is why we selected this lung carcinoma for our tests. After we were unable to detect any specific positive bacterial FISH signal in the lung abscess material, we were unfortunately also unable to do so in the lung carcinoma tissue.

Figure 39. Adenocarcinoma of the lung, H&E staining, overview

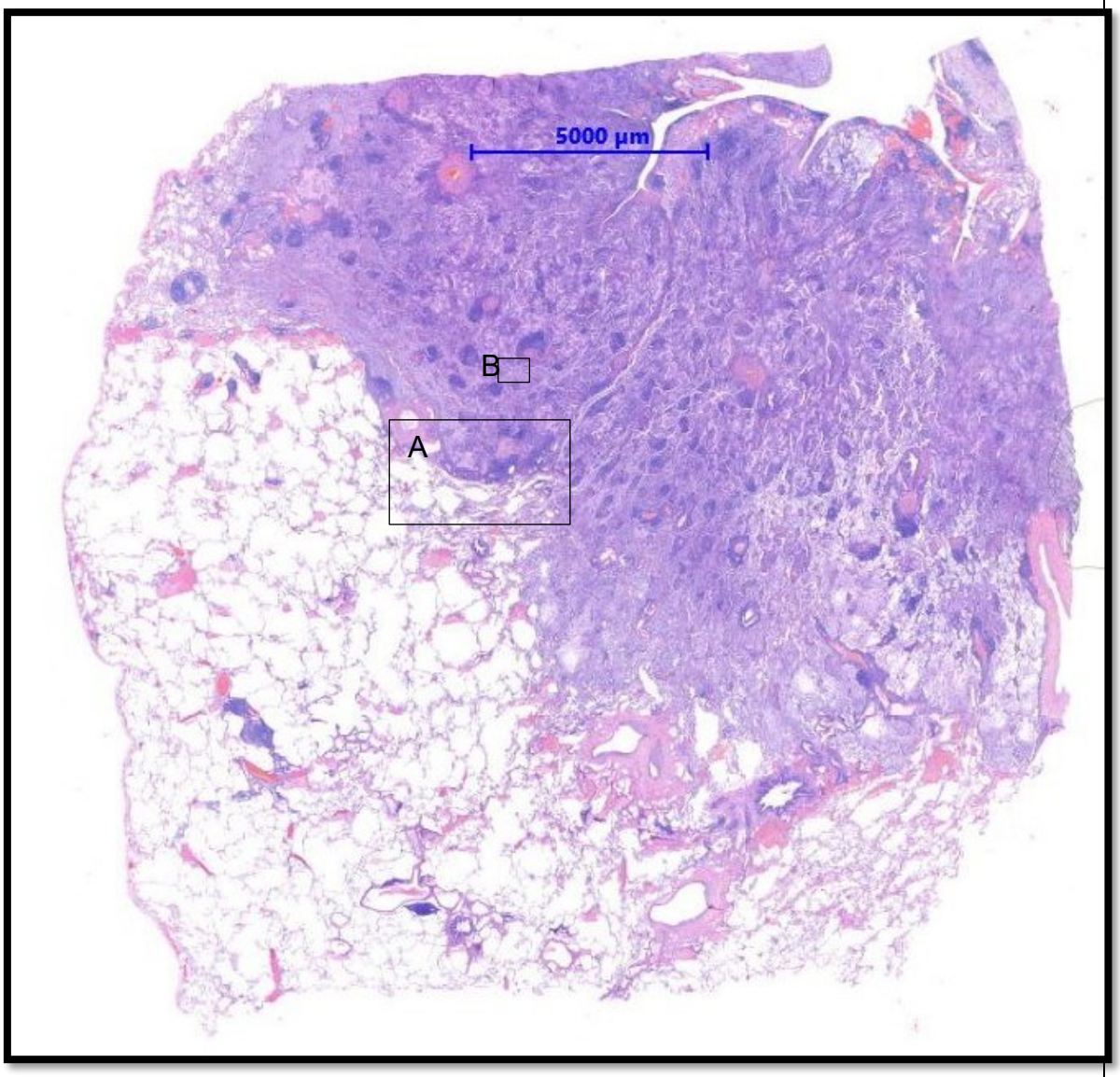

Invasion front divide normal lung parenchyma and adenocarcinoma

Figure 40. Magnification of Figure 39.-A

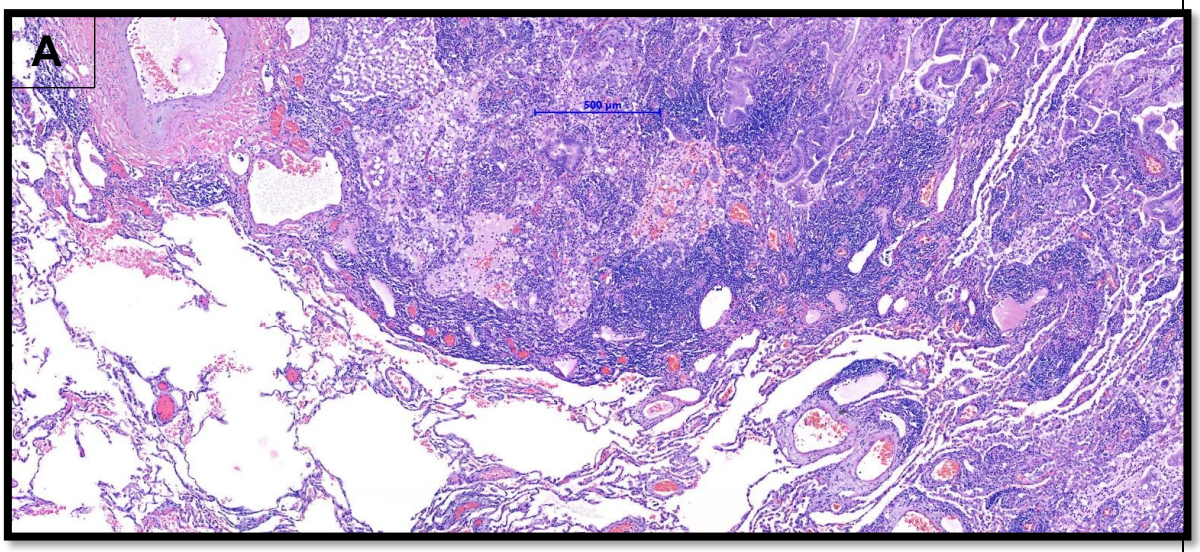

Invasion front - detail

Figure 41. Magnification of Figure 39.-B

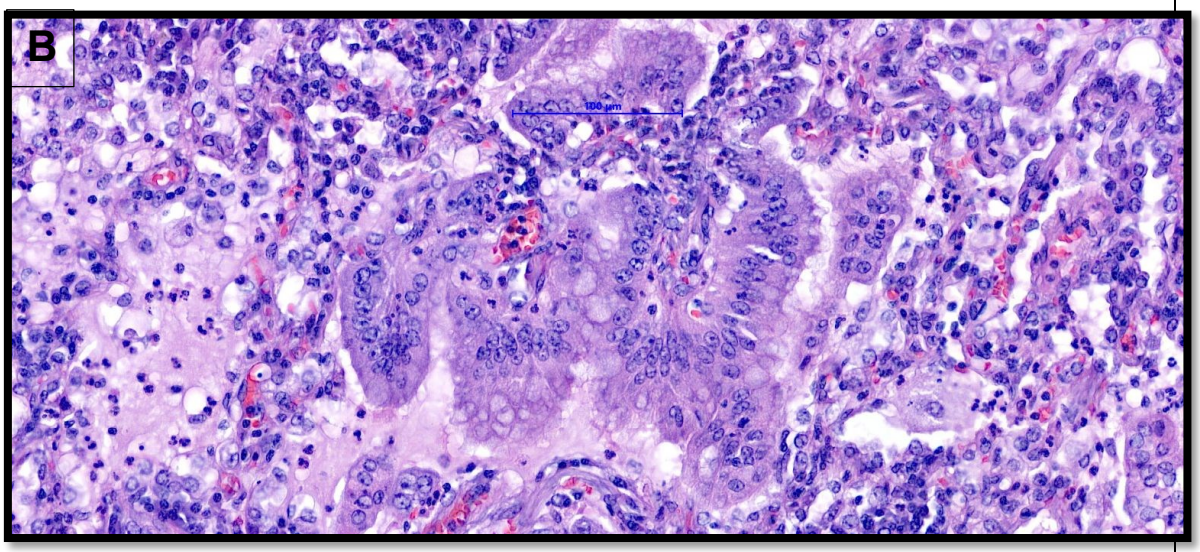

Adenocarcinoma architecture, inflammatory cells

The non-specific signals and the autofluorescence were too strong in this tissue to be able to detect such a specific bacterial signal (Figure 42.6. + 43.3.). The unspecific signals, in turn, are easy to recognize when the image of the probe signal (Figure 43.2.) is compared with the image of the background signal (Figure 43.3.). The signals and their intensity are almost identical. A rough local assignment between H&E and FISH was unfortunately no longer feasible due to the time intervals and the spatial intervals between the cuts.

Figure 42. Adenocarcinoma of the lung, FISH staining, adapted protocol

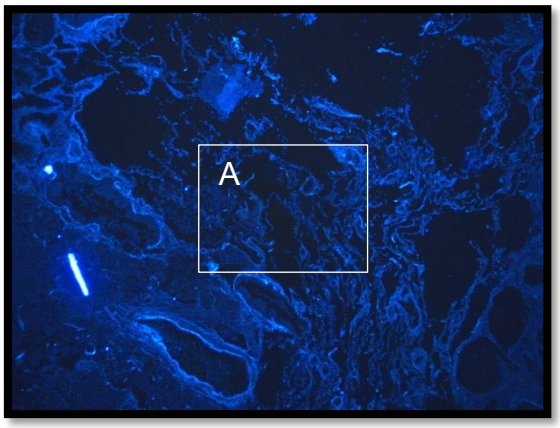

42.1. DAPI - EX387nm, x4

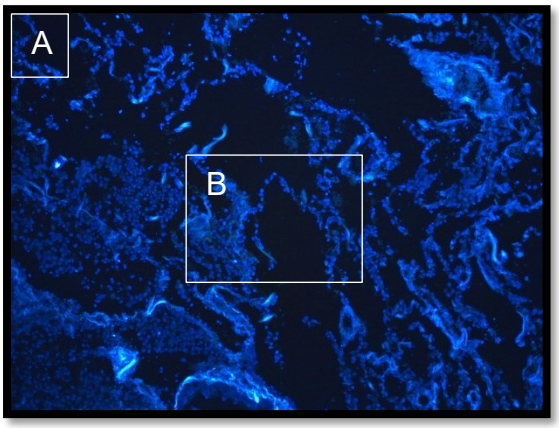

42.2. DAPI - EX387nm, x10

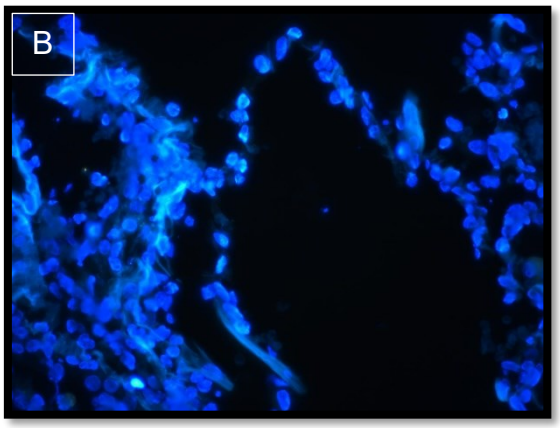

42.3. DAPI - EX387nm, x40

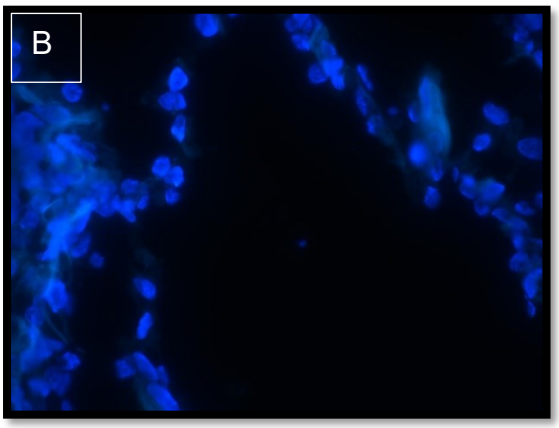

42.4. DAPI - EX387nm, x60

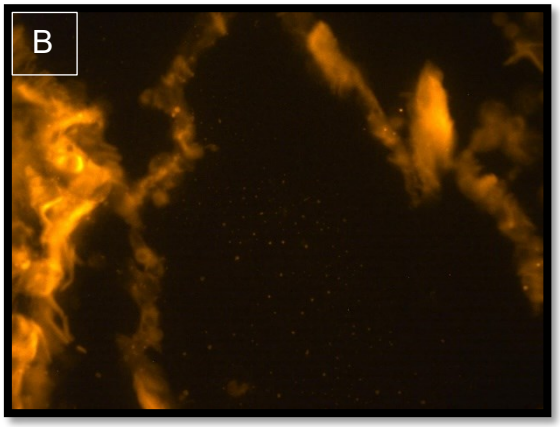

42.5. Probe - EX543nm, x60

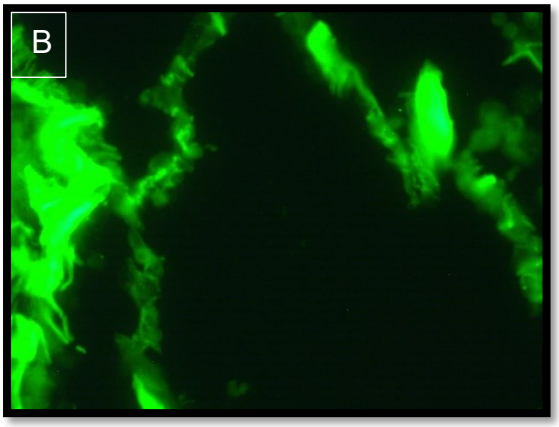

42.6. Background - EX494nm, x60

Detectable tumor cells with typical malignancy criteria in the DAPI filter, no specific signal in probe filter. Background and probe filters are almost identical.

Figure 43. Adenocarcinoma of the lung, FISH staining, adapted protocol

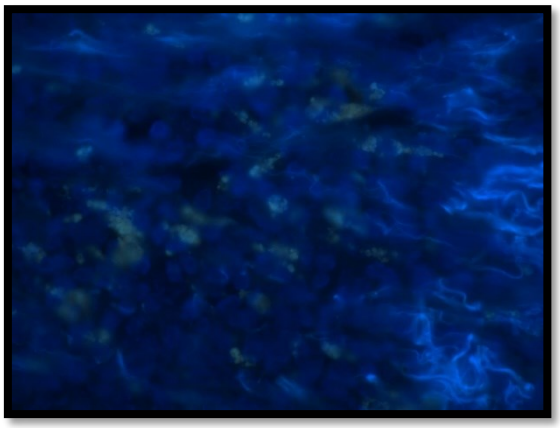

43.1. DAPI - EX387nm, x60

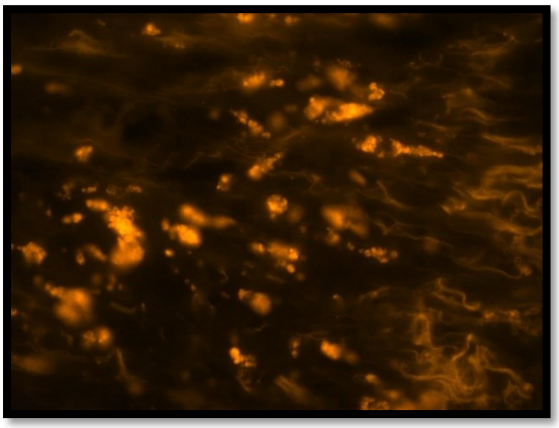

43.2. Probe - EX543nm, x60

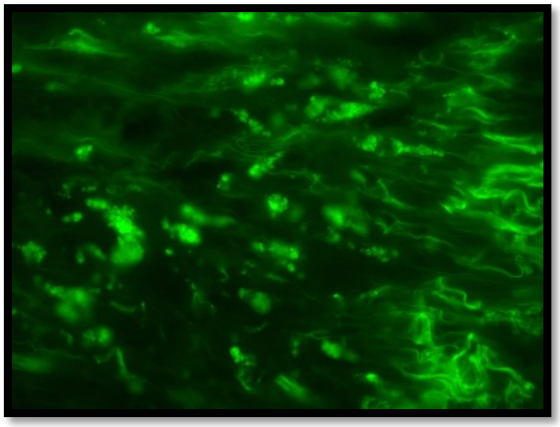

43.3. Background - EX494nm, x60

Massive interference signal which is detectable in all three filters.

3.4. Summary of results:

The following table summarizes the results of our work, classified by test material, in comparison with the original protocols of Madhusudhan et al. (117) and Fu et al. (47).

Table 2. Summary of results classified by test material

Cell block	*Madhusudhan et al.*	*Fu et al.*	*Adapted protocol*
Specificity *(correct negative)*	Correct negative in non-EUB	Correct negative in non-EUB	Correct negative in non-EUB
Sensitivity *(correct positive)*	Gram-negative and Mycobacteria: good performance, Gram-positive staphylococci: intermediate performance	Gram-negative and Mycobacteria: good performance, Gram-positive staphylococci: intermediate performance	Gram-negative and Mycobacteria: intermediate performance (overdigested), Gram-positive staphylococci: intermediate performance
Background/ Auto-fluorescence	Good = low	Poor performance = high	Good = low
Signal intensity	Gram-negative and Mycobacteria: strong, Gram-positive staphylococci: weak	Gram-negative and Mycobacteria: strong, Gram-positive staphylococci: intermediate	Gram-negative and Mycobacteria: intermediate (overdigested), Gram-positive staphylococci: intermediate
Interpretation	Well practicable (with Probe + DAPI + Background images)	Well practicable (with Probe + DAPI + Background images)	Well practicable (with Probe + DAPI + Background images)

GI tissue	*Madhusudhan et al.*	*Fu et al.*	*Adapted protocol*
Specificity *(correct negative)*	Correct negative in non-EUB	Correct negative in non-EUB	Correct negative in non-EUB
Sensitivity *(correct positive)*	Intermediate – some bacteria detectable	Poor performance – no bacteria detectable	Good performance – bacteria detectable
Background/ Auto-fluorescence	Bad = high	Bad = high	Intermediate
Signal intensity	Intermediate	-	Strong
Interpretation	Not easy with low signal intensity and background issues	-	Possible with higher signal intensity and slightly less background issues

Lung tissue	*Madhusudhan et al.*	*Fu et al.*	*Adapted protocol*
Specificity *(correct negative)*	Correct negative in non-EUB	Correct negative in non-EUB	Correct negative in non-EUB
Sensitivity *(correct positive)*	Poor performance – no bacteria detectable	Poor performance – no bacteria detectable	Poor performance – no bacteria detectable
Background/ Auto-fluorescence	Bad = high – very strong background and interfering signals	Bad = high – very strong background and interfering signals	Bad = high – very strong background and interfering signals
Signal intensity	-	-	-
Interpretation	No specific bacterial signal	No specific bacterial signal	No specific bacterial signal

General	*Madhusudhan et al.*	*Fu et al.*	*Adapted protocol*
*Costs**	Intermediate (high lysostaphin concentration)	Low	Low
Hands-on time	Intermediate - completable in one day	High – need two days	Intermediate - completable in one day
Time consumption	High (Prepare reagents…)	High (Prepare reagents…)	High (Prepare reagents…)

*FISH is generally very cost-effective compared to many other sophisticated detection methods.

4. Discussion/Outlook:

With the aim of visualizing tumor-associated bacteria, we asked ourselves the question of methodology. With FISH, we chose a widely used and frequently applied method that has already been used in many areas for visualization experiments (see chapter 1.3.1.). By preparing cell blocks from pure bacteria, we were able to take the first steps towards establishing panbacterial FISH. The interpretation of bacterial cell block material with i) DAPI (387nm, blue spectrum) counterstains as positive controls, ii) the definition of the background at an extinction of 494nm (green spectrum) and iii) the specific probe signal at 543nm (orange spectrum), allowed us to specifically detect bacterial signals against non-specific interfering signals and background noises. In the further process, we adapted general conditions to the needs of the tissue context. First with inflammatory pathologies, before we tested and evaluated our adapted protocol for tumors. With a successful detection in the colon tumor material, we were able to achieve a partial success of 16S rRNA FISH establishment in the tumor tissue context, although the main goal of visualizing

bacteria in lung tumor tissue could not be achieved, most likely because the interference signals and the autofluorescence of the lung tissue were stronger in intensity than the specific probe signal. Therefore, no specific bacterial signals could be detected. With 16S rRNA FISH, a traditional detection method for visualization of bacteria exists, which works reliably. However, it should be noted that the establishment of this method is very time-consuming and there are many factors that can be adjusted to optimize the method. It should also be considered that experienced handling and experienced microscopy of the results are necessary in order to achieve good results. It therefore remains a method that also depends on the examiner.

To give the following discussion a certain organization, we would first like to present and discuss possible further adaptations of the FISH protocol that we consider to be useful. We would then like to discuss the limitations of our method before discussing possible clinical applications of FISH analysis in context of the microbiome and the tumor microbiome.

4.1. FISH adaptions:

One of the easiest and most promising adjustments to make is certainly to extend the hybridization time. According to Young et al. (92), hybridization cannot be "too long" or "overcolor", so that an extension of the hybridization time from 2h to 12-24h probably leads to an improvement in signal intensity. However, it will be necessary to check the post hybridization wash steps I + II, as the slide may need to be washed more intensively to remove unspecific binding after the extended hybridization time. Another simple modification to improve the signal intensity and signal sensitivity might be to increase the sodium dodecyl sulfate (SDS) concentration in the hybridization buffer. With a reasonable range of 2% to 10% SDS concentration, a significant improvement can possibly be achieved. Together with the option of changing the formalin concentration in the macroscopic work-up, these opportunities offering an increasing of the non-specific permeabilization of bacteria (92). After we have adapted our specific enzymatic permeabilization to the hybridization time (2h) and SDS concentration (2%) described in our protocol, it is possible that the combination with an increased non-specific permeabilization (SDS concentration increase and/or hybridization time extension) leads to an excessive digestion of the bacteria and thus to a loss of detection accuracy.

Santos et al. (118) describe, among other things, the possibility of changing the concentration of formamide. A variation range of approx. 10-50% is described here, whereby the detection accuracy of different bacteria reacts differently well/badly to the change in concentration. Consequentially, the hybridization temperature may have to be adjusted according to the function of formamide (92,118).

Dextran sulfate is also a common reagent in FISH protocols. It can reduce the proportion of free water and thus improve the spatial proximity of the probe and their target sequence. This increases the probability of specific binding of both reaction partners (92). While Young et al. (92) speak of a common concentration between 50-100mg/ml, Rocha et al. (119) describe a significantly different signaling result of Gram-positive and Gram-negative bacteria at different dextran sulfate concentrations between 2% - 10% in accordance with pH changes. Therefore, they recommend an adaptation to either Gram-positive bacteria or Gram-negative bacteria (119). For example, Fu et al. (47) chose a concentration of 10% dextran sulfate for their protocol. In addition to increasing the binding specificity, dextran sulfate should also be able to reduce the background signal (118), which could be crucial in the context of FISH application in lung tissue.

The often-used reagents bovine serum albumin (BSA) and tRNA from *E. coli* can also be integrated into the hybridization buffer to block unspecific binding and thus reduce the background signal (92). For example, Fu et al. (47) and Nejman et al. (46) used both BSA at a concentration of 0.02% and tRNA from *E. coli* at a concentration of 1mg/ml in their FISH protocols. Young et al. (92) recommend choosing a BSA concentration between 1mg/ml - 10mg/ml. Regarding the tRNA concentration, they also refer to an extremely wide range of variation and great dependence on the size and type of tissue (92).

Vanadyl-ribonucleoside complex in its function as an RNAase inhibitor can protect the 16S rRNA target sequence from premature non-specific digestion and thus improve method accuracy. Nejman et al. (46) use 2 mM of this substance in their hybridization buffer, whereas Young et al. recommend a concentration of 10 mM (92).

About the reduction of autofluorescence, which greatly disturbed our method especially in the lung tissue context (see Background images from lung tissue), there is the recommendation by Young et al. (92) to treat the sections with 0.1%

Sudan Black in 70% ethanol in addition to the background signal reduction options mentioned above.

To further optimize specific enzymatic digestion, adding the enzyme mutanolysin to the digestion could close a large gap in Gram-positive bacteria. In our enzymatic digestion, we only digested the staphylococci specifically with lysostaphin, while the lysozyme and proteinase K showed an effect primarily against Gram-negative bacteria and mycobacteria in our test series. It is therefore possible that large groups of Gram-positive bacteria such as streptococci are not digested in our enzymatic digestion. It has been described that mutanolysin as N-acetylmuramidase can cleave cell wall components of *Streptococcus spp., Enterococcus spp., Lactobacillus spp., Lactococcus spp*. and *Listeria spp.,* among others (120). However, what we were able to show with our enzymatic dilution series is, that the permeabilization for example in the protocols as carried out by Fu et al. (47) and Nejman et al. (46) might be to a large extent due to the non-specific permeabilization by detergents and formalin. With the described very low enzyme concentrations of these protocols, in our reproduction experiments hardly any specific bacterial signal was detectable in the cell block material, which in principle already require less aggressive digestion than tissue. Also, the morphology of bacteria was not preserved in the results of e.g. Fu et al. (47), Nejman et al. (46) and Madhusudhan et al. (117), whereas in our results the morphology of bacteria remained clearly recognizable. A point that seems at least debatable to us and emphasizes the importance of the comprehensible presentation of results. It is relevant to show the individual images (DAPI + probe + background) in combination with the digitally processed images in order to be able to understand which signals are exactly specific probe signals, how strong the background signal is and which signals are false positive interference signals.

4.2. Limitations of 16S rRNA FISH analysis in FFPE tissue:

There might be several limitations that we have to consider in the context of our protocol and in the context of the whole idea of visualizing the tumor microbiome using FISH.

Probably the biggest challenge of this analysis lies in the nature of the bacteria themselves. The incredible variety of different components of the bacterial cell walls and their architecture in the different bacterial species (121) make an approach in

which all bacteria are to be digested to such an extent that they are perfectly detectable and have not been digested too far, almost impossible. In our series of experiments, we have seen what logically results from the composition of the cell wall components of bacteria and at the same time represents the principle of Gram staining (121–123). Thin-walled Gram-negative bacteria are much easier to digest than thick-walled Gram-positive bacteria. Santos et al. (118) and Rocha et al. (119) also consistently describe the differences in the reactions of Gram-positive bacteria and Gram-negative bacteria in their optimization suggestions and conclude that there should be different protocols for the detection of Gram-positive bacteria on the one hand and Gram-negative bacteria on the other. The extremely superficial classification of bacteria into Gram-positive and Gram-negative is probably far too simple and with the ever-increasing complexity of the bacterial kingdom, an even more detailed description of the characteristics of the bacteria and their reactions to possible changes in FISH protocols is required. With our homemade cell block control, we only tested three different bacterial species for our protocol. There is also the problem of efficiently checking the correctness of the bacterial signal. Although previous positive controls can be run (here cell block material), we have found that even the DAPI counterstaining is not reproducible in every specific bacterial signal (possible overlapping with nuclear materials), so that a precise determination of the global detection of the bacteria present in the stained tissue is a real challenge.

The integration of mutanolysin into specific permeabilization could close a major gap in the field of Gram-positive bacteria. While lysostaphin can only cleave *Staphylococcus*-specific cell wall components, mutanolysin would be able to cleave bacterial cell walls in a much broader Gram-positive range and thus make them permeable for the probe (120). The results in Figure 34. (Chapter 3.3.2.2.) could therefore also be explained by the fact that the cocci in the lung abscess were simply different from staphylococci. *Streptococcus pneumoniae* for example is a common pathogen of pneumonia and consecutive lung abscesses and could not have been adequately digested with our rather short unspecific digestion and the described gap in the Gram-positive range of our specific enzymatic digestion and thus could not be stained at all (124).

In addition to the limitations underlying the composition of the bacteria, there are of course also limitations underlying the method itself and its preparation. For example,

the thickness of a section (5 µm in this case) determines the offset of individual sections. If sections of different stains (e.g. H&E or Gram and FISH) are compared - with the background information that the bacterial size is between 0.2-5µm (125) - it must be noted that the majority of bacteria that can be detected in one section cannot be detected identically in the other section.

What was a big challenge for us and unfortunately still hasn't been solved perfectly is the homogeneous distribution of all reagents applied to the slide. We have tried to optimize this through constant agitation. Of course, the composition of the tissue section also plays an important role here - the size, the surface conditions and the composition of different tissue types (e.g. very loose fatty tissue vs. very dense cellular structures of a squamous cell carcinoma). It is easy to imagine that the absolute quantity of reagents - to stay with the example - does not have to be as high in the area of fatty tissue as in the area of squamous cell carcinoma in order to adequately digest the local bacteria, for example. The absolute amount of reagent pipetted directly onto the slide would of course also have to be set in direct relation to the size of the individual piece of tissue (length x width).

A limitation that should by no means be underestimated in broader sense is the immense amount of time required to take all the factors mentioned above into account. The literature on various FISH protocols is diverse and our suggestions for improvement (see above) are certainly not all-encompassing. The microscopy of FISH analyses is also initially time-consuming and requires some experience in order to be carried out efficiently. Nevertheless, the implementation/continuation of this project would certainly enrich tumor microbiome research in general and could also offer a new diagnostic approach (see below 4.4.).

4.3. Optimized experimental setup:

To further optimize the protocol for tumor tissue, tumors with clear inflammatory signs should be selected again. If necessary, further optimization can also be carried out with inflammatory pathologies (as we have done). In our opinion, there are various options for making a precise statement about the tumor-associated bacteria and their pathophysiological role with an optimized protocol.

For example, immunohistochemical staining could be used to visualize lipoteichoic acid (cell wall component of Gram-positive bacteria) and lipopolysaccharides (cell wall component of Gram-negative bacteria) (121). These signals could then be

compared with the FISH signals in order to find a correlation between these signals and thus validate the correctness of the FISH analysis.

Furthermore, immunohistochemical methods could be used to stain B lymphocytes (CD 20) and T lymphocytes (CD 3, subtypes CD 4 and CD 8) in order to possibly find specific, corresponding distribution patterns that would confirm an interaction between bacteria and the immune system. The fact that chronic inflammation and the microbiome are linked to tumor development and tumor progression via immune cells has already been shown in the lung tumor context (29,30,69,82,84,85,88,89), but not on a visual level.

Since a microbiome analysis in most organs and a rough knowledge of the present microorganisms is already available, as published by Dickson et al. in the lung context (24–26), FISH analysis offers the possibility to refine the probes for certain bacterial species-specific sequences. These results could then be checked for distribution patterns and immunohistochemical correlation again and thus contribute decisively to the idea of "indicator germs" (see chapter 4.4.)

The microbial and immune cell distribution patterns and correlations could then be tested in a further step in different entities of tumors, just as the experimental setup would allow a comparative evaluation of the primary tumor and the associated metastases as also an evaluation of different tumor stages would be possible. Tsay et al. (69) have already described an influence of the changing microbiome (dysbiosis) on lung tumor progression, which could possibly be visualized in this way.

The decisive factor for all possibilities of visual evaluation will be that all sections of the tissue were made in direct succession in order to limit the offset per section (here 5µm) and thus significantly increase the informative value. Of course, this requires an established and reliable protocol for all methods used.

4.4. Future benefits of established 16S rRNA FISH analysis in tumor tissue:

As mentioned in 4.3., some already published results, like the connection between chronic inflammation and dysbiosis and the potential initiation of carcinogenesis (29,30,69,82,84,85,88,89), could be confirmed visually by high-quality FISH analysis. Using panbacterial and bacterial species-specific probes, a precise mapping of the microbial distribution in tissues could be created and also of tumor-

associated microbes in tumors. This means that PCR-based results from microbiome analyses can also be confirmed visually. In addition, the visual method is always a method that is much less susceptible to contamination, with which PCR-based methods sometimes have massive problems (90). Under the microscope, the level of the signals can be detected very precisely in comparison to the surrounding tissue, thus enabling reliable identification of the bacteria localized in the tissue. Once the bacteria have been fixed in the tissue as part of the macroscopic processing and fixation, microscopy and the level of the bacteria in relation to the surrounding tissue make it possible to rule out contamination. Bacteria brought in from the outside would be detected microscopically at a very superficial level and not in direct relation to the surrounding tissue.

Another interesting area of application is in the field of diagnostics. In lung tumors the differentiation between primary tumors and metastasis is always important. In special cases of lung tumor diagnostics, it is about the distinction between (i) primary mucinous adenocarcinoma of the lung vs. metastasis into the lung of a mucinous adenocarcinoma of the colon and (ii) primary squamous cell carcinoma in the lung vs. metastasis into the lung of a known squamous cell carcinoma of the mouth/throat region. Here it is often difficult to make a differential diagnosis even with highly developed pathological diagnostic methods. In order to understand why 16S rRNA FISH analysis could bring a real revolution in routine diagnostics, we must first recapitulate some physiological facts and research results. First, we need to recall the physiological colonization of the areas where the primary tumor in question is located (14,15,44). In this case, the mouth and throat area and the colon (126–130). We compare this with the physiological microbiome of the lungs (26,30,128,129,131) and find differences. We now do the same with corresponding primary tumors and again find clear differences (35,62,70,84,132), whereby individual differences must be pointed out. In a second step, we must reconsider the results of Fu et al. (47). They were able to prove that intratumoral pathogens can participate and influence the path of metastasis. With this knowledge, it can now be hypothesized that it is possible to identify certain “indicator germs”, as Sepich-Poore et al. have already mentioned this idea in general in their review (90), for (i) the metastasis into the lung from the mucinous adenocarcinoma of the colon and for (ii) the metastasis into the lung from the squamous cell carcinoma of the mouth/throat region, which allow an explicit differentiation from the primary tumor in the lung. To

do this, a high percentage of these indicator germs would have to follow the metastatic path from the primary tumor and should never be detectable in a primary lung tumor. With specific probes for these indicator germs, this complex question could be answered using a simple and affordable FISH analysis. In this way, a high-quality and optimized FISH analysis that stains very specific bacteria could find its way into routine pathology diagnostics.

5. Summary:

To summarize, we must honestly admit that we have only carried out a small part of possible adaptations of a panbacterial FISH analysis in this work and that much work remains to be done. Nevertheless, besides an acceptable specific enzymatic digestion on which further modifications are possible, we were able to present a comprehensible general way of establishing a bacterial FISH. Important and memorable points of our work are certainly on the one hand the partially preserved morphology of the bacteria in the tissue context, as our results clearly show, and on the other hand the comprehensible presentation of different extinctions and digital processed images, which allow a precise interpretation. The discussion of different adaptation ideas and limitations to be considered will hopefully provide a good basis for future optimization attempts.

6. References:

1. STATISTICS AUSTRIA. Number of cancer patients 15% higher by 2030 | Enhanced Reader [Internet]. 2024 [cited 2024 Mar 12]. Available from: https://www.statistik.at/fileadmin/announcement/2024/01/20240125Krebsstatistik2022EN.pdf

2. Emrich K, Kraywinkel K. Epidemiology of small cell lung cancer in Germany: An update. Onkologe. 2021 Sep 1;27(9):858–61.

3. Kraywinkel K, Barnes B. Epidemiologie des kleinzelligen Lungenkarzinoms in Deutschland. Onkologe. 2017;23:334–9.

4. Kraywinkel K, Schönfeld I. Epidemiology of non-small cell lung cancer in Germany. Onkologe. 2018 Dec 1;24(12):946–51.

5. Herold G. Innere Medizin. Vol. 2023. Köln: Dr. med. Gerd Herold; 2023. 402–408 p.

6. Wörmann B. Empfehlungen der Fachgesellschaft zur Diagnostik und Therapie hämatologischer und onkologischer Erkrankungen Leitlinie Lungenkarzinom, nicht-kleinzellig (NSCLC) [Internet]. Berlin; 2023. Available from: www.onkopedia.com

7. Wörmann B. Empfehlungen der Fachgesellschaft zur Diagnostik und Therapie hämatologischer und onkologischer Erkrankungen Leitlinie Lungenkarzinom, kleinzellig (SCLC) [Internet]. Berlin; 2023. Available from: www.onkopedia.com

8. Nicholson AG, Tsao MS, Beasley MB, Borczuk AC, Brambilla E, Cooper WA, et al. The 2021 WHO Classification of Lung Tumors: Impact of Advances Since 2015. Journal of Thoracic Oncology. 2022 Mar 1;17(3):362–87.

9. Böcker DHHKM. Pathologie. 5th ed. München: Elsevier GmbH; 2012. 506–513 p.

10. Andre F, Arnold D, Ascierto PA, Bielack S, Yves Blay J, Cappuzzo F, et al. appendix 2 2nd ESMO Consensus Conference in Lung Cancer: locally advanced stage III non-small-cell lung cancer Annals of Oncology special articles. Annals of Oncology. 2015;26:1573–88.

11. Hendriks LE, Kerr KM, Menis J, Mok TS, Nestle U, Passaro A, et al. Oncogene-addicted metastatic non-small-cell lung cancer: ESMO Clinical Practice Guideline for diagnosis, treatment and follow-up☆ 2023 [cited 2024 Jul 19]; Available from: https://doi.org/10.1016/j.annonc.2022.12.009

12. Requena T, Velasco M, Homeostasis M;, Simbiosis ;, Enfermedad ; Revista Clínica Española The human microbiome in sickness and in health PALABRAS CLAVE. Rev Clin Esp [Internet]. 2021 [cited 2024 Apr 4];221:233–40. Available from: www.elsevier.es/rce

13. Berg G, Rybakova D, Fischer D, Cernava T, Vergès MCC, Charles T, et al. Microbiome definition re-visited: old concepts and new challenges. Microbiome [Internet]. 2020 Jun 30 [cited 2024 Apr 4];8(1):1–22. Available from: https://microbiomejournal.biomedcentral.com/articles/10.1186/s40168-020-00875-0

14. Sender R, Fuchs S, Milo R. Revised Estimates for the Number of Human and Bacteria Cells in the Body. 2016 [cited 2024 Mar 13]; Available from: https://erc.europa.eu/funding-and-grants

15. Kostic AD. The human microbiome: A coming of age story. Vol. 30, Cell Host and Microbe. Cell Press; 2022. p. 449–53.

16. Manos J. The human microbiome in disease and pathology. APMIS [Internet]. 2022 Dec 1 [cited 2024 Apr 5];130(12):690–705. Available from: https://pubmed-1ncbi-1nlm-1nih-1gov-10013b5ij29e4.han.medunigraz.at/35393656/

17. Bivar Xavier K. Bacterial interspecies quorum sensing in the mammalian gut microbiota. C R Biol [Internet]. 2018 May 1 [cited 2024 Apr 5];341(5):297–9. Available from: https://doi.org/10.1016/j.crvi.2018.03.006

18. Nishida A, Inoue R, Inatomi O, Bamba S, Naito Y, Andoh A. Gut microbiota in the pathogenesis of inflammatory bowel disease. Clin J Gastroenterol. 2018 Feb 1;11(1).

19. Sheehan D, Moran C, Shanahan F. The microbiota in inflammatory bowel disease. J Gastroenterol. 2015 May 1;50(5):495–507.

20. Schneeberger M, Everard A, Gómez-Valadés AG, Matamoros S, Ramírez S, Delzenne NM, et al. Akkermansia muciniphila inversely correlates with the onset of inflammation, altered adipose tissue metabolism and metabolic disorders during obesity in mice. Scientific Reports 2015 5:1 [Internet]. 2015 Nov 13 [cited 2024 Apr 5];5(1):1–14. Available from: https://www.nature.com/articles/srep16643

21. Li J, Lin S, Vanhoutte PM, Woo CW, Xu A. Akkermansia muciniphila protects against atherosclerosis by preventing metabolic endotoxemia-induced inflammation in Apoe-/- Mice. Circulation [Internet]. 2016 Jun 14 [cited 2024 Apr 5];133(24):2434–46. Available from: https://www-1ahajournals-1org-10013b5ij2c8e.han.medunigraz.at/doi/abs/10.1161/CIRCULATIONAHA.115.019645

22. El Hage R, Hernandez-Sanabria E, Van de Wiele T. Emerging trends in "smart probiotics": Functional consideration for the development of novel health and industrial applications. Front Microbiol. 2017 Sep 29;8(SEP):291773.

23. Tropini C, Earle KA, Huang KC, Sonnenburg JL. The Gut Microbiome: Connecting Spatial Organization to Function. Cell Host Microbe. 2017 Apr 12;21(4):433–42.

24. Dickson RP, Erb-Downward JR, Freeman CM, McCloskey L, Falkowski NR, Huffnagle GB, et al. Bacterial topography of the healthy human lower respiratory tract. mBio. 2017 Jan 1;8(1).

25. Dickson RP, Erb-Downward JR, Falkowski NR, Hunter EM, Ashley SL, Huffnagle GB. The lung microbiota of healthy mice are highly variable, cluster by environment, and reflect variation in baseline lung innate immunity. Am J Respir Crit Care Med. 2018 Aug 15;198(4):497–508.

26. Dickson RP, Erb-Downward JR, Martinez FJ, Huffnagle GB. The Microbiome and the Respiratory Tract. Annu Rev Physiol [Internet]. 2016 Feb 2 [cited 2024 Mar 13];78:481. Available from: /pmc/articles/PMC4751994/

27. Dickson RP, Erb-Downward JR, Freeman CM, McCloskey L, Beck JM, Huffnagle GB, et al. Spatial variation in the healthy human lung microbiome and the adapted island model of lung biogeography. Ann Am Thorac Soc

[Internet]. 2015 Jun 1 [cited 2024 Apr 5];12(6):821–30. Available from: www.clinicaltrials.gov

28. Frayman KB, Wylie KM, Armstrong DS, Carzino R, Davis SD, Ferkol TW, et al. Differences in the lower airway microbiota of infants with and without cystic fibrosis. Journal of Cystic Fibrosis. 2019 Sep 1;18(5):646–52.

29. O'Dwyer DN, Dickson RP, Moore BB. The Lung Microbiome, Immunity, and the Pathogenesis of Chronic Lung Disease. The Journal of Immunology. 2016 Jun 15;196(12):4839–47.

30. O'Dwyer DN, Dickson RP, Moore BB. The Lung Microbiome, Immunity, and the Pathogenesis of Chronic Lung Disease. J Immunol [Internet]. 2016 Jun 15 [cited 2024 Mar 11];196(12):4839–47. Available from: https://pubmed-1ncbi-1nlm-1nih-1gov-10013b5m8232d.han.medunigraz.at/27260767/

31. Erb-Downward JR, Thompson DL, Han MK, Freeman CM, McCloskey L, Schmidt LA, et al. Analysis of the Lung Microbiome in the "Healthy" Smoker and in COPD. PLoS One [Internet]. 2011 [cited 2024 Apr 5];6(2):e16384. Available from: https://journals.plos.org/plosone/article?id=10.1371/journal.pone.0016384

32. Charlson ES, Diamond JM, Bittinger K, Fitzgerald AS, Yadav A, Haas AR, et al. Lung-enriched Organisms and Aberrant Bacterial and Fungal Respiratory Microbiota after Lung Transplant. https://doi.org/101164/rccm201204-0693OC [Internet]. 2012 Dec 14 [cited 2024 Apr 5];186(6):536–45. Available from: www.atsjournals.org

33. Sze MA, Dimitriu PA, Hayashi S, Elliott WM, McDonough JE, Gosselink J V., et al. The Lung Tissue Microbiome in Chronic Obstructive Pulmonary Disease. https://doi.org/101164/rccm201111-2075OC [Internet]. 2012 Dec 14 [cited 2024 Apr 5];185(10):1073–80. Available from: www.atsjournals.org

34. Wang Q, Li F, Liang B, Liang Y, Chen S, Mo X, et al. A metagenome-wide association study of gut microbiota in asthma in UK adults. BMC Microbiol [Internet]. 2018 Sep 12 [cited 2024 Apr 5];18(1):1–7. Available from: https://bmcmicrobiol.biomedcentral.com/articles/10.1186/s12866-018-1257-x

35. Sepich-Poore GD, Zitvogel L, Straussman R, Hasty J, Wargo JA, Knight R. The microbiome and human cancer. Vol. 371, Science. American Association for the Advancement of Science; 2021.

36. [Papyrus Ebers- the greatest Egyptian medical document] - Digital Collections - National Library of Medicine [Internet]. [cited 2024 Mar 13]. Available from: https://collections.nlm.nih.gov/catalog/nlm:nlmuid-101434622-img

37. Busch W. Berliner klinische Wochenschrift. 1866 [cited 2024 Mar 13]. p. 245–6 #251 - Berliner klinische Wochenschrift v.3 1866. - Full View | HathiTrust Digital Library. Available from: https://babel.hathitrust.org/cgi/pt?id=mdp.39015079976141&view=1up&seq=251

38. Busch W. Berliner klinische Wochenschrift. 1868 [cited 2024 Mar 13]. p. 137–8 #147 - Berliner klinische Wochenschrift v.5 1868. - Full View | HathiTrust Digital Library. Available from: https://babel.hathitrust.org/cgi/pt?id=mdp.39015020939958&view=1up&seq=147

39. Fehleisen F. Deutsche medizinische Wochenschrift. 1882 [cited 2024 Mar 13]. p. 553–4 #567 - Deutsche medizinische Wochenschrift v.8 1882. - Full View | HathiTrust Digital Library. Available from: https://babel.hathitrust.org/cgi/pt?id=mdp.39015023225710&seq=567

40. Starnes CO. Coley's toxins in perspective. Nature 1992 357:6373 [Internet]. 1992 [cited 2024 Mar 13];357(6373):11–2. Available from: https://www-1nature-1com-10013b5m82b98.han.medunigraz.at/articles/357011a0

41. Livingston-Wheeler therapy. CA Cancer J Clin. 1990 Mar 1;40(2):103–8.

42. White MK, Pagano JS, Khalili K. Viruses and Human Cancers: a Long Road of Discovery of Molecular Paradigms. Clin Microbiol Rev [Internet]. 2014 [cited 2024 Mar 13];27(3):463. Available from: /pmc/articles/PMC4135891/

43. Zapatka M, Borozan I, Brewer DS, Iskar M, Grundhoff A, Alawi M, et al. The landscape of viral associations in human cancers. Nat Genet [Internet]. 2020 Mar 1 [cited 2024 Mar 11];52(3):320–30. Available from: https://pubmed-1ncbi-1nlm-1nih-1gov-10013b5m8251b.han.medunigraz.at/32025001/

44. Huttenhower C, Gevers D, Knight R, Abubucker S, Badger JH, Chinwalla AT, et al. Structure, function and diversity of the healthy human microbiome. Nature. 2012 Jun 14;486(7402):207–14.

45. Charlson ES, Bittinger K, Haas AR, Fitzgerald AS, Frank I, Yadav A, et al. Topographical continuity of bacterial populations in the healthy human respiratory tract. Am J Respir Crit Care Med. 2011 Oct 15;184(8):957–63.

46. Nejman D, Livyatan I, Fuks G, Gavert N, Zwang Y, Geller LT, et al. The human tumor microbiome is composed of tumor type-specific intracellular bacteria. Science (1979). 2020 May 29;368(6494):973–80.

47. Fu A, Yao B, Dong T, Chen Y, Yao J, Liu Y, et al. Tumor-resident intracellular microbiota promotes metastatic colonization in breast cancer. Cell. 2022 Apr 14;185(8):1356-1372.e26.

48. Galeano Niño JL, Wu H, LaCourse KD, Kempchinsky AG, Baryiames A, Barber B, et al. Effect of the intratumoral microbiota on spatial and cellular heterogeneity in cancer. Nature [Internet]. 2022 Nov 24;611(7937):810–7. Available from: https://www.nature.com/articles/s41586-022-05435-0

49. Geller LT, Barzily-Rokni M, Danino T, Jonas OH, Shental N, Nejman D, et al. Potential role of intratumor bacteria in mediating tumor resistance to the chemotherapeutic drug gemcitabine. Science (1979). 2017 Sep 15;357(6356):1156–60.

50. Pernigoni N, Zagato E, Calcinotto A, Troiani M, Pereira Mestre R, Calì B, et al. Commensal bacteria promote endocrine resistance in prostate cancer through androgen biosynthesis [Internet]. Available from: https://www.science.org

51. Shiao SL, Kershaw KM, Limon JJ, You S, Yoon J, Ko EY, et al. Commensal bacteria and fungi differentially regulate tumor responses to radiation therapy. Cancer Cell. 2021 Sep 13;39(9):1202-1213.e6.

52. Uribe-Herranz M, Rafail S, Beghi S, Gil-De-Gómez L, Verginadis I, Bittinger K, et al. Gut microbiota modulate dendritic cell antigen presentation and radiotherapy-induced antitumor immune response. J Clin Invest [Internet]. 2020 Jan 2 [cited 2024 Mar 11];130(1):466–79. Available from:

https://pubmed-1ncbi-1nlm-1nih-1gov-10013b5m8232d.han.medunigraz.at/31815742/

53. Matson V, Fessler J, Bao R, Chongsuwat T, Zha Y, Alegre ML, et al. The commensal microbiome is associated with anti-PD-1 efficacy in metastatic melanoma patients. Science (1979). 2018;359(6371):104–8.

54. Routy B, Le Chatelier E, Derosa L, Duong CPM, Alou MT, Daillère R, et al. Gut microbiome influences efficacy of PD-1-based immunotherapy against epithelial tumors. Science (1979) [Internet]. 2018 Jan 5 [cited 2024 Mar 11];359(6371):91–7. Available from: https://www.science.org/doi/10.1126/science.aan3706

55. Gopalakrishnan V, Spencer CN, Nezi L, Reuben A, Andrews MC, Karpinets T V., et al. Gut microbiome modulates response to anti–PD-1 immunotherapy in melanoma patients. Science [Internet]. 2018 Jan 1 [cited 2024 Mar 11];359(6371):97. Available from: /pmc/articles/PMC5827966/

56. Derosa L, Hellmann MD, Spaziano M, Halpenny D, Fidelle M, Rizvi H, et al. Negative association of antibiotics on clinical activity of immune checkpoint inhibitors in patients with advanced renal cell and non-small-cell lung cancer. Ann Oncol [Internet]. 2018 Jun 1 [cited 2024 Mar 11];29(6):1437–44. Available from: https://pubmed-1ncbi-1nlm-1nih-1gov-10013b5m8240d.han.medunigraz.at/29617710/

57. Pinato DJ, Howlett S, Ottaviani D, Urus H, Patel A, Mineo T, et al. Association of Prior Antibiotic Treatment With Survival and Response to Immune Checkpoint Inhibitor Therapy in Patients With Cancer. JAMA Oncol [Internet]. 2019 Dec 1 [cited 2024 Mar 11];5(12):1774–8. Available from: https://pubmed-1ncbi-1nlm-1nih-1gov-10013b5m8240d.han.medunigraz.at/31513236/

58. Tanoue T, Morita S, Plichta DR, Skelly AN, Suda W, Sugiura Y, et al. A defined commensal consortium elicits CD8 T cells and anti-cancer immunity. Nature [Internet]. 2019 Jan 31 [cited 2024 Mar 11];565(7741):600–5. Available from: https://pubmed-1ncbi-1nlm-1nih-1gov-10013b5m821d3.han.medunigraz.at/30675064/

59. Di Modica M, Gargari G, Regondi V, Bonizzi A, Arioli S, Belmonte B, et al. Gut microbiota condition the therapeutic efficacy of trastuzumab in HER2-positive breast cancer. Cancer Res. 2021 Apr 1;81(8):2195–206.

60. Griffin ME, Espinosa J, Becker JL, Luo JD, Carroll TS, Jha JK, et al. Enterococcus peptidoglycan remodeling promotes checkpoint inhibitor cancer immunotherapy. Science (1979). 2021 Aug 27;373(6558):1040–6.

61. Kwong TNY, Wang X, Nakatsu G, Chow TC, Tipoe T, Dai RZW, et al. Association Between Bacteremia From Specific Microbes and Subsequent Diagnosis of Colorectal Cancer. Gastroenterology. 2018 Aug 1;155(2):383-390.e8.

62. Poore GD, Kopylova E, Zhu Q, Carpenter C, Fraraccio S, Wandro S, et al. Microbiome analyses of blood and tissues suggest cancer diagnostic approach. Nature. 2020 Mar 26;579(7800):567–74.

63. Zeller G, Tap J, Voigt AY, Sunagawa S, Kultima JR, Costea PI, et al. Potential of fecal microbiota for early-stage detection of colorectal cancer. Mol Syst Biol. 2014 Nov;10(11):766.

64. Gorkiewicz G. Microbiome Diagnostics—Useful for Medical Practice? J Gastroenterol Hepatol Erkrank. 2021 Dec 1;19(4):98–104.

65. Halwachs B, Madhusudhan N, Krause R, Nilsson RH, Moissl-Eichinger C, Högenauer C, et al. Critical issues in mycobiota analysis. Front Microbiol. 2017 Feb 14;8(FEB).

66. Parhi L, Alon-Maimon T, Sol A, Nejman D, Shhadeh A, Fainsod-Levi T, et al. Breast cancer colonization by Fusobacterium nucleatum accelerates tumor growth and metastatic progression. Nat Commun [Internet]. 2020 Dec 1 [cited 2024 Mar 11];11(1). Available from: https://pubmed-1ncbi-1nlm-1nih-1gov-10013b5m8232d.han.medunigraz.at/32591509/

67. Janney A, Powrie F, Mann EH. Host–microbiota maladaptation in colorectal cancer. Vol. 585, Nature. Nature Research; 2020. p. 509–17.

68. Riquelme E, Zhang Y, Zhang L, Montiel M, Zoltan M, Dong W, et al. Tumor Microbiome Diversity and Composition Influence Pancreatic Cancer Outcomes. Cell. 2019 Aug 8;178(4):795-806.e12.

69. Tsay JCJ, Wu BG, Sulaiman I, Gershner K, Schluger R, Li Y, et al. Lower airway dysbiosis affects lung cancer progression. Cancer Discov. 2021 Feb 1;11(2):293–307.

70. Dadkhah E, Sikaroodi M, Korman L, Hardi R, Baybick J, Hanzel D, et al. Gut microbiome identifies risk for colorectal polyps. BMJ Open Gastroenterol. 2019 May 1;6(1).

71. Conry RM, Westbrook B, Mckee S, Norwood TG. Talimogene laherparepvec: First in class oncolytic virotherapy. Hum Vaccin Immunother [Internet]. 2018 [cited 2024 Mar 11];14. Available from: https://doi.org/10.1080/21645515.2017.1412896

72. Zhou S, Gravekamp C, Bermudes D, Liu K. Tumour-targeting bacteria engineered to fight cancer. Vol. 18, Nature Reviews Cancer. Nature Publishing Group; 2018. p. 727–43.

73. Kramer MG, Masner M, Ferreira FA, Hoffman RM. Bacterial therapy of cancer: Promises, limitations, and insights for future directions. Front Microbiol. 2018 Jan 23;9(JAN).

74. Forbes NS. Engineering the perfect (bacterial) cancer therapy. Vol. 10, Nature Reviews Cancer. 2010. p. 785–94.

75. Chowdhury S, Castro S, Coker C, Hinchliffe TE, Arpaia N, Danino T. Programmable bacteria induce durable tumor regression and systemic antitumor immunity. Nat Med. 2019 Jul 1;25(7):1057–63.

76. Charbonneau MR, Isabella VM, Li N, Kurtz CB. Developing a new class of engineered live bacterial therapeutics to treat human diseases. Vol. 11, Nature Communications. Nature Research; 2020.

77. Chowdhury S, Castro S, Coker C, Hinchliffe TE, Arpaia N, Danino T. Programmable bacteria induce durable tumor regression and systemic antitumor immunity. Nat Med. 2019 Jul 1;25(7):1057–63.

78. Chieng Yeo C, Min JJ, Tripathi K, Chuah LH, Gabriela Kramer M, Masner M, et al. Bacterial Therapy of Cancer: Promises, Limitations, and Insights for Future Directions. 2018 [cited 2024 Mar 11]; Available from: www.frontiersin.org

79. Hanahan D, Weinberg RA. The Hallmarks of Cancer Review evolve progressively from normalcy via a series of pre. Cell. 2000;100:57–70.

80. Hanahan D. Hallmarks of Cancer: New Dimensions. Vol. 12, Cancer Discovery. American Association for Cancer Research Inc.; 2022. p. 31–46.

81. Segal LN, Alekseyenko A V., Clemente JC, Kulkarni R, Wu B, Chen H, et al. Enrichment of lung microbiome with supraglottic taxa is associated with increased pulmonary inflammation. Microbiome. 2013 Jul 1;1(1).

82. Segal LN, Clemente JC, Tsay JCJ, Koralov SB, Keller BC, Wu BG, et al. Enrichment of the lung microbiome with oral taxa is associated with lung inflammation of a Th17 phenotype. Nat Microbiol. 2016 Apr 4;1(5).

83. Dickson RP, Morris A. Macrolides, inflammation and the lung microbiome: Untangling the web of causality. Vol. 72, Thorax. BMJ Publishing Group; 2017. p. 10–2.

84. Jin C, Lagoudas GK, Zhao C, Bullman S, Bhutkar A, Hu B, et al. Commensal Microbiota Promote Lung Cancer Development via γδ T Cells. Cell. 2019 Feb 21;176(5):998-1013.e16.

85. Tsay JCJ, Wu BG, Badri MH, Clemente JC, Shen N, Meyn P, et al. Airway microbiota is associated with upregulation of the PI3K pathway in lung cancer. Am J Respir Crit Care Med. 2018 Nov 1;198(9):1188–98.

86. Lee SH, Sung JY, Yong D, Chun J, Kim SY, Song JH, et al. Characterization of microbiome in bronchoalveolar lavage fluid of patients with lung cancer comparing with benign mass like lesions. Lung Cancer. 2016 Dec 1;102:89–95.

87. Greathouse KL, White JR, Vargas AJ, Bliskovsky V V., Beck JA, von Muhlinen N, et al. Interaction between the microbiome and TP53 in human lung cancer. Genome Biol. 2018 Aug 24;19(1).

88. Palucka AK, Coussens LM. The Basis of OncoImmunology. Cell [Internet]. 2016 Mar 3 [cited 2024 Mar 13];164(6):1233. Available from: /pmc/articles/PMC4788788/

89. Marsland BJ, Gollwitzer ES. Host–microorganism interactions in lung diseases. Nature Reviews Immunology 2014 14:12 [Internet]. 2014 Nov 25 [cited 2024 Mar 13];14(12):827–35. Available from: https://www-1nature-1com-10013b5m82da5.han.medunigraz.at/articles/nri3769

90. Sepich-Poore GD, Guccione C, Laplane L, Pradeu T, Curtius K, Knight R. Cancer's second genome: Microbial cancer diagnostics and redefining clonal evolution as a multispecies process: Humans and their tumors are not aseptic, and the multispecies nature of cancer modulates clinical care and clonal evolution. Vol. 44, BioEssays. John Wiley and Sons Inc; 2022.

91. Cui C, Li SW. Fluorescence In situ Hybridization: Cell-Based Genetic Diagnostic and Research Applications. Fluorescence In situ Hybridization: Cell-Based Genetic Diagnostic and Research Applications Front Cell Dev Biol [Internet]. 2016;4:89. Available from: www.frontiersin.org

92. Young AP, Jackson DJ, Wyeth RC. A technical review and guide to RNA fluorescence in situ hybridization.

93. Bishop R, Stead DA. Applications of fluorescence in situ hybridization (FISH) in detecting genetic aberrations of medical significance. Bioscience Horizons: The International Journal of Student Research [Internet]. 2010 Mar 1 [cited 2024 Apr 8];3(1):85–95. Available from: https://dx.doi.org/10.1093/biohorizons/hzq009

94. Gall JG, Lou M, Kline P, Giles NH. FORMATION AND DETECTION OF RNA-DNA HYBRID MOLECULES IN CYTOLOGICAL PREPARATIONS. Proc Natl Acad Sci U S A [Internet]. 1969 [cited 2024 Mar 14];63(2):378. Available from: /pmc/articles/PMC223575/?report=abstract

95. Rudkin GT, Stollar BD. High resolution detection of DNA–RNA hybrids in situ by indirect immunofluorescence. Nature 1977 265:5593 [Internet]. 1977 Feb 1 [cited 2024 Mar 14];265(5593):472–3. Available from: https://www-1nature-1com-10013b5xy00f6.han.medunigraz.at/articles/265472a0

96. Bauman JGJ, Wiegant J, Borst P, van Duijn P. A new method for fluorescence microscopical localization of specific DNA sequences by in situ hybridization of fluorochrome-labelled RNA. Exp Cell Res. 1980 Aug 1;128(2):485–90.

97. Singer RH, Ward DC. Actin gene expression visualized in chicken muscle tissue culture by using in situ hybridization with a biotinated nucleotide analog. Proc Natl Acad Sci U S A [Internet]. 1982 [cited 2024 Mar 14];79(23):7331. Available from: /pmc/articles/PMC347333/?report=abstract

98. Arrigucci R, Bushkin Y, Radford F, Lakehal K, Vir P, Pine R, et al. FISH-Flow, a protocol for the concurrent detection of mRNA and protein in single cells using fluorescence in situ hybridization and flow cytometry HHS Public Access Author manuscript. Nat Protoc [Internet]. 2017 [cited 2024 Mar 14];12(6):1245–60. Available from: http://www.nature.com/reprints/index.html.

99. El-Heliebi A, Kashofer K, Fuchs J, Jahn SW, Viertler C, Matak A, et al. Visualization of tumor heterogeneity by in situ padlock probe technology in colorectal cancer. Histochem Cell Biol. 2017 Aug 1;148(2):105–15.

100. Rowley JD. A New Consistent Chromosomal Abnormality in Chronic Myelogenous Leukaemia identified by Quinacrine Fluorescence and Giemsa Staining. Nature 1973 243:5405 [Internet]. 1973 [cited 2024 Apr 9];243(5405):290–3. Available from: https://www-1nature-1com-10013b5ij3912.han.medunigraz.at/articles/243290a0

101. Mitelman F, Johansson B, Mertens F. The impact of translocations and gene fusions on cancer causation. Nature Reviews Cancer 2007 7:4 [Internet]. 2007 Mar 15 [cited 2024 Apr 9];7(4):233–45. Available from: https://www-1nature-1com-10013b5ij3912.han.medunigraz.at/articles/nrc2091

102. Case RJ, Boucher Y, Dahllöf I, Holmström C, Ford Doolittle W, Kjelleberg S. Use of 16S rRNA and rpoB Genes as Molecular Markers for Microbial Ecology Studies. Appl Environ Microbiol [Internet]. 2007 [cited 2024 Apr 8];73(1):278–88. Available from: http://www.tree-puzzle.de

103. Tsukuda M, Kitahara K, Miyazaki K. Comparative RNA function analysis reveals high functional similarity between distantly related bacterial 16 S

rRNAs. Scientific Reports 2017 7:1 [Internet]. 2017 Aug 30 [cited 2024 Apr 8];7(1):1–8. Available from: https://www-1nature-1com-10013b5ij356f.han.medunigraz.at/articles/s41598-017-10214-3

104. Shah J, Mark O, Weltman H, Barcelo N, Lo W, Wronska D, et al. Fluorescence In Situ Hybridization (FISH) Assays for Diagnosing Malaria in Endemic Areas. PLoS One [Internet]. 2015 Sep 2 [cited 2024 Apr 8];10(9). Available from: /pmc/articles/PMC4558036/

105. Greuter D, Loy A, Horn M, Rattei T. ProbeBase-an online resource for rRNA-targeted oligonucleotide probes and primers: New features 2016. Nucleic Acids Res. 2016;44(D1):D586–9.

106. Greuter D, Loy A, Horn M, Rattei T. https://probebase.csb.univie.ac.at/pb_report/probe/159. 2016. probeBase .

107. Rolls G. and Sampias C. Überblick & Best Practice H- und E-Färbung | Leica Biosystems [Internet]. [cited 2024 Apr 9]. Available from: https://www.leicabiosystems.com/de-at/knowledge-pathway/he-staining-overview-a-guide-to-best-practices/

108. Simple and Robust FISH and CISH Procedures Hybridizer Hybridizer. [cited 2024 Mar 18]; Available from: www.dako.com

109. Nawaz N, Wen S, Wang F, Nawaz S, Raza J, Iftikhar M, et al. Lysozyme and Its Application as Antibacterial Agent in Food Industry. Molecules [Internet]. 2022 Oct 1 [cited 2024 Feb 21];27(19). Available from: /pmc/articles/PMC9572377/

110. Wu JA, Kusuma C, Mond JJ, Kokai-Kun JF. Lysostaphin Disrupts Staphylococcus aureus and Staphylococcus epidermidis Biofilms on Artificial Surfaces. Antimicrob Agents Chemother [Internet]. 2003 Nov [cited 2024 Feb 21];47(11):3407. Available from: /pmc/articles/PMC253758/

111. Bastos M do C de F, Coutinho BG, Coelho MLV. Lysostaphin: A Staphylococcal Bacteriolysin with Potential Clinical Applications. Pharmaceuticals [Internet]. 2010 [cited 2024 Feb 21];3(4):1139. Available from: /pmc/articles/PMC4034026/

112. Selene Gómez-Acata E, Centeno CM, Falcón LI. Methods for extracting ’omes from microbialites. 2019 [cited 2024 Feb 21]; Available from: www.elsevier.com/locate/jmicmeth

113. Kubista M, Akerman B, Norden B. Characterization of interaction between DNA and 4’,6-diamidino-2-phenylindole by optical spectroscopy. Biochemistry [Internet]. 1987 [cited 2024 Feb 17];26(14):4545–53. Available from: https://pubmed-1ncbi-1nlm-1nih-1gov-10013b5vl0452.han.medunigraz.at/3663606/

114. Ahmad E, Ali A, Nimisha, Kumar Sharma A, Ahmed F, Mehdi Dar G, et al. Molecular approaches in cancer. Clinica Chimica Acta. 2022 Dec 1;537:60–73.

115. Spindler N, Moter A, Wiessner A, Gradistanac T, Borger M, Rodloff AC, et al. Fluorescence in situ hybridization (Fish) in the microbiological diagnostic of deep sternal wound infection (dswi). Infect Drug Resist. 2021;14:2309–19.

116. Eichinger S, Kikhney J, Moter A, Wießner A, Eichinger WB. Fluorescence in situ hybridization for identification and visualization of microorganisms in infected heart valve tissue as addition to standard diagnostic tests improves diagnosis of endocarditis. Interact Cardiovasc Thorac Surg. 2019 Nov 1;29(5):678–84.

117. Madhusudhan N, Pausan MR, Halwachs B, Durdević M, Windisch M, Kehrmann J, et al. Molecular profiling of keratinocyte skin tumors links staphylococcus aureus overabundance and increased human β-defensin-2 expression to growth promotion of squamous cell carcinoma. Cancers (Basel). 2020 Mar 1;12(3).

118. Santos RS, Guimarães N, Madureira P, Azevedo NF. Optimization of a peptide nucleic acid fluorescence in situ hybridization (PNA-FISH) method for the detection of bacteria and disclosure of a formamide effect. J Biotechnol. 2014 Oct 10;187:16–24.

119. Rocha R, Santos RS, Madureira P, Almeida C, Azevedo NF. Optimization of peptide nucleic acid fluorescence in situ hybridization (PNA-FISH) for the

detection of bacteria: The effect of pH, dextran sulfate and probe concentration. J Biotechnol. 2016 May 20;226:1–7.

120. Yokogawa K, Kawata S, Nishimura S, Ikeda Y, Yoshimura Y. Mutanolysin, bacteriolytic agent for cariogenic Streptococci: partial purification and properties. Antimicrob Agents Chemother [Internet]. 1974 [cited 2024 Mar 19];6(2):156–65. Available from: https://journals.asm.org/journal/aac

121. Hof H, Dörries R. Medizinische Mikrobiologie. Vol. 4. Stuttgart: Thieme; 2009. 276–289 p.

122. Moyes RB, Reynolds J, Breakwell DP. Differential staining of bacteria: Gram stain. Curr Protoc Microbiol [Internet]. 2009 [cited 2024 Mar 19];Appendix 3(SUPPL. 15). Available from: https://pubmed-1ncbi-1nlm-1nih-1gov-10013b5xy1804.han.medunigraz.at/19885931/

123. O'toole GA. Classic Spotlight: How the Gram Stain Works. 2016;

124. Hof H, Dörries R. Medizinische Mikrobiologie. Vol. 4. Stuttgart: Thieme; 2009. 612–616 p.

125. Hof H, Dörries R. Medizinische Mikrobiologie. Vol. 4. Stuttgart: Thieme; 2009. 5–6 p.

126. Oishi T, Muratani T, Tanaka T, Sato M, Urara K, Ouchi K, et al. Study of Normal Flora in the Pharynx of Healthy Children. Jpn J Infect Dis [Internet]. 2021 [cited 2024 Mar 20];74(5):450–7. Available from: https://pubmed-1ncbi-1nlm-1nih-1gov-10013b5xy1bbc.han.medunigraz.at/33642434/

127. Prakash Gaonkar P, Patankar SR, Tripathi N, Sridharan G. Oral bacterial flora and oral cancer: The possible link? 2018 [cited 2024 Mar 20]; Available from: www.jomfp.in

128. Schulze J. Humanes Mikrobiom - Wie Mensch und Mikrobe zusammenwirken. Thieme Group - Deutsche Heilpraktikerzeitung [Internet]. 2014 [cited 2024 Mar 20];4–11. Available from: https://www.thieme-connect.com/products/ejournals/pdf/10.1055/s-0034-1396949.pdf

129. Davis CP. Normal Flora. Definitions [Internet]. 1996 Feb 2 [cited 2024 Mar 20]; Available from: https://www-1ncbi-1nlm-1nih-1gov-10013b5xy1bbc.han.medunigraz.at/books/NBK7617/

130. Gomez A. Heritable oral microbes and their importance in microbiome research for public health. Vol. 30, Cell Host and Microbe. Cell Press; 2022. p. 439–43.

131. Musher DM, Jesudasen SJ, Barwatt JW, Cohen DN, Moss BJ, Rodriguez-Barradas MC. Open Forum Infectious Diseases Normal Respiratory Flora as a Cause of Community-Acquired Pneumonia.

132. Kordahi MC, Stanaway IB, Avril M, Chac D, Blanc MP, Ross B, et al. Genomic and functional characterization of a mucosal symbiont involved in early-stage colorectal cancer. Cell Host Microbe. 2021 Oct 13;29(10):1589-1598.e6.

7. Supplement:

7.1. Ad 3.1.2.1. Acute appendicitis:

Figure 44. Ad Figure 16. - Detailed magnification and localization

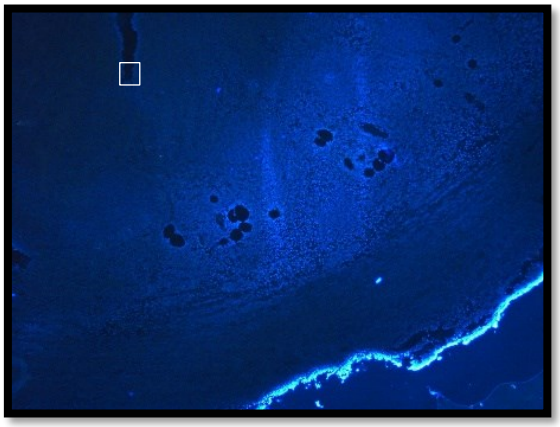

44.1. DAPI - EX387nm, x4a

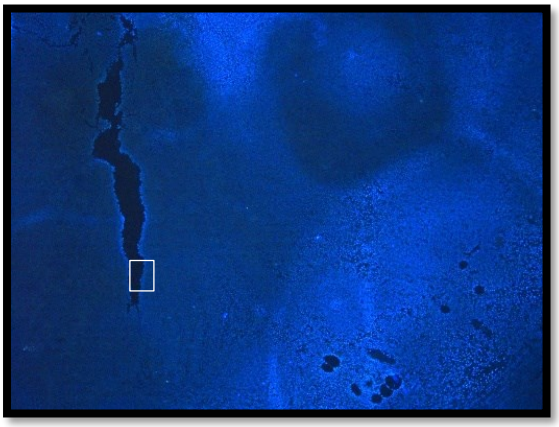

44.2. DAPI - EX387nm, x4

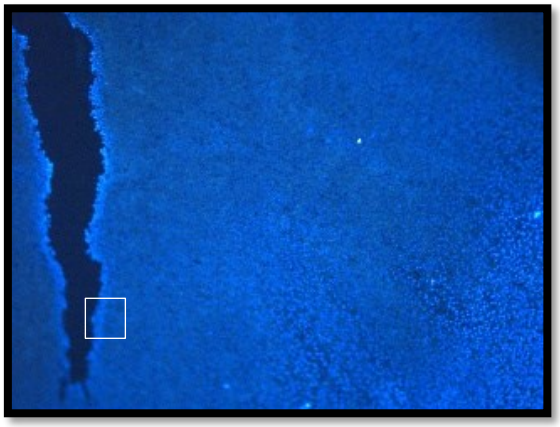

44.3. DAPI - EX387nm, x10

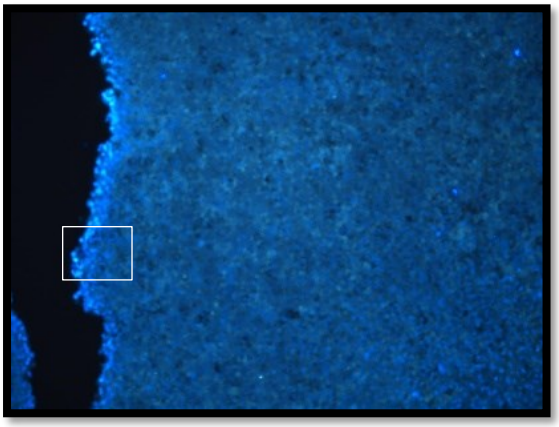

44.4. DAPI - EX387nm, x20

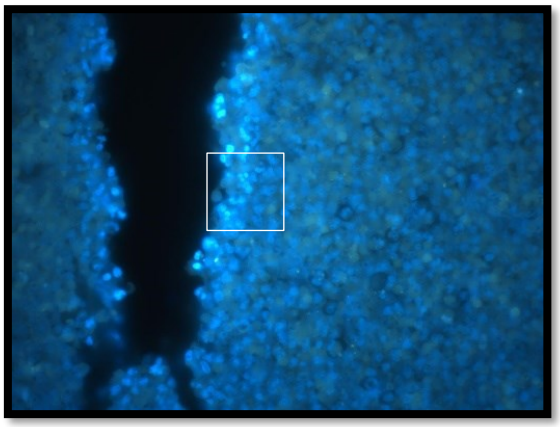

44.5. DAPI - EX387nm, x40

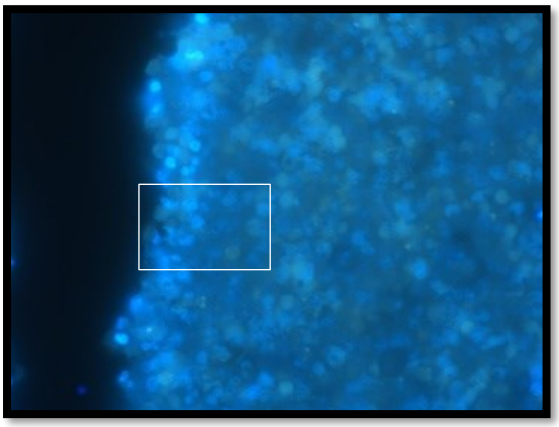

44.6. DAPI - EX387nm, x60

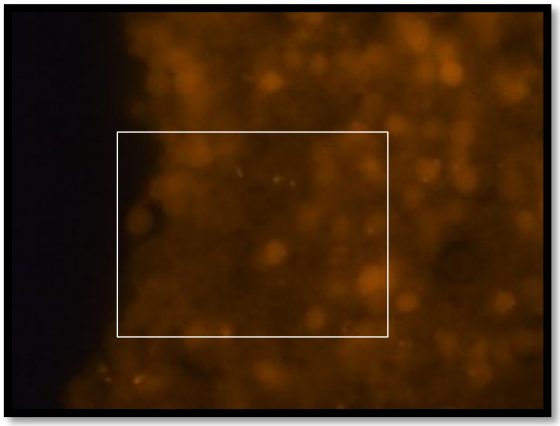

44.7. Probe - EX543nm, x100

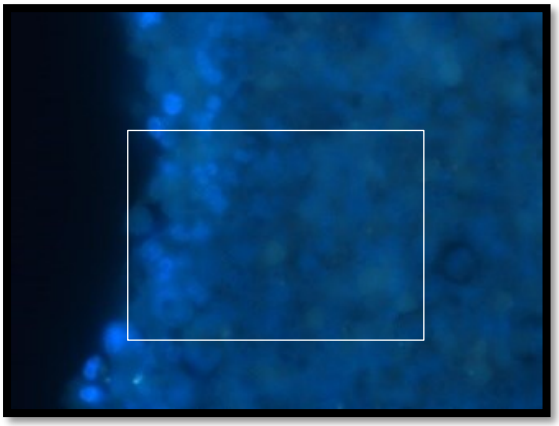

44.8. DAPI - EX387nm, x100

The exact sequence of magnifications of the DAPI images and thus the exact localization of the specific bacterial signals can be traced here.

7.2. Ad 3.3.2.1. Acute appendicitis:

Figure 45. Ad Figure 30. - Detailed magnification and localization

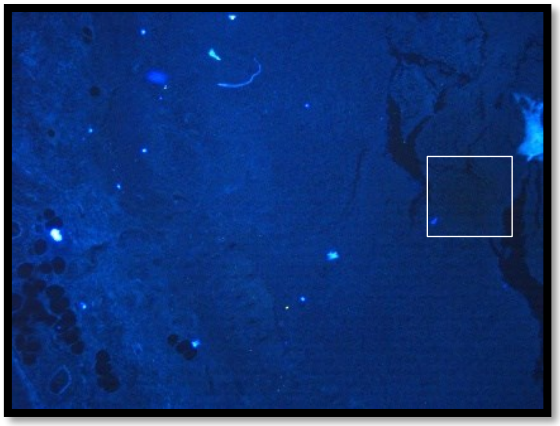

45.1. DAPI - EX387nm, x4

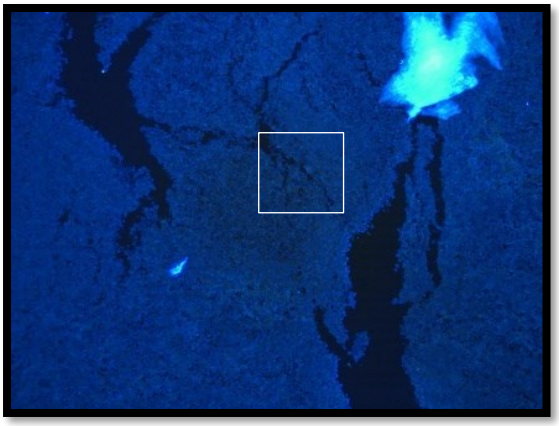

45.2. DAPI - EX387nm, x10

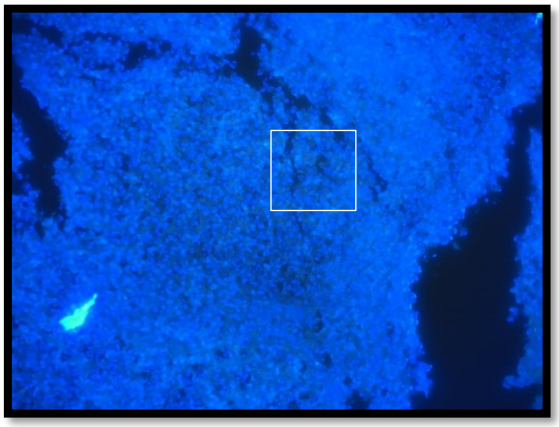

45.3. DAPI - EX387nm, x20

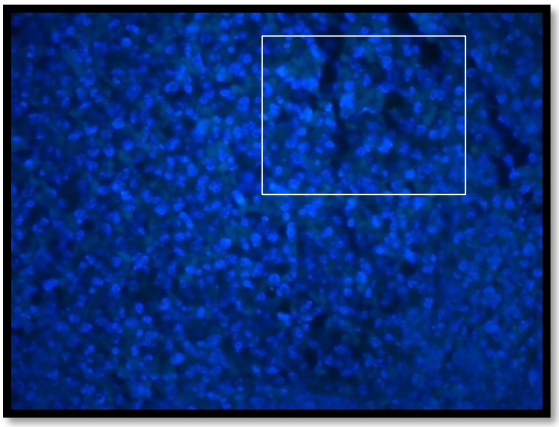

45.4. DAPI - EX387nm, x40

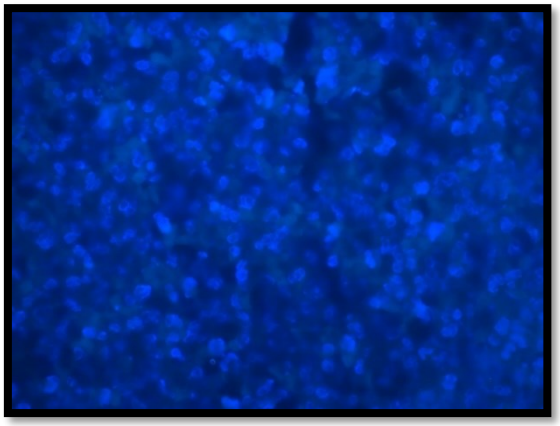

45.5. DAPI - EX387nm, x60

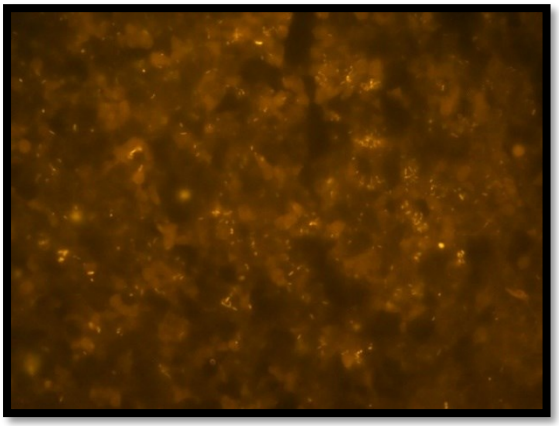

45.6. Probe - EX543nm, x60

The exact sequence of magnifications of the DAPI images and thus the exact localization of the specific bacterial signals can be traced here.

7.3. Ad 3.3.3.1. Adenocarcinoma of the colon:

Figure 46. More results of the adenocarcinoma of the colon

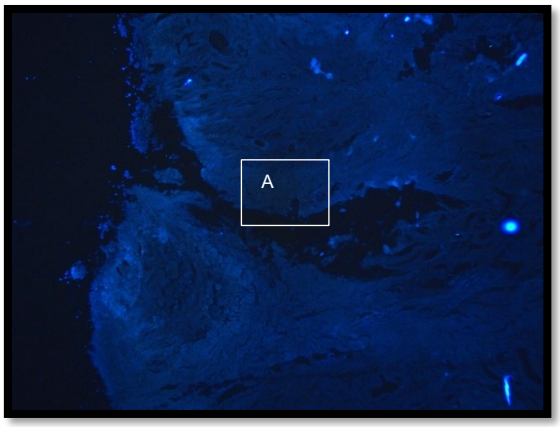

46.1. DAPI-1 - EX387nm, x4

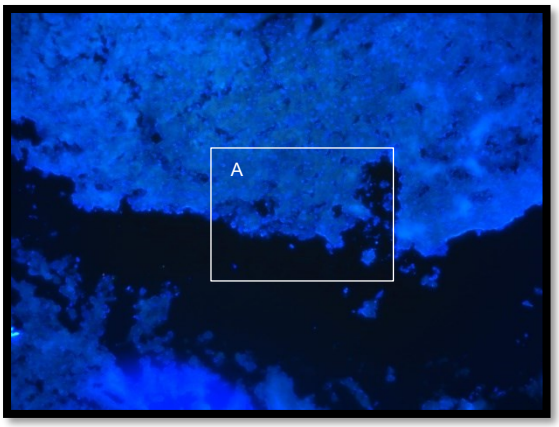

46.2. DAPI-1 - EX387nm, x20

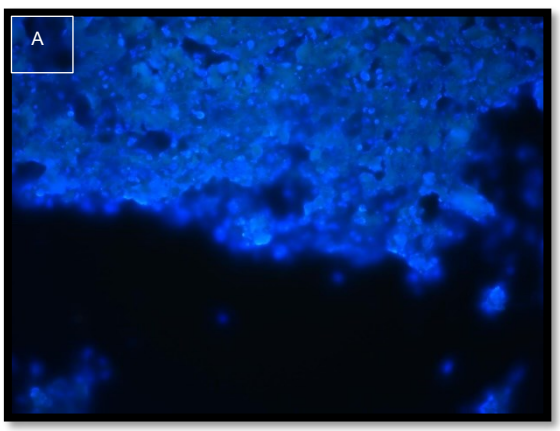

46.3. DAPI-1 - EX387nm, x40

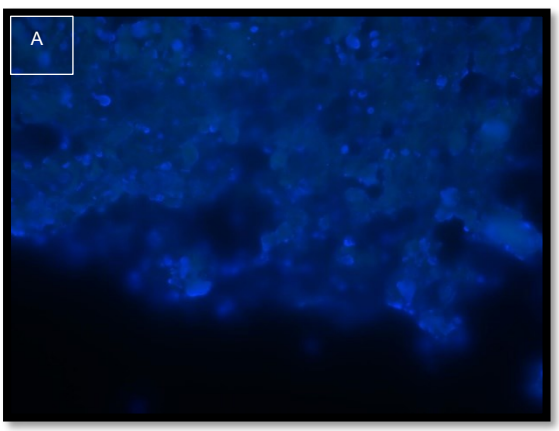

46.4. DAPI-1 - EX387nm, x60

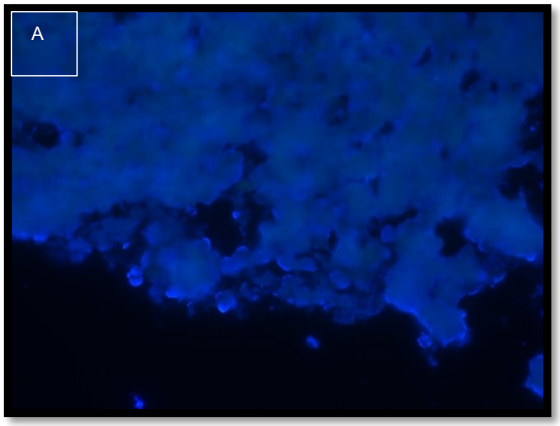

46.5. DAPI-2 - EX387nm, x60

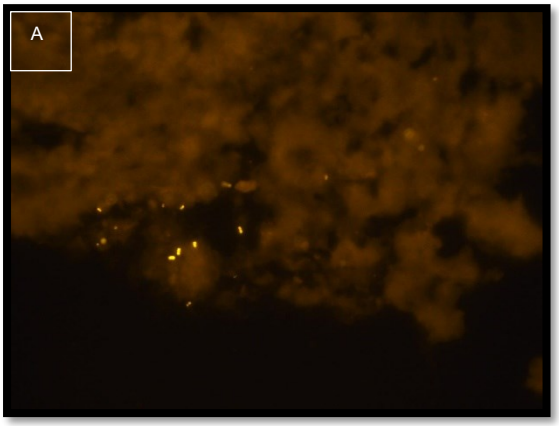

46.6. Probe-2 - EX543nm, x60

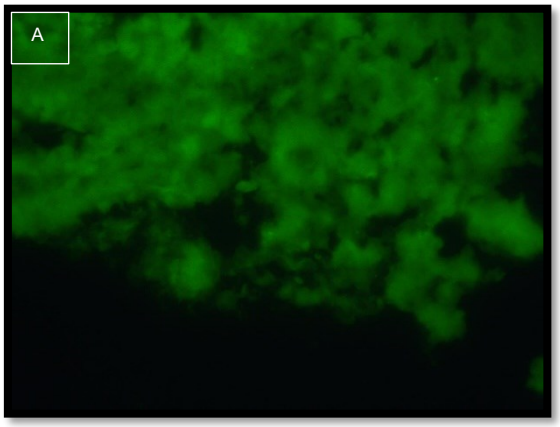

46.7. Background-2 - EX494nm, x60

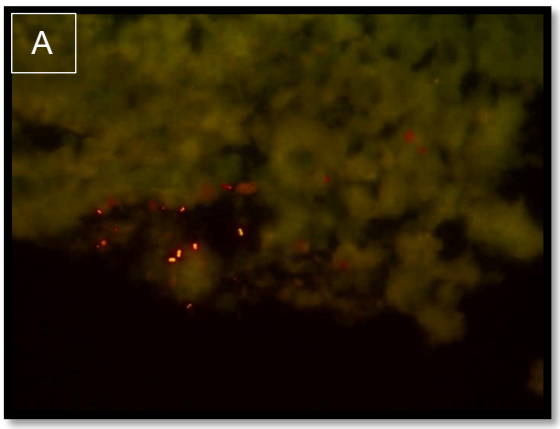

46.8. Difference-2 background – probe

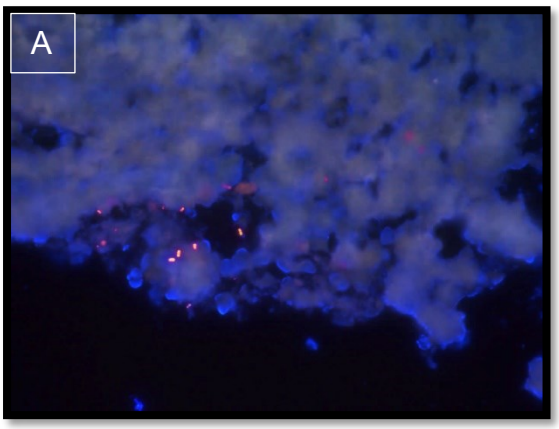

46.9. overlay-2 „difference“ + DAPI

Cocci or coccoid rods in tumor tissue that can be detected with a strong specific signal. While the DAPI -1 image series (46.1. – 46.4.) allows an orientation on the microscopy plane of the nuclei in focus in the area of the bacterial signals, the image-2 series (46.5. – 46.9.) shows the microscopy plane of the bacterial signals in focus.

Figure 47. More results of the adenocarcinoma of the colon

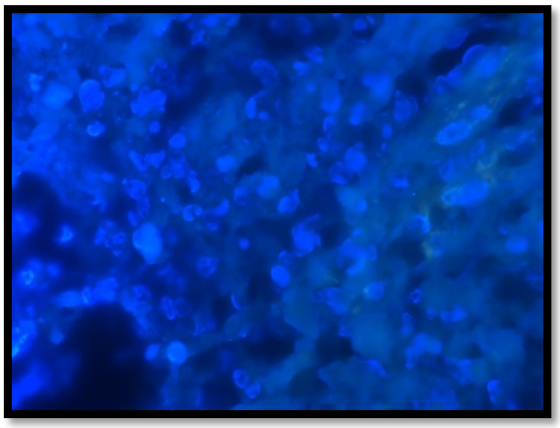

47.1. DAPI - EX387nm, x100

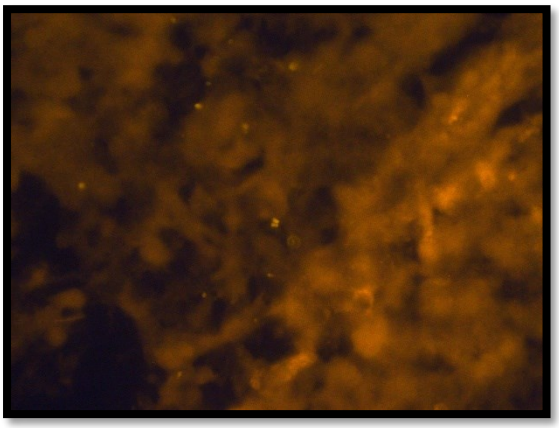

47.2. Probe - EX543nm, x100

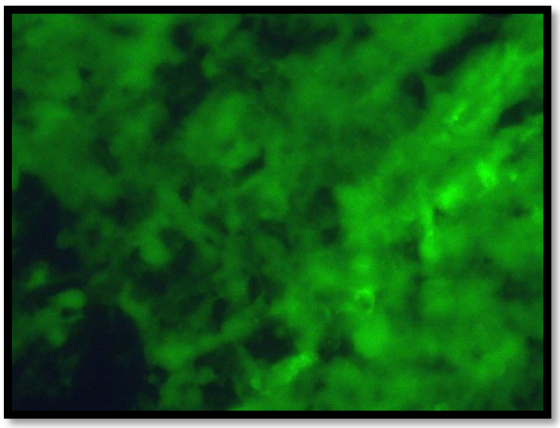

47.3. Background - EX494nm, x100

47.4. Difference background – probe

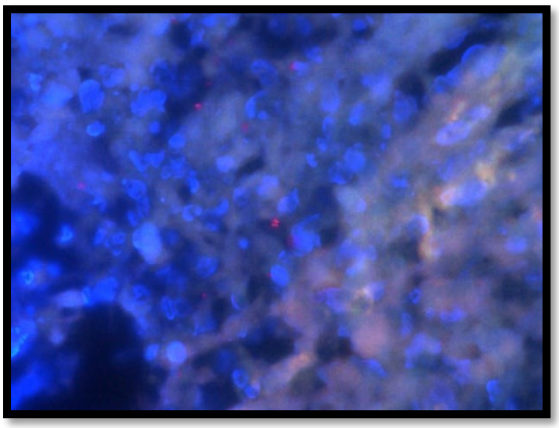

47.5. overlay „difference“ + DAPI

A clearly identifiable, morphologically preserved pair of rods surrounded by de-rounded, polymorphic cell nuclei of tumor cells.

Figure 48. More results of the adenocarcinoma of the colon

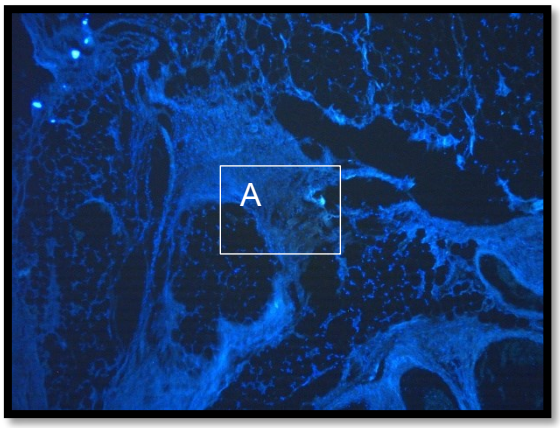

48.1. DAPI-1 - EX387nm, x4

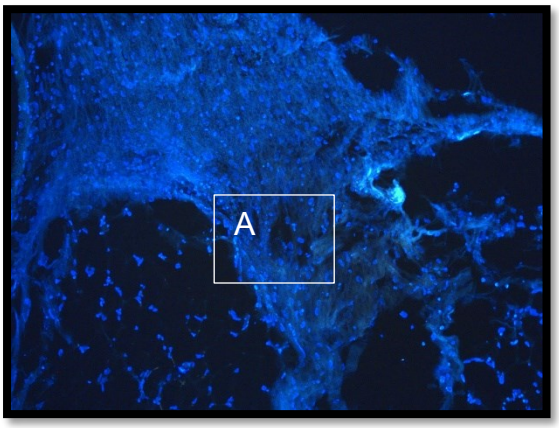

48.2. DAPI-1 - EX387nm, x10

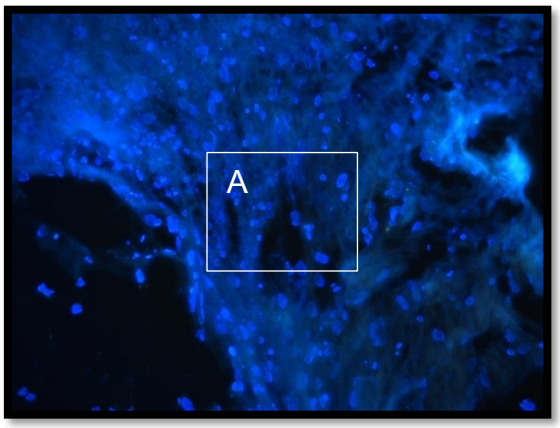

48.3. DAPI-1 - EX387nm, x20

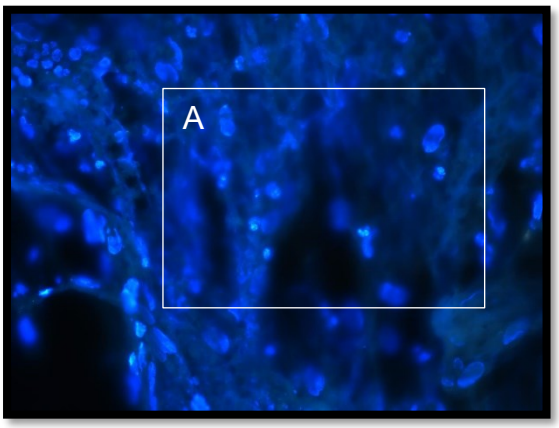

48.4. DAPI-1 - EX387nm, x40

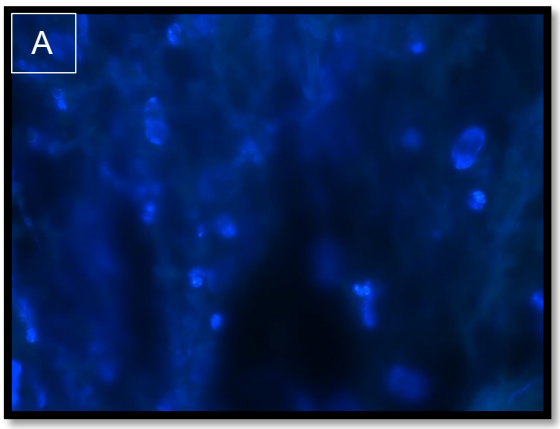

48.5. DAPI-1 - EX387nm, x60

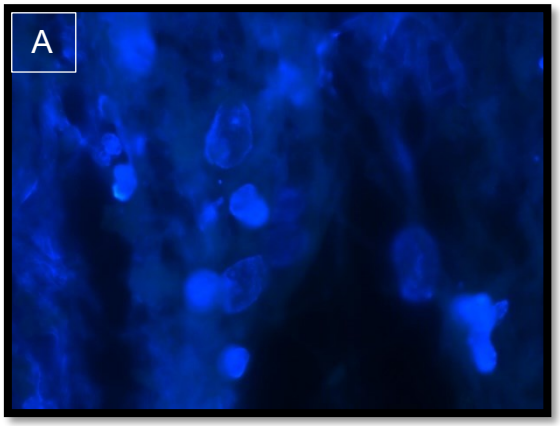

48.6. DAPI-2 - EX387nm, x100

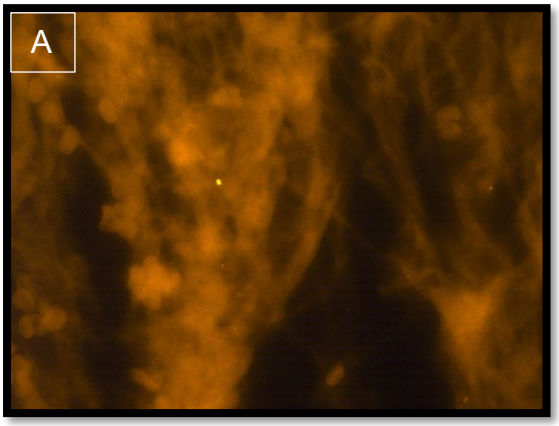

48.7. Probe-2 - EX543nm, x100

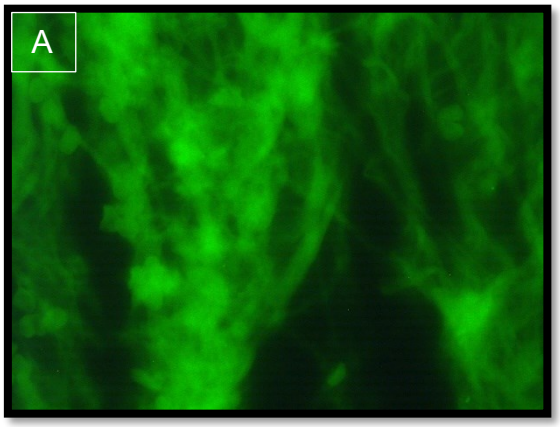

48.8. Background-2 - EX494nm, x100

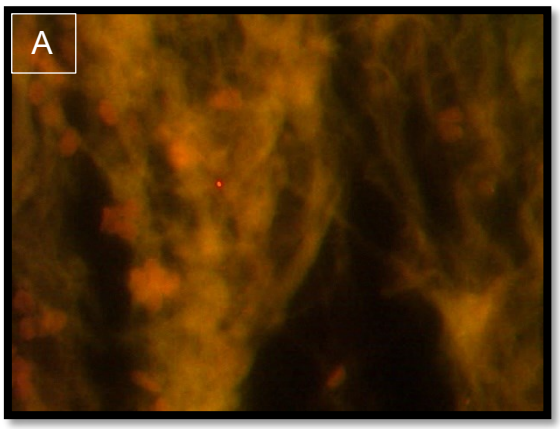

48.9. Difference-2 background – probe

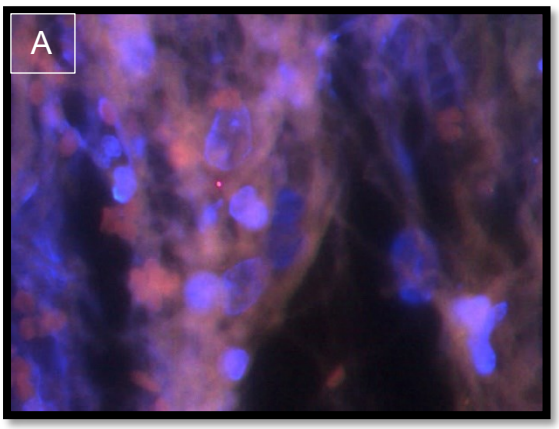

48.10. overlay-2 „difference“ + DAPI

The magnification image series DAPI-1 (48.1. – 48.5.) can be used for orientation. The DAPI-1 x60 image (48.5.) is in the same localization as the DAPI-2 x100 image (48.6.), but in a different microscopy plane to be able to show surrounding cell nuclei in focus. In 48.6. – 48.10. a clearly specific bacterial signal is recognizable in the direct surrounding of atypical cell nuclei, which is particularly evident in the overlay image.

Figure 49. More results of the adenocarcinoma of the colon

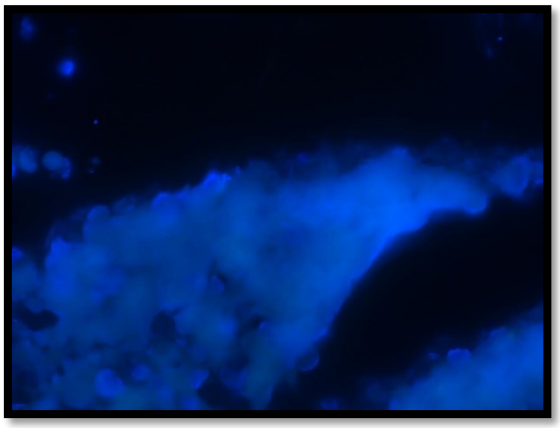

49.1. DAPI-1 - EX387nm, x100

49.2. Probe-1 - EX543nm, x100

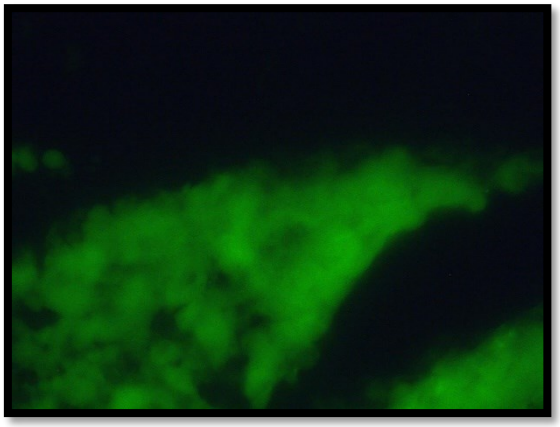

49.3. Background-1 - EX494nm, x100

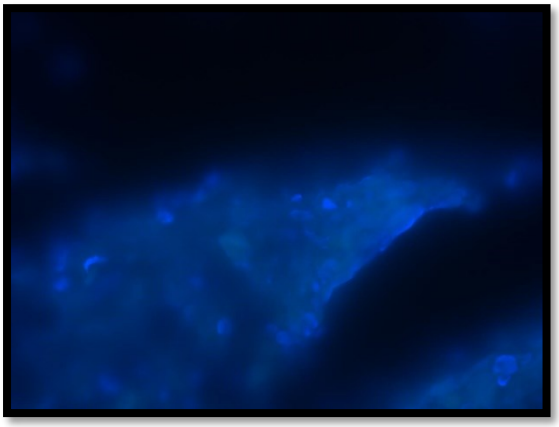

49.4. DAPI-2 - EX387nm, x100

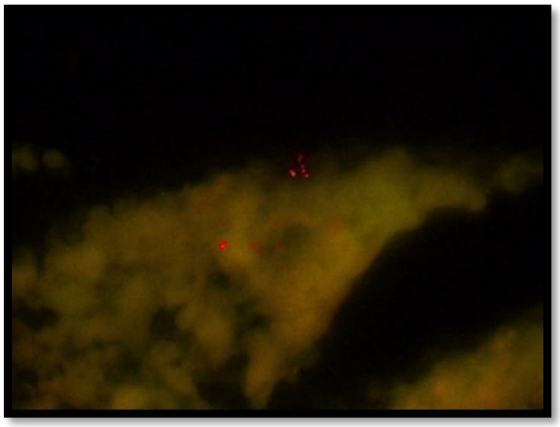

49.5. Difference background-1 – probe-1

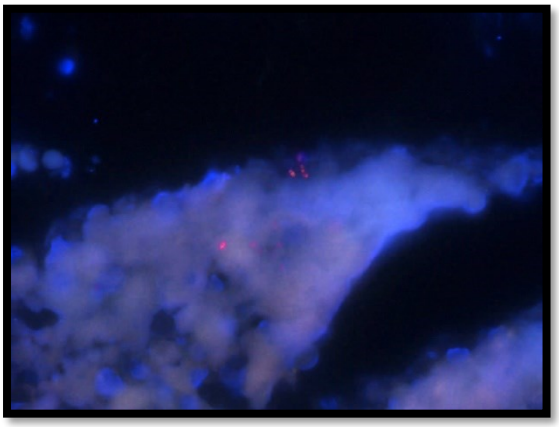

49.6. overlay-1 „difference“ + DAPI-1

Cocci/coccoid rods are clearly visible within the nucleus region. Image-1 series (49.1. – 49.3., 49.5. + 49.6.) is the microscopy plane of the bacterial signal in the probe filter, while DAPI-2 image (49.4.) has the surrounding nuclei partially in focus.

Figure 50. More results of the adenocarcinoma of the colon

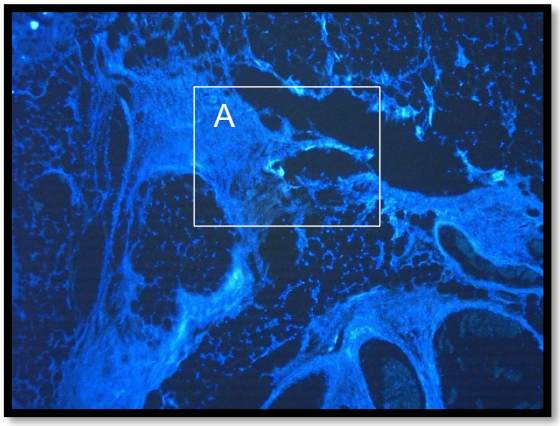

50.1. DAPI-1 - EX387nm, x4

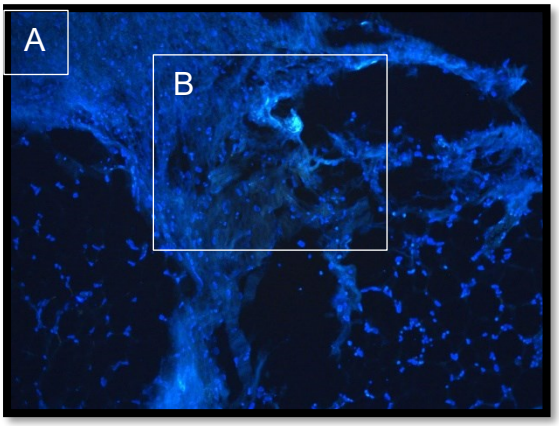

50.2. DAPI-1 - EX387nm, x10

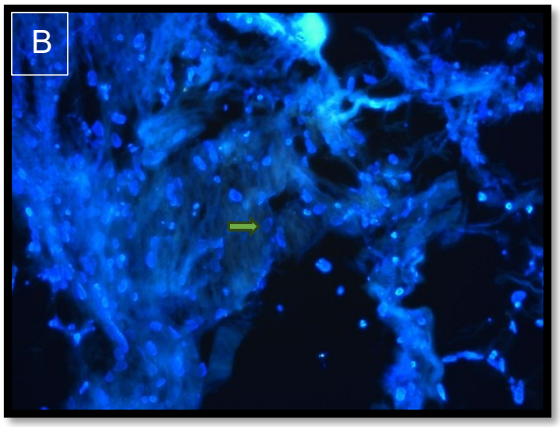

50.3. DAPI-1 - EX387nm, x20

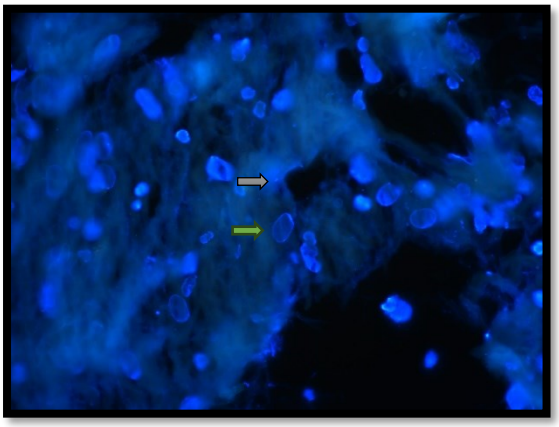

50.4. DAPI-1 - EX387nm, x40

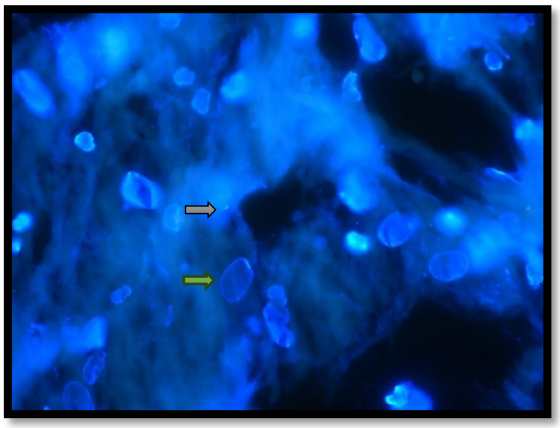

50.5. DAPI-1 - EX387nm, x60

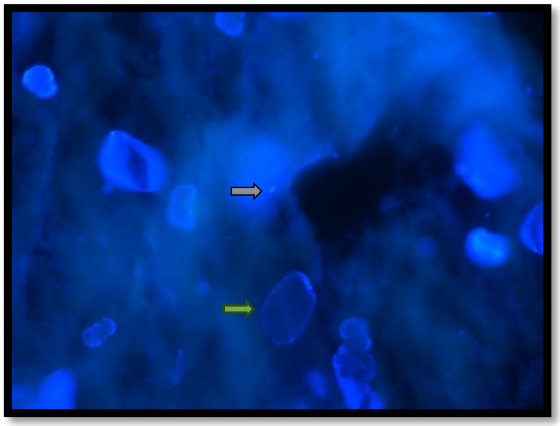

50.6. DAPI-1 - EX387nm, x100

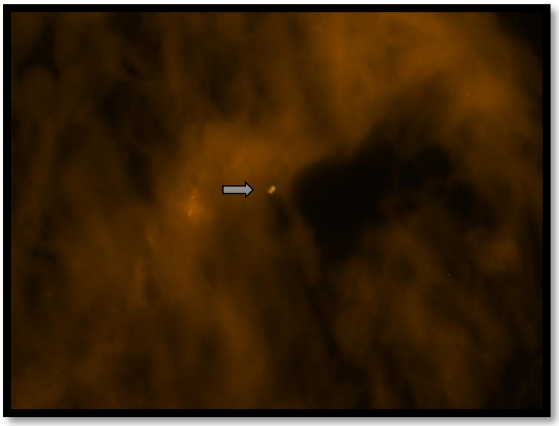

50.7. Probe-1 - EX543nm, x100

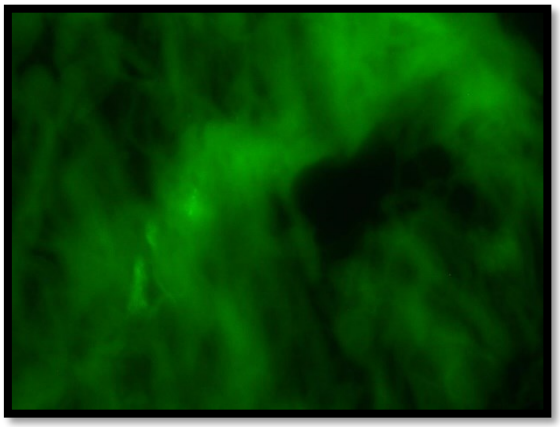

50.8. Background-1 - EX494nm, x100

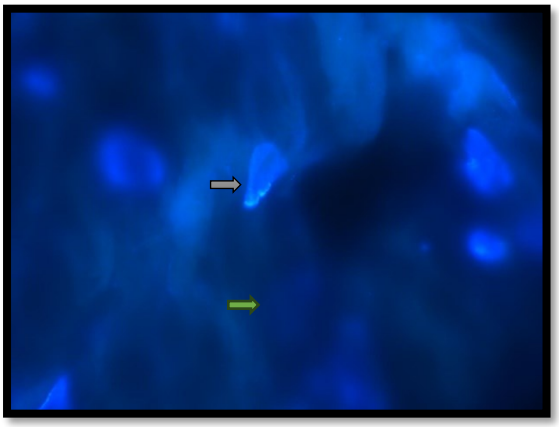

50.9. DAPI-2 - EX387nm, x100

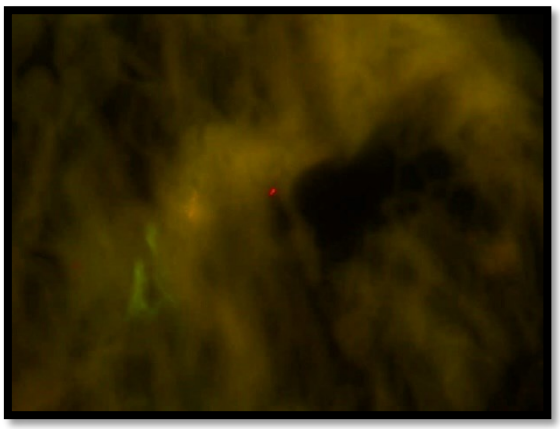

50.10. Difference background-1 – probe-1

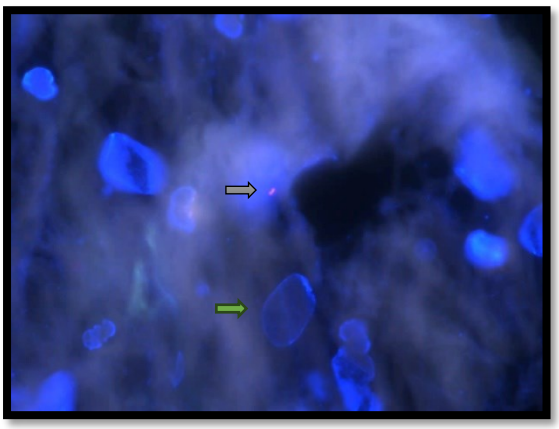

50.11. overlay „difference“ + DAPI-1

The image-1 series is used for orientation and shows the atypical cell nuclei (⇨) in direct positional relationship to the DAPI-positive bacterial signals (⇨) in the large magnifications, which is particularly easy to recognize in the overlay (50.11.). The DAPI-2 image (50.9.) shows the atypical cell nucleus lying directly above the bacterial signal in sharp focus. Whether the bacterium is located directly near the nucleus intracellularly or outside is not definitively recognizable.